TECHNICAL UNIVERSITY OF LIBEREC

FACULTY OF SCIENCE, HUMANITIES AND EDUCATION, DEPARTMENT OF PHYSICS

Studentská 2, 461 17 Liberec 1, Czech Republic

PHYSICAL PRINCIPLES OF ELECTROSTATIC SPINNING

FYZIKÁLNÍ PRINCIPY ELEKTROSTATICKÉHO ZVLÁKŇOVÁNÍ

DISSERTATION THESIS

Ing. Petr Mikeš

Liberec, 2011

TECHNICAL UNIVERSITY OF LIBEREC

FACULTY OF SCIENCE, HUMANITIES AND EDUCATION, DEPARTMENT OF PHYSICS

Studentská 2, 461 17 Liberec 1, Czech Republic

PHYSICAL PRINCIPLES OF ELECTROSTATIC SPINNING

DISSERTATION THESIS

Author:	Ing. Petr Mikeš
Supervisor:	Prof. RNDr. David Lukáš, CSc.
Consultant:	Doc. RNDr. Antonín Kopal, CSc.

Name of study field:	Physical engineering, 3901V012
Extent of dissertation thesis:	122 pages
	64 pictures
	3 tables
	136 formulas

Place and year of dissertation's defense: Liberec, 2011

…….. ……..

Místo a datum Podpis autora

Prohlášení

Byl jsem seznámen s tím, že na mou disertační práci se plně vztahuje zákon č. 121/2000 Sb. o právu autorském, zejména § 60 – školní dílo.
Beru na vědomí, že Technická univerzita v Liberci (TUL) nezasahuje do mých autorských práv užitím mé disertační práce pro vnitřní potřebu TUL.
Užiji-li disertační práci nebo poskytnu-li licenci k jejímu využití, jsem si vědom povinnosti informovat o této skutečnosti TUL; v tomto případě má TUL právo ode mne požadovat úhradu nákladů, které vynaložila na vytvoření díla, až do jejich skutečné výše.
Disertační práci jsem vypracoval samostatně s použitím uvedené literatury a na základě konzultací s vedoucím diplomové práce a konzultantem.

…… ……

V Liberci dne Ing. Petr Mikeš

Poděkování

Tato práce byla podpořena grantem GAČR No. 102/08/H081 „Nestandardní aplikace fyzikálních polí.“ Rád bych poděkoval svému školiteli Prof. RNDr. Davidu Lukášovi, CSc.. za odborné vedení, užitečné připomínky, vstřícnou pomoc při řešení vědeckých problémů a vytvoření optimálních podmínek pro mou experimentální i teoretickou práci.
Děkuji také svému kolegovi Ing. Pavlovi Pokornému za pomoc při přípravě experimentů a přínosnou diskuzi. Mnoho díků patří mému konzultantovi Doc. RNDr. Antonínu Kopalovi, CSc. a Prof. Konstantinu Korněvovi za důležité konzultace. Poděkování patří také Ing. Tomáši Trojkovi, PhD. a Prof. Ing. Tomáši Čechákovi, CSc. za vstřícnost a pomoc při realizaci spektrálních měření. Nakonec bych rád poděkoval svým rodičům Ireně Mikešové a Zdeňkovi Mikešovi za morální a finanční podporu během mých studií.

Acknowledgment

This work has been supported by GACR, grant No. 102/08/H081 “Unusual application of physical fields”. I would like to thank to my supervisor Prof. RNDr. David Lukáš, CSc. for my leading, expertise, accommodating help with solution of scientific problems and creation of optimal conditions for my experimental and theoretical work. I would like to thank as well to my colleague Ing. Pavel Pokorný for great help with preparation of experiments as well as for fruitful conversations. Many thanks belong to my consultant Doc. RNDr. Antonín Kopal, CSc. and Prof. Konstantin Kornev for an important consultations. Thanks belongs as well to Ing. Tomáš Trojek, PhD. and Prof. Ing. Tomáš Čechák, CSc. for helpfulness and help with preparation and realization of spectral measurements. At the end I would like to thank to my parents Irena Mikešová and Zdeněk Mikeš for moral and financial support during my studies.

Abstrakt

Proces elektrostatického zvlákňování vytváří nanovlákna působením vysokého napětí na polymerní roztok. Bylo dokázáno, že nanovlákna zachovávají určité množství náboje během jejich ukládání a některá zůstávají nabitá i několik hodin poté. Trysky vzniklé elektrostatickým zvlákňováním mohou vytvářet cylindrické elektrody, které koncentrují ve svém okolí extrémně vysoké hodnoty intenzity elektrického pole za atmosférických podmínek. Tyto vlastnosti elektrostatického zvlákňování jsou jen nedostatečně prozkoumány a interakce elektrického pole jimi generována s okolními plyny je téměř neznámá. Tato práce pojednává o objevení jednoduchých experimentálních zařízení založených na elektrostatickém zvlákňování, které generují Röentgenovo záření do energií 20 keV za atmosférických podmínek jenž je detekováno pomocí radiografických filmů a křemíkového detektoru nízko energetického Röentgenova záření. Tento jev byl vysvětlen pomocí teorie zvané Counterion condensation. Proces lze využít pro nejrůznější aplikace jako je například přenosné zdroje Röentgenova záření nebo jako anomální částicové urychlovače v jaderné fyzice.

Formování nanovlákenných trysek je také možně provádět v prostředí obsahující radon. Radon se rozpadá na produkty, které jsou převážně kladně nabité díky jejich β rozpadu a tyto kladně nabité radonové dcery jsou poté přitahovány a zachycovány záporně nabitými vlákny. Tohoto jevu lze využít pro aktivní filtraci ionizovaného záření.

Klíčová slova: Elektrostatické zvlákňování, nanovlákna, Röentgenovo záření, Oheň svatého Eliáše, depozice dceřiných produktů radonu.

Abstract

Electrospinnig is a process to create nanofibres by application of high voltage on the polymer solution. It is proved that nanofibres keep some amount of charge during their deposition and some of them are charged even few hours after that. Electrospinning jets can serve as fine cylindrical electrodes to create extremely high electric field intensity in their vicinity at atmospheric conditions. However, this quality of electrospinning is only scarcely investigated, and the interactions of electric fields generated by them with ambient gasses are nearly unknown. Here is the report on the discovery that simple experimental set-ups employing electrospinning generate X-ray beams up to energies of 20 keV at atmospheric conditions detected by radiographic film and then spectrally measured by Silicon Lithium-Drifted Low Energy X ray Detector. Some theoretical explanation by the process of Counterion condensation has been built up as well. This process can be used for several applications such are for example portable X-ray sources or the design of anomalous particle accelerators in nuclear physics.

The forming of the jet could be running in gas environment contains Radon. Radon decay creates progenies which are positively charged due to their β decay and these positively charged Radon daughters are then attracted and trapped by negatively charged nanofibers. This process can be used as active filters of ionized radiation.

Keywords: Electrospinning, nanofibers, X-rays, St. Elmo’s fire, Radon daughter’s deposition**.**

CONTENTS

Notation 3

1. Introduction 5

1.1. Goals of the thesis 5

1.2 Electrospinning 6

1.3 Author's own contribution to the thesis 8

2. Introduction to the basic electrostatic parameters 10

2.1 Coulomb law 10

2.2 Electrostatic potential 11

2.3 Electrostatic energy 13

2.4 Electric pressure of ideally conductive materials 14

2.5 Electrostatic field of capacitors 17

2.6 Electric field in fluid dielectrics 19

2.6.1 Clausius-Mossotti relation 21

2.6.2 Onsager relation 22

2.6.3 Electric pressure in dielectric liquids 23

2.7 Asymmetric capacitors 24

3. Basics of hydrodynamics 34

3.1 The equation of continuity 34

3.2. Euler's equation 36

3.3 Capillary pressure 38

3.4 Surface tension 39

3.5 Viscosity 40

4. Electric forces in fluids 45

4.1 Application of the electric force on ideally conductive liquids 45

4.2 Analysis of dispersion law for ideally conductive liquids 47

4.3 Application of the electric force on the dielectric liquids 49

4.4 Analysis of the dispersion law for dielectric liquids 50

5. Observation of St. Elmo's fire in laboratory conditions 54

5.1 Numerical analysis 55

6. Detection and measurement of X-rays generated by electrospinning 58
6.1 Detection by radiographic film 58
6.1.1 Characteristics of radiographic film 59
6.1.2 Detection of radiation during electrospinning process using various film shielding 60
6.1.3 Effects that might mimic X-rays 65
6.1.4 Experiment with carton frame 66
6.1.5 Experiments carried out in a photographic laboratory 67
6.1.6 Static samples 69
6.2 Spectral measurement 71
7. Electromagnetic radiation with main focus on X-rays 80
7.1 Energy levels 81
7.2 Characterization of selected subdivisions of electromagnetic spectrum 82
7.2.1 Extreme ultraviolet region 82
7.2.2 Röentgen radiation (X-rays) 83
7.3 Mechanisms of generation of X-rays. 85
7.3.1 Bremsstrahlung 85
7.3.2 X-ray radiation produced by acceleration of single point charge 85
7.3.3 Thermal Bremsstrahlung 87
7.3.4 Characteristic radiation 89
7.3.5 X-ray emission by heavy ions, Particle Induced X-ray Emission 90
7.3.6 X-ray emission during thunderstorms 92
7.3.7 X-ray flashes produced by stick-slip friction in peeling tape 92
8. Theoretical approach 94
8.1 Poisson – Boltzmann theory 94
8.2 Counterion condensation theory 97
9. Deposition of radon progeny 101
9.1 Experimental setup for radon daughter's deposition 102
10. Summary and Outlook 107
11. References 109
Appendix 115

NOTATION

A	Amplitude of the wave	$[m]$
$\vec{a}$	Acceleration	$[m/s^2]$
$\vec{B}$	Magnetic induction	$[kg \cdot s^{-1} \cdot C^{-1}]$
C	Capacity	$[C/V]$
c	Speed of light in vacuum	$[m/s]$
E	Energy	$[kg \cdot m^2/s^2]$
$\vec{E}$	Intensity of electric field	$[V/m]$
$\vec{F}$	Coulomb force	$[kg \cdot m/s^{-2}]$
f	Frequency	$[s^{-1}]$
g	Gravitational acceleration	$[m/s^2]$
h	Depth of the liquid	$[m]$
k	Wave number	$[m^{-1}]$
k_B	Boltzmann constant	$[kg \cdot m^2 \cdot s^{-2} \cdot K^{-1}]$
M	Molecular weight	$[kg]$
M_i	The mass of the ion	$[kg]$
m_e	The mass of the electron	$[kg]$
N_A	Avogadro constant	$[mol^{-1}]$
P	Polarization density	$[C/m^2]$
$\vec{p}$	Dipole moment	$[C \cdot m]$
p_e	Electric pressure	$[kg \cdot m^{-1} \cdot s^{-2}]$
p_h	Hydrostatic pressure	$[kg \cdot m^{-1} \cdot s^{-2}]$
p_c	Capillary pressure	$[kg \cdot m^{-1} \cdot s^{-2}]$
Q	Total charge	$[s \cdot A]$
q	Electric charge	$[s \cdot A]$
R	Radiated power of accelerated particle	$[kg \cdot m^2/s^3]$
$\vec{r}$	Vector displacement	$[m]$
S	Surface	$[m^2]$
T	Temperature	$[K]$
t	Time	$[s]$
U	Electrostatic energy	$[V]$
V	Volume	$[m^3]$
$\vec{v}$	Speed	$[m/s]$
Z	Atom's number	
ε_0	Permittivity of vacuum	$[F/m]$
ε_r	Relative permittivity	$[F/m]$
φ	Electrostatic potential	$[V]$

Φ	Velocity potential	$[m^2/s]$
γ	Surface tension	$[kg/s^2]$
η	Dynamic viscosity	$[kg \cdot m^{-1} \cdot s^{-1}]$
λ	Wavelength	$[m]$
μ_0	Permeability of the vacuum	$[N/A^2]$
ρ_m	Mass density	$[kg/m^3]$
ρ	Volume charge density	$[C/m^3]$
σ	Surface charge density	$[C/m^2]$
τ	Linear charge density	$[C/m]$
ν	Kinematic viscosity	$[m^2/s]$
ω	Angular frequency	$[rad/s^2]$
ξ	Wave deflection	$[m]$

1. Introduction

Nanotechnology has been under the scope of interest during last decades as a promising research for future materials. It deals with sizes of submicron dimensions but rigorous definitions of nanotechnology have the dimensions less than 100 nm. First concept of nanotechnology was established by Feynman's talk given at an American Physical Society meeting at Caltech on December 1959, where he affirmed the famous phrase: "There is plenty of room at the bottom". For many scientists, nanotechnology is manipulating with individual atoms or molecules. One part of nanotechnology is creation of nanofibers with diameters less than 1μm. Nanofibers are usually made from polymeric solutions, consisted by individual macromolecules.

Serious physical explanations of some phenomena observed in "nanoworld" are still missing. Some basic principles of quantum theory built in last century gives explanations of behavior of elementary particles comprising an atom and inside an atom, but nano-objects are usually consisted from many of these elementary particles and therefore this quantum theory starts proceed into collective phenomena based on macromolecular structures. "Classical macroscopic" theory is not good enough for explanation of some processes observed in "nanoworld". Therefore the new theory has to be built.

1.1 Goals of the thesis

This work aims to creation of some cornerstones of physical principles of electrostatic spinning (electrospinning) process, which is the basic method for nanofibrous creation. Some of improvements of current theory were already determined and are introduced in this work, for example an implementation of relative thin films and permittivity into the dispersion law (chapters 3 and 4) or preliminary theory with inclusion of viscosity (chapter 3). But the comparison with experiment is still missing.

The main goal of this work is the clarification of origin and parameters of detected high energetic electromagnetic radiation. Discovery of Röentgen radiation produced at atmospheric conditions during electrospinning process can be very helpful for the understanding of physical phenomena occurring during electrospinning process. It can be as well very helpful for many future applications. Thesis has been aligned in the same rank as the time of discoveries was going on. It starts with description of first observations by radiographic films, and continues with measurement of its spectrum. Then it was necessary to have a brief description of generation of X-rays detected during electrospinning (chapter 7)

and at the end, some theoretical explanation of generation of X-rays by electrospinning process has been created. More detailed studies of both radiographic and spectral measurements have to be made.

The last goal was the observation of Radon daughter's deposition during electrospinning process. In chapter 9 is the report about the radon progeny deposition driven by electrospinning which can be used for several applications as active filters of ionized particles.

1.2 Electrospinning

Electrospinning is the process for creation of nanofibers by application of high electrostatic field on a surface of a polymeric solution. This process is in its principle very simple, but as was already mentioned it is affected by many parameters. First report of electrospinning was discovered by John Zeleny (1914) in his atmospheric observations. He applied high voltage on the tip of the sharp needle for creation of high corona discharge to simulate the lightning in laboratory conditions. But the tip of the needle started to vituperate by these corona discharges and therefore he used column of water instead. He was the first person who observed electrostatic spraying in laboratory conditions. But he didn't find any application at that time and published it as an interesting, but useless phenomenon. Anyway it was the first step for future creation of nanofibers. In this work, only basic principles of electrospinning will be explained because there were next books written about this process. The first monography about electrospinning was written by Ramakrishna (2005), Andrady (2008), Filatov (2007) or the monographic article written by Reneker (2008) or Lukas (2008). But the description of electrospinning process isn't the main topic of this work. This work aims mainly to unexceptional phenomena observed during electrospinning which are for example radon daughter's deposition, St. Elmo's fire and mainly detection of X-rays.

Anyway it is useful to briefly describe basic principles of electrospinning. As was already mentioned, electrospinning is a process for nanofibrous creation by application of high electrostatic field on the surface of polymeric solution. It has three main stages. At the beginning, Taylor (1969) cone is created by the destabilization of the liquid surface by application of electrostatic field. If the field is strong enough, jet is emitted from the tip of the Taylor cone and most of the solvent is evaporated during this phase. This stage is usually called stable part. If the viscosity (concentration of the polymer) is not high enough,

electrospraying instead of electrospinning will occur. It means that nanodroplets instead of nanofibers are created. Liquid jet will be disintegrated into the droplets by Rayleigh (1882) instability and in some cases it can create St. Elmo's fire (see chapter 5). A robust approach for the analysis of the stable jet region was introduced by Xiao-Hong Qin and co-workers (2004). There is a crucial impact on dielectric parameters of the polymeric solution during the stable part due to the massive solvent's evaporation and there weren't any studies of impact of relative permittivity on the electrospinning process until this work (for analysis of dielectric properties see chapter 4). When the most of the solvent is evaporated, jet starts to circulate and form the spiral or it starts to split into thinner fibers. This stage is called whipping zone. Due to the impossibility of observation of whipping zone by accessible methods, there isn't any satisfactory theory and experimental observations until these days. Some first theoretical explanation was made by Reneker and Yarin (2008). But the observation of X-rays during the nanofiber's deposition, which is the main topic of this work, can be helpful for the description of this last and hidden part of nanofiber's creation. As can be clearly seen, electrospinning is very simple process but with many variable parameters which can drastically change its behavior. Schematic view with all these three main parts of an electrospinning jet can be seen in Fig. 1.1.

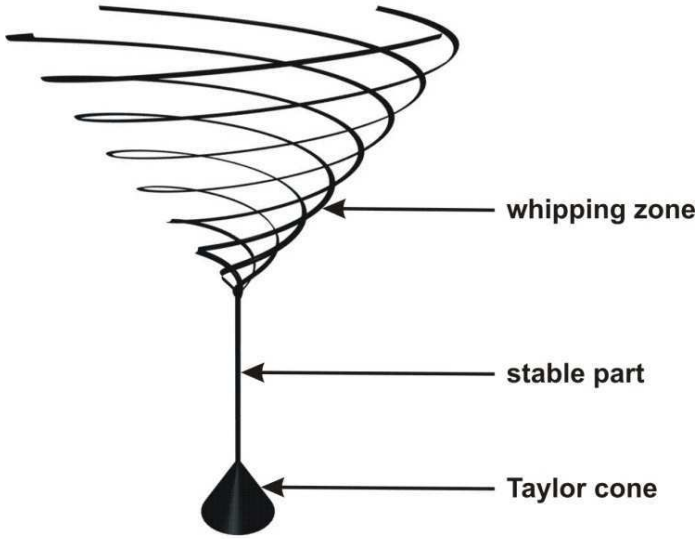

Figure 1.1: Stable and unstable zones of a liquid jet in an electrospinning zone.

Electrospinning until beginning of 21st century, was an interesting natural phenomenon but without any possibility of effective application for mass production. Therefore it is important to tell few words about other specifications of this method. Until the

year of 2004, electrospinning was possible only using the needle filled by the polymeric solution which is the method with low productivity. The productivity can be simply increased by application of an array of needles, but it brings other problems of clogging of needles, see Theron (2005). Therefore another solution had to be discovered. Yarin (2004) and his colleagues found a method of spinning from the free liquid surface and named it needless electrospinning. The real revolution method was later developed by Jirsak (2005) et al by using of rotating cylinder in the polymeric solution. Many jets from the surface of the cylinder are created and their invention was then appointed as Nanospider. This work is not focused on technological development but on explanation of physical problems, connected to this wonderful and interesting natural process. All mentioned technical details about electrospinning can be found in works mentioned above.

First physical description of destabilization of liquid surface and the formation of Taylor's cones was worked out by Lukas (2008) with his students. They had to use several approximations such are incompressible and ideally conductive liquids. It gives some nice results comparable with experiment. Their main keystone is the relations between hydrostatic, capillary and electrostatic forces. This theory is good initial point for future enhancements and some its base stones are determined in chapter 4.

1.3 Author's own contribution to the thesis

- Calculation of all examples in chapter 2 which are helpful for many theoretical as well as experimental results such for example Counter ion condensation theory or Nanospider technology.
- Inclusion of relative permittivity into the dispersion laws for charged liquid surface and their analysis (chapters 2.6 and 4.3). There is a massive evaporation of solvent and therefore distinct change of relative permittivity during jet's elongation.
- Inclusion of viscosity into the theory of electrospinning process (chapter 3.5). Viscosity seems to play the crucial impact on the thickness of the fibers.
- Derivation and analysis of dispersion law for thin films of charged liquid surface as the real liquid surfaces has finite depths (chapter 4.2).
- Analysis and comparison of theoretical approaches of St Elmo's fire as this phenomenon was observed during electrospraying process in laboratory conditions (chapter 5).

- All radiographic experiments were prepared as a first detection of X-rays as well as measurement of its space distribution (chapter 6.1)
- All X-rays spectral distributions were measurements on Si-lithium drifted detector as the elimination of parasite effects as well as proving of X-rays generated by the electrospinning process (chapter 6.2).
- Generation of X-rays by electrospinning process was explained by the Counterion condensation theory. Derivation and analysis of potential gradient in Manning zone showed the possibility of acceleration of ions into the energy of X-rays region of electromagnetic spectra. (chapter 8)
- The last unexpected phenomenon of electrospinning is the Radon daughter's deposition. Several measurements in laboratory as well as in radon chamber were prepared to prove it. Precise PVDF yarns were prepared for filtering of ionized radiation (chapter 9).

2. Introduction to the basic electrostatic parameters

There were many text books or monographs written about electrostatics. A great course was written by Richard Feynman (1971). He involves a brilliant description of basics of electrostatics and adds more complex examples in later chapters. The book continues in description of electromagnetism, but as we observed, there isn't almost any influence of magnetic field on nanofibre creation. Here, only the first twelve chapters of his second course are important for us. Another brilliant book was written by Lev Davidovic Landau and Evgeny Mikhailovich Lifshitz (1960). They solved more complex problems in this book, which readers are supposed to meet in some basics coursers of physics. These courses should be provided for instance by the Open Courseware by Walter Lewin from Massachusetts Institute of Technology (MIT). It is possible to watch these courses online on internet: (http://ocw.mit.edu/OcwWeb/web/courses/av/index.htm) . A brief overview of basic electrostatic laws which will be used later for description of electrospinning is introduced further. Basics knowledge of electrostatics is crucial for understanding and explanation of electrospinning phenomenon. Many of these fundamental laws are introduced without a broad description, since one can use books mentioned above.

2.1 Coulomb law

Electrostatics starts as a rule with definition of well known Coulomb law which describes force between two charges q_1 and q_2 with distance *r* between them.

$$\vec{F}_{21} = \frac{1}{4\pi\varepsilon_o\varepsilon_r} \cdot \frac{q_1 \cdot q_2}{r^2} \cdot \frac{\vec{r}}{|\vec{r}|}, \qquad (2.1)$$

where ε_0 is a permittivity of vacuum, ε_r is a relative permittivity of used material and $\vec{r}$ is the vector displacement to point (1) from (2).

A force exerted per a single positive unit charge is called intensity of electrostatic field or field strength and is denoted as $\vec{E}$. This is a very important quantity of electrostatic theory,

$$\vec{F} = q\vec{E}\,. \qquad (2.2)$$

Electric field can be represented by field lines. Sometimes these lines can be very complex in shapes and a problem is hard to solve analytically (see Fig. 2.1). Sharp body edges always keep higher values of electrostatic field around them, as can be seen in figure 2.1 D.

2.2 Electrostatic potential

Another important parameter of electrostatic field theory is an electrostatic potential φ. It is a scalar quantity, typically measured in Volts. Areas with same potentials can be in 2D represented by lines called equipotentials. Field lines are always perpendicular to them (see Fig 2.1). Knowledge of these lines plays a crucial role for electrospinning explanation. The proper definition of electrostatic potential uses electric field of two points:

$$\varphi(\vec{r}) = -\int_0^{\vec{r}} \vec{E} \cdot d\vec{r} + C \cdot \tag{2.3}$$

This can be expressed by derivation obtaining another definition of electric field:

$$\vec{E} = -\vec{\nabla}\varphi. \tag{2.4}$$

Another condition for electrostatic potential is that

$$\vec{\nabla} \times \vec{E} = 0 \quad \text{or} \quad \oint \vec{E} dl = 0,$$

It simply means that any work cannot be made, when the charge is transferred around any closed curve without generation of magnetic induction. This is the special form of the second Maxwell's equation of electromagnetism, which full formula is:

$$\vec{\nabla} \times \vec{E} = \frac{\partial \vec{B}}{\partial t}. \tag{2.5}$$

If $\vec{\nabla} \times \vec{E} \neq 0$, some magnetic induction per unit of time has to be created during electric charge transportation, see Maxwell's equations in Feynman (1971). One can now use Gauss's law which in general form is: $\oint_S \vec{v} \cdot d\vec{S} = \int_V (\vec{\nabla} \cdot \vec{v}) dV$, where *S* is the closed surface bordering volume *V*. Gauss's law can be used to derive Coulomb's law and vice versa

$$\vec{\nabla} \cdot \vec{E} = -(\vec{\nabla} \cdot \vec{\nabla})\varphi = -\vec{\nabla}^2 \varphi = \frac{\rho}{\varepsilon_0}, \tag{2.6}$$

what is the first Maxwell's equation for electrostatic conservative field, where ρ is total charge density. Total charge can be expressed as: $Q_{all} = \int_S \rho dV$ for continual charge distribution and $Q_{all} = \sum_S q_i$ for discrete charge distribution inside surface *S*. For non-charged or inside some closed conductive object, which is commonly called Faraday's cage, is the electric field zero:

$$\vec{\nabla}^2 \varphi = 0. \tag{2.7}$$

This equation is usually called as Laplace's equation. By combination of (2.2) and (2.3), we get formula for electric potential of point charge placed in $\vec{r} = 0$:

$$\varphi = \frac{1}{4\pi\varepsilon_0\varepsilon_r} \cdot \frac{q}{r} \tag{2.8}$$

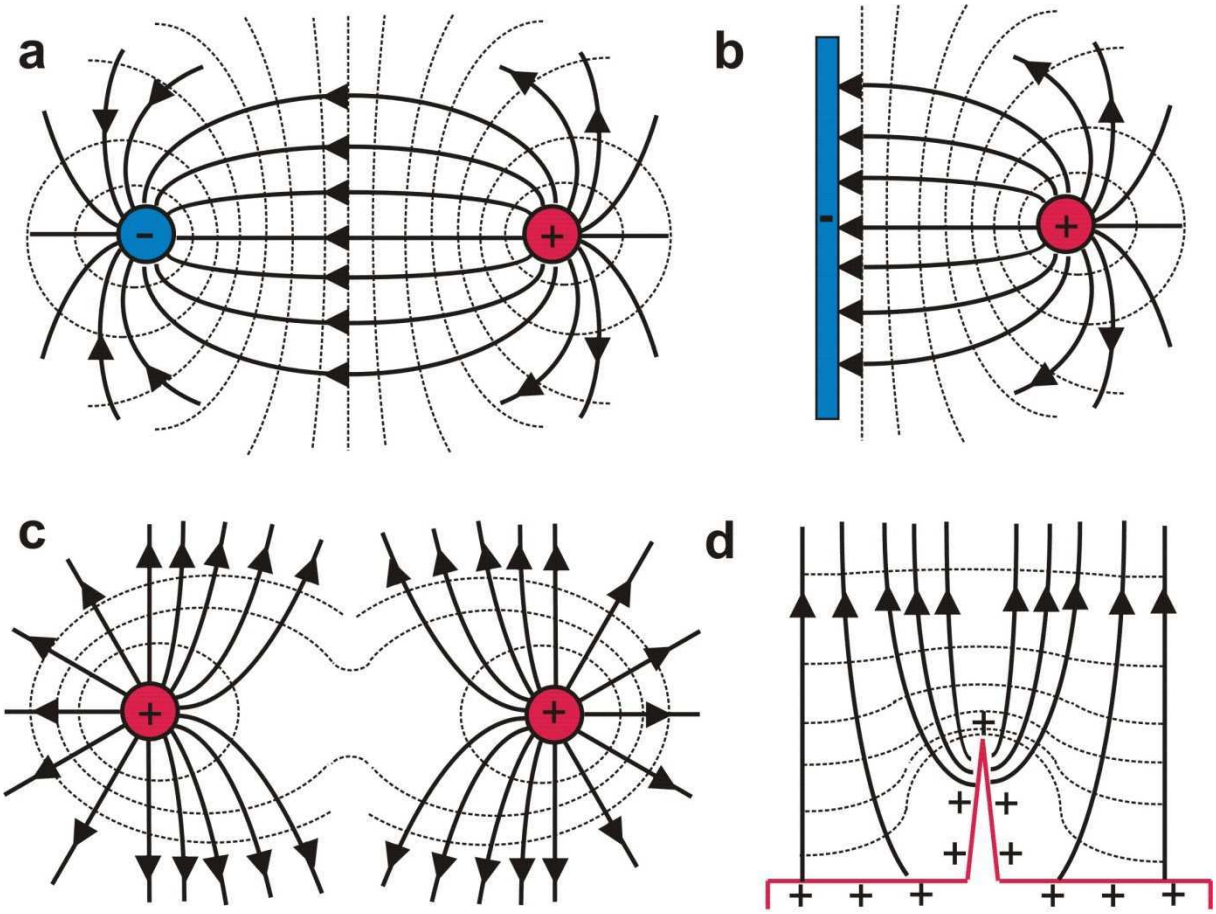

Figure 2.1: Electric field represented by filed lines (solid lines) and equipotentials (dash lines) for various examples. (a) Electric field between two charges with different polarity,(b) electric field between a charge and charged plate with different polarity, (c) electric field between two charges with the same polarity, (d) electric field around a sharp charged object.

2.3 Electrostatic energy

Another important quality for the theory of electrostatic field is its electrostatic potential energy. There is a great explanation of this quantity made by Feynman (1971), in chapter 8 ,Kopal (2008) or Griffiths (1999). Only very basic definitions of electrostatic energy will be explained here. At the beginning one can have a look on the basic definition of electrostatic energy. With using of the principle of superposition, the electrostatic energy U of reciprocal locations of system of point charges can be expressed as a sum of the energies of all possible pairs of charges q_i and q_j $(i, j = 1,...,n)$ with distances r_{ij} in between them:

$$U = \frac{1}{2}\sum \frac{q_i q_j}{4\pi\varepsilon_0 r_{ij}}, \tag{2.9}$$

which simply means the total work which has to be done to bring all charges together. The factor $1/2$ is introduced, because all pairs are counted twice. Another approach how to calculate the electrostatic energy of electric field is to use the charge density ρ. Each volume element dV contains the element of charge ρdV. So the formula (2.9) can be rewritten by the integral expression of principle of superposition:

$$U = \frac{1}{2}\int \frac{\rho(1)\rho(2)}{4\pi\varepsilon_0 r_{12}} dV_1 dV_2 . \tag{2.10}$$

Formula (2.10) can be rewritten by using of definition of electrostatic potential, formula (2.8), for continuously distributed charge U_1 and for formulation of two discrete charges U_2:

$$U_1 = \frac{1}{2}\int_V \rho(1)\varphi(1)dV_1 , \quad U_2 = q_1 \frac{q_2}{4\pi\varepsilon_0 r_{12}} = q_1\varphi(1) = q_2\varphi(2) \quad . \tag{2.11}$$

Because the energy is not the term of charges but the term of the fields they produce, the formula (2.11) is numerically equal to:

$$U = \frac{\varepsilon_0}{2}\int \vec{E}\cdot\vec{E}dV , \tag{2.12}$$

which is the energy of electrostatic field. Energy per unit volume, also called energy density, is:

$$u = \frac{\varepsilon_0 \vec{E}^2}{2}, \tag{2.13}$$

and the total energy is therefore: $U = \int_V u dV$. Energy of the electromagnetic radiation will be explained later.

2.4 Electric pressure of ideally conductive materials

Electric pressure is another basic concept in electrospinning. Having a charged sphere with surface element dS and $\vec{E}_1$ being the contribution to the total field from charges that reside on surface of this element and $\vec{E}_2$ is the field contribution of all other charges around the element dS. The total field strength therefore will be sum of both contributions: $\vec{E} = \vec{E}_1 + \vec{E}_2$. Field strength $\vec{E}_1$ is for conductors orthogonal to the surface. Electric field strength inside the element has to be equal to zero, therefore $-\vec{E}_1 + \vec{E}_2 = 0$ and E_2 has to be collinear to E_1. That is why $\vec{E}_1 = \vec{E}_2 = \frac{1}{2}\vec{E}$, see Fig 2.2. For more details: Lukas (2009).

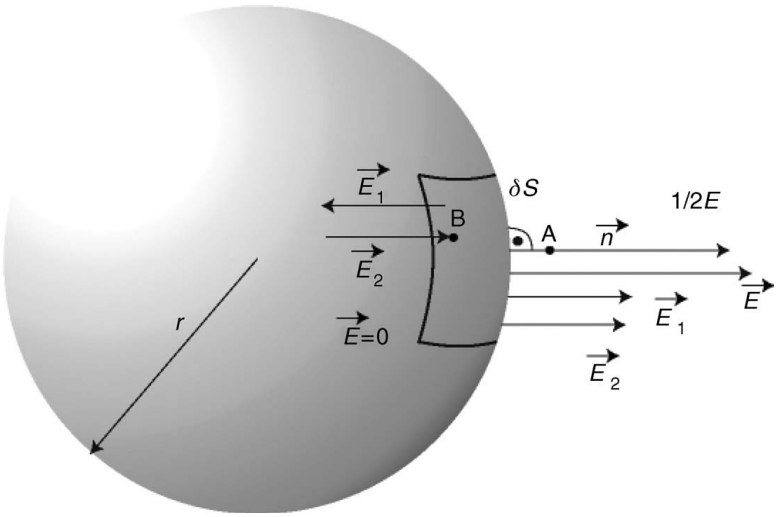

Fig.: 2.2: A charged, perfectly conductive sphere with a radius r has a normal $\vec{n}$ perpendicular to an elementary area, δS, of its surface. Point A is just outside the droplet, while point B is inside it. $\vec{E}_1$ is the contribution to the total field from charges that reside on surface of this element and $\vec{E}_2$ being the rest field intensity contribution of all others charges around the element dS.

The surface of the sphere is charged and both contributions of the electric field $\vec{E}_1$ and $\vec{E}_2$ have the same direction perpendicular to the surface and form together consequent electric field outside the sphere. The charge on the element dS can be expressed as $\sigma \cdot dS$, where

σ is a surface charge density and it generates an intensity of electrostatic field $\vec{E}_1$. So the force acting on this charge is caused by the electric field strength $\vec{E}_2$ that interacts with the charge $\sigma \cdot dS$:

$$d\vec{F} = \sigma \cdot dS \cdot \vec{E}_2 = \frac{1}{2}\sigma \cdot dS \cdot \vec{E}\,. \tag{2.14}$$

When the electric force acting on charge of the element is known, one can find formula for electric pressure:

$$p_e = \frac{dF_n}{dS} = \frac{1}{2}\sigma \cdot E = \frac{1}{2}\varepsilon_0 \cdot E^2, \tag{2.15}$$

electric pressure is defined as orthogonal compound electric force F_n acting on dS. Surface charge density can be expressed as $\sigma = \varepsilon_0 \cdot E$. To make formula (2.15) usable for electrospinning theory, one has to find its dependence on a surface deflection.
The basic formula for the deflection ζ can be expressed as a harmonic function:

$$\zeta = A \cdot \exp[i(kx - \omega t)], \tag{2.16}$$

with amplitude A, wave number k, angular frequency ω and time t. Electrostatic potential can be implemented as well with the knowledge of its deflection of the harmonic function (2.16) in vertical dimension $z = \zeta$ where $\zeta \to 0$:

$$\varphi_\zeta = D \cdot e^{-k\zeta} \cdot \exp[i(kx - \omega t)]. \tag{2.17}$$

Detailed expression of this formula can be found in Feynman (1971) in chapter 7.5.
Electrostatic potential on the deflected wave as a function of the field in ground level E_0 is:

$$\varphi_\zeta = E_0 \cdot \zeta \tag{2.18}$$

With respect to equation (2.17) and condition $\zeta \to 0$ and therefore $e^{-k\zeta} \to 1$, one can a find relation between constants A and D and rewrite (2.18) as:

$$\varphi_\zeta = A \cdot E_0 \cdot e^{-k\zeta} \cdot \exp[i(kx - \omega t)] \tag{2.19}$$

Deflection of the wave by the electric pressure is important for theory of electrospinning. It will be used for determination of dispersion law which is the main equation for description of destabilization of liquid surface by the electric field, see Lukas (2008).

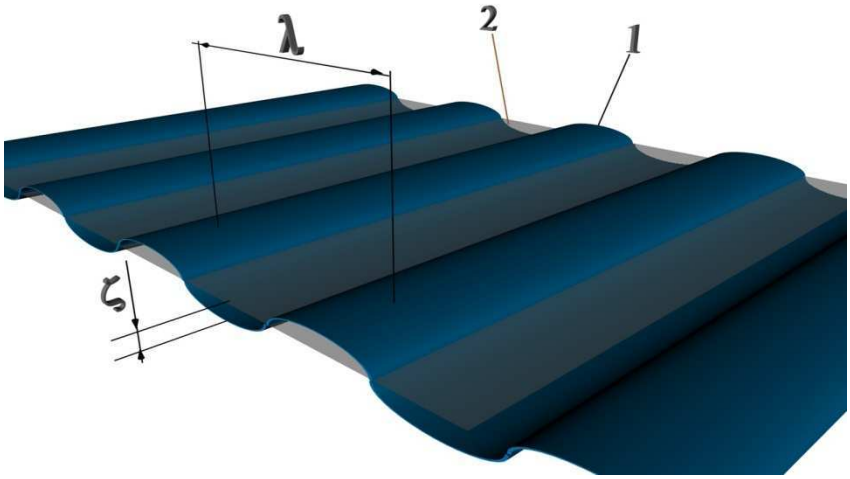

Figure 2.3: Schematic view of the surface of the liquid body. (1): non deflected plane liquid surface with constant intensity of electric field $\vec{E}_0$ *and (2): deflected liquid body by the electric field of intensity* $\vec{E}_\zeta$ *where* ζ *is an amplitude and* λ *is a wavelength of the deflected surface.*

One can implement two compounds of electric field of this system for the purpose of electrospinning description. First $\vec{E}_0$ is the field of stable surface of the liquid, and $\vec{E}_\zeta$ denotes the field on a wavy surface. Therefore the total field strength is a sum of both compounds (see Fig. 2.3). So the formula (2.15) can be rewritten as:

$$p_e = \frac{1}{2}\varepsilon_0 \cdot (\vec{E}_0 + \vec{E}_\zeta)^2 = \frac{1}{2}\varepsilon_0 (\vec{E}_0^{\,2} + 2\vec{E}_0\vec{E}_\zeta + \vec{E}_\zeta^{\,2}) \cong$$
$$\cong \frac{1}{2}\varepsilon_0 (\vec{E}_0^{\,2} + 2\vec{E}_0\vec{E}_\zeta). \qquad (2.20)$$

Since $\vec{E}_\zeta << \vec{E}_0$, $\vec{E}_\zeta^{\,2}$ can be neglected in equation (2.20). It is necessary to impose formulas for electrostatic potentials due to their dependency on wave deflection.

Because $E_\zeta = -\partial\varphi_\zeta / \partial\zeta$, therefore:

$$\vec{E}_\zeta = k \cdot \vec{E}_0 \cdot \zeta \qquad (2.21)$$

With this result one can write formula (2.20) as:

$$p_e = \frac{1}{2}\varepsilon_0 \cdot \vec{E}_0^{\,2} + \varepsilon_0 \cdot k \cdot \vec{E}_0^{\,2} \cdot \zeta \qquad (2.22)$$

Only the second part of formula (2.22) is time dependant, $\zeta = \zeta(x,t)$.

2.5 Electrostatic field of capacitors

A brief decryption of electric forces acting on ideally conductive liquid surface was done in previous chapter. Real materials used for electrospinning are not ideally conductive. It is necessary to start with description of capacitors before the inclusion of nonconductive liquids. The simplest example is plate capacitor (two oppositely charged plates with distance d between them) with various materials between electrodes. Geometry of such a capacitor is sketched in Fig. 2.4.

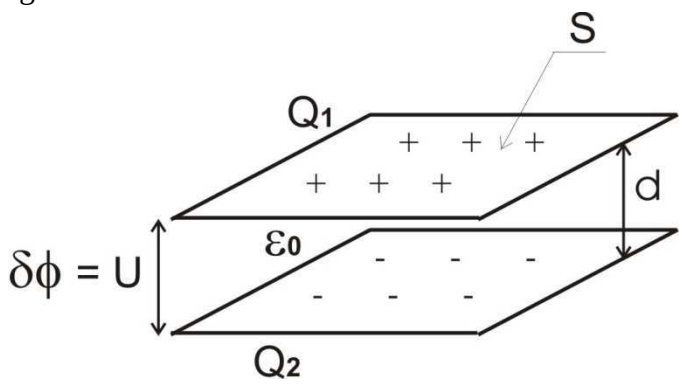

Fig. 2.4: A sketch of a simple capacitor with vacuum between electrodes. Q_1 =- Q_2 are charges of electrodes; d is a distance between them; ε_0 is a permittivity of vacuum and U is a voltage which is equal to the potential difference.

Intensity of electrostatic field for vacuum can be expressed as $E = \sigma / \varepsilon_0$ where σ is a surface charge density. Capacity *C* of the plate capacitor with vacuum can be therefore calculated by simple formula:

$$C = \frac{Q}{U} = \frac{\sigma S}{\frac{\sigma}{\varepsilon_0} \cdot d} = \frac{\varepsilon_0 S}{d}, \qquad (2.23)$$

where capacity *C* is an ability to store electrical charge with unit called Farad [F=C/V]. Capacity of the plate capacitor without any material between capacitor plates depends only on its geometry, i.e. on the distance between plates *d* and surface *S*. A question now is how some another material affect capacity of the capacitor inserted between its electrodes. If a conductive material of a thickness *b* is added between electrodes, the charges will immediately move to the edges of the inserted element. This is because charge inside the conductors is transferred by electrons which can travel in conductive zone freely. Capacity will therefore be:

$$C = \frac{\varepsilon_0 S}{d-b} = \frac{\varepsilon_0 S}{d(1-b/d)} = \varepsilon_r \frac{\varepsilon_0 S}{d}, \tag{2.24}$$

where ε_r is relative permittivity and for metals $\varepsilon_r \to \infty$ when $b \to d$. One can see that capacity will increase. It is not very surprising, because if we decrease distance between electrodes, the capacity will automatically increase.

Another situation occurs when dielectric material is added in between the electrodes, instead of a conductor. Dielectrics can be polarized by application of external electric field. It simply means that it starts to form dipoles which are then formed as a response to the polarity of external electric field. The reason for it is that the nucleus of each atom is slightly moved from its central position or the trajectories of the electrons are deformed. Such an example can be seen in Fig. 2.5b.

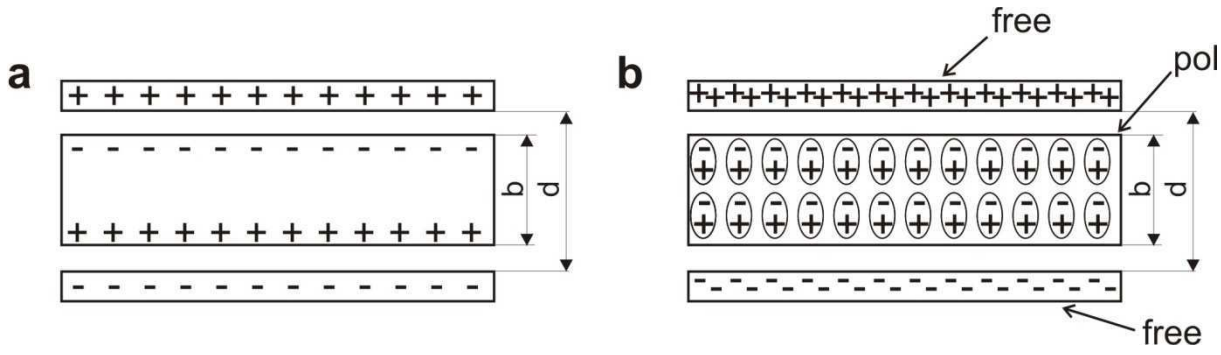

Fig. 2.5: Capacitors with different materials added between its electrodes. (a) conductor, (b) dielectric.

The same happened for liquids which are dielectrics. Already known free charge density σ_{free} is on the surface of the electrodes without any dielectric. Another polarized charge density σ_{pol} has to be considered inside the dielectrics. Intensity of electrostatic field will therefore be:

$$E = \frac{\sigma_{free} - \sigma_{pol}}{\varepsilon_0} = \frac{\sigma_{free} - \chi\varepsilon_0 E}{\varepsilon_0} = \frac{\sigma_{free}}{\varepsilon_0(1+\chi)} = \frac{\sigma_{free}}{\varepsilon_0\varepsilon_r}, \tag{2.25}$$

where χ is electric susceptibility and ε_r is already mentioned relative permittivity, which is an important quality determining material's electric parameters. More detailed study of such problem can be found in chapter 10 and 11 of Vol II written by Feynman (1971).

2.6 Electric field in fluid dielectrics

Anyway, it is useful regarding to electrospinning, to have a brief look how the electric field affects molecules inside a liquid dielectrics. Clausius (1849) and Mossoti (1850) found a relation for non-polar liquids and Onsager (1936) upgraded this formula for weakly polar liquids.

Due to the explanation of theory of electrospinning, it is convenient to find the formula for electrostatic pressure including the dielectric parameters of the liquid. One can start with the definition of Maxwell stress tensor which for dielectrics in absence of magnetic field has a form:

$$\tau_{ik} = -P_0(\rho_m, T)\delta_{ik} - \frac{\varepsilon_0 E^2}{2}\left[\varepsilon_r - \rho_m\left(\frac{\partial \varepsilon_r}{\partial \rho_m}\right)_T\right]\delta_{ik} + \varepsilon_0 \varepsilon_r E_i E_k , \qquad (2.26)$$

where δ_{ik} is Kronecker's delta and P_0 is the pressure in the medium in the absence of electric field, ρ_m is the mass density and T is the temperature. Its complete derivation is not the main topic of this work. It was done by Landau (1960) in chapter 15 and Griffiths (1999) showed derivation of this formula in vacuum. Anyway Maxwell stress tensor is the general formula for all forms of matter. It is convenient for liquids to find the formula for volume density of the electric force acting on the fluid: $\vec{f} = \vec{F} / dV$. One can use well known formula giving the volume forces in terms of the stress tensor: $f_i = \partial \sigma_{ik} / \partial x_k$. According to Helmholtz (1868) we can get known formula:

$$\vec{f} = -\vec{\nabla} P_0(\rho_m, T) + \frac{\varepsilon_0}{2}\vec{\nabla}\left[\vec{E}^2 \rho_m\left(\frac{\partial \varepsilon_r}{\partial \rho_m}\right)_T\right] - \frac{\varepsilon_0}{2}\vec{E}^2\vec{\nabla}\varepsilon_r . \qquad (2.27)$$

Its detailed derivation can be found in Landau's (1960) book in paragraph 15 or Abraham and Becker (1932).

Relative permittivity is a function only of ρ_m and T , and its gradient can therefore be written as $\vec{\nabla}\varepsilon_r = \left(\partial \varepsilon_r / \partial T\right)_\rho \vec{\nabla} T + \left(\partial \varepsilon_r / \partial \rho_m\right)_T \vec{\nabla}\rho_m$ and for uncompressible liquids and for constant temperature, the formula (2.28) can be simplified:

$$\vec{f} = -\vec{\nabla} P_0(\rho_m, T) + \frac{\varepsilon_0}{2}\rho_m\vec{\nabla}\left[\vec{E}^2\left(\frac{\partial \varepsilon_r}{\partial \rho_m}\right)_T\right]. \qquad (2.28)$$

It is now easy to find the formula for electrostatic pressure and one can focus only on its electric part.

Formula for electrostatic pressure of ideally conductive materials was evolved in chapter 2.4. Let focus on the polarization of dielectrics in external electric field. The formula for the pressure in dielectric liquids was evolved by Abraham and Becker (1932). They determined the excess of electrical pressure Δp_e. By choosing of two points and one of the points as a base with zero electric field and obtained:

$$\frac{\Delta p_e}{\rho_m} = \int_{pe0}^{pe} \frac{dp_e}{\rho_m} = \frac{1}{2}\varepsilon_0 \vec{E}^2 \frac{\partial \varepsilon_r}{\partial \rho_m},$$

or, if the dielectric has a weak compressibility:

$$\Delta p_e = p_e - p_{e0} = \frac{1}{2}\varepsilon_0 \vec{E}^2 \frac{\partial \varepsilon_r}{\partial \rho_m}\rho_m. \tag{2.29}$$

So the formula for electrostatic pressure can be simply written as:

$$p_e = \frac{\varepsilon_0 \vec{E}^2}{2}\rho_m \left(\frac{\partial \varepsilon_r}{\partial \rho_m}\right)_T. \tag{2.30}$$

One can compare equation (2.30) with previously obtained formula (2.22) for electrostatic pressure of ideally conductive materials. It is necessary to find dependency of relative permittivity on mass density of the liquid.

2.6.1 Clausius-Mossotti relation

As was mentioned at the beginning of this chapter, relation for nonpolar liquids was firstly found by Clausius (1849) and Mossoti (1850). We assume that each molecule inside the external electric field with intensity $\vec{E}$ has a dipole moment equal to:

$$\vec{p} = \alpha \varepsilon_0 \vec{E}, \tag{2.31}$$

where α is a polarizability of molecule. The polarization $\vec{P}$ for several molecules with number density N can be found as

$$\vec{P} = N\vec{p} = N\alpha\varepsilon_0\vec{E} = \frac{N_A \rho_m \alpha}{M}\varepsilon_0 \vec{E}, \tag{2.32}$$

for medium with mass density ρ_m and molecular weight M, where N_A is the Avogadro's number. It is important to find how electric field is experienced by an individual molecule relative to the average electric field in the medium. Suppose that dielectrics are polarized by uniform external electric field $\vec{E}_0$ which is directed along the z-axis. To establish boundary between macroscopic and microscopic range of phenomena affecting the molecule, one has to

find a sphere of a radius a around this particular molecule. Outside this sphere, the dielectrics are considered as continuous medium and inside the sphere the dielectrics is a collection of polarized molecules. The polarized charge σ_{pol} on the surface of the sphere in spherical polar coordinates is:

$$\sigma_{pol} = -P\cos\theta . \tag{2.33}$$

This formula can be used to calculate magnitude of the electric field in *z*-axis E_z at the molecule with surface element of the sphere $dS = 2\pi a^2 \sin\theta d\theta$:

$$E_z = -\frac{1}{4\pi\varepsilon_0}\int \frac{\sigma_{pol}\cos\theta}{a^2} ds = \frac{P}{2\varepsilon_0}\int_0^{\pi} \cos^2\theta \sin\theta d\theta = \frac{P}{3\varepsilon_0} . \tag{2.34}$$

It can be easily demonstrated, that $E_\theta = E_\varphi = 0$ and therefore the electric filed at the molecule will be only its *z* part, due to the chosen direction of our coordinating spherical system (z, θ, φ) with respect to the external electric field in *z*-axis:

$$E_z = \frac{P}{3\varepsilon_0} . \tag{2.35}$$

So the intensity of the electric field seen by the individual molecule will therefore be a sum of the intensity $\vec{E}_0$ and the intensity generated by its surface charge density (2.35):

$$\vec{E} = \vec{E}_0 + \frac{\vec{P}}{3\varepsilon_0} . \tag{2.36}$$

By the combination of the definition of polarization $\vec{P} = \varepsilon_0(\varepsilon_r - 1)\vec{E}_0$ (see Feynman 1971) and formulas (2.32) and (2.36), one can obtain:

$$\frac{\varepsilon_r - 1}{\varepsilon_r + 2} = \frac{N_A \rho_m \alpha}{3M} , \tag{2.37}$$

which is the well known Clausius-Mossotti relation. But it is obvious that one has to find partial derivative of relative permittivity with respect to the mass density of the liquid, which is necessary for finding of the formula for electrostatic pressure (2.30):

$$\frac{d\varepsilon_r}{d\rho} = \frac{(\varepsilon_r - 1)(\varepsilon_r + 2)}{3\rho} , \tag{2.38}$$

detailed mathematical operations can be found in appendix A3. Another way how to obtain Clausius-Mossotti relation was done by Feynman (1971) or by Kittel (1963). Feynman used indexes of refraction instead the relative permittivity because the square root of index of

refraction of some material is equal to its relative permittivity. His expression of Clausius-Mossotti formula is:

$$\frac{n^2-1}{n^2+2}=\frac{N_A\rho_m\alpha}{3M}, \tag{2.39}$$

but the Clausius-Mossoti relation works only for non-polar liquids; therefore Onsager (1936) developed another theory which includes weakly polar liquids.

2.6.2 Onsager relation

Formula for dielectric constants of pure polar liquids can be according to Onsager (1936) expressed:

$$\frac{(\varepsilon_r-n^2)(2\varepsilon_r+n^2)}{\varepsilon_r}=\frac{N_A\rho_m\alpha}{3M}, \tag{2.40}$$

and one can see the difference between Clausius-Mossoti and Onsager relations. But for the same reason, it is convenient to find the partial derivative of relative permittivity with respect to the mass density of the liquid :

$$\frac{d\varepsilon_r}{d\rho_m}=\frac{\varepsilon_r(\varepsilon_r-n^2)(2\varepsilon_r+n^2)}{[2(\varepsilon_r)^2+n^4]\rho_m}\ . \tag{2.41}$$

Both relations for non polar a weakly polar liquids have been sufficiently verified in practice by Hakim and Higham (1962).

2.6.3 Electric pressure in dielectric liquids

With using of Clausius-Mossotti and Onsager relations for non polar and weakly polar liquids, one can find the formula of electrostatic pressure in this media. The dependence on mass density was already determined in previous part of this chapter. So one can now easily find the formula in the range of validity of Clausius-Mossotti approach:

$$\Delta p_{CM}=\frac{1}{2}\varepsilon_0\vec{E}^2\frac{(\varepsilon_r-1)(\varepsilon_r+2)}{3}, \tag{2.42}$$

and according to Onsager:

$$\Delta p_e=\frac{1}{2}\varepsilon_0\vec{E}^2\frac{\varepsilon_r(\varepsilon_r-n^2)(2\varepsilon_r+n^2)}{[2(\varepsilon_r)^2+n^4]} \tag{2.43}$$

Both formulas for electrostatic pressure will be used for dispersion laws and then analyzed in chapter 4 which will help to describe behavior of needle-less electrospinning of dielectric liquids.

2.7 Asymmetric capacitors

Understanding of electrostatic field around nanofibres requires solutions of the first Maxwell's equation (2.6), (2.7) for basic alignments of ideally conductive cylinders with finite radius. Some examples will be solved and these solutions will be useful for the theory of electrospinning or for explanation of radiation phenomenon.

Example E.1: The cylinder between two parallel plates.

The first example will be very useful for explanation of electrospinning device called Nanospider. It is the asymmetric capacitor consisting a plan parallel infinite and ideally conductive cylinder and a plate with distance *h* between them. To simplify this problem one can use the method of charge mirroring and imagine another plate of the same distance from the cylinder as upper plate to make the symmetric capacitor. Field lines in the middle of the capacitor have to be perpendicular to both plates. This alignment can be seen in Fig E1. It is convenient to use cylindrical coordinates due to the cylindrical shape of our fiber.

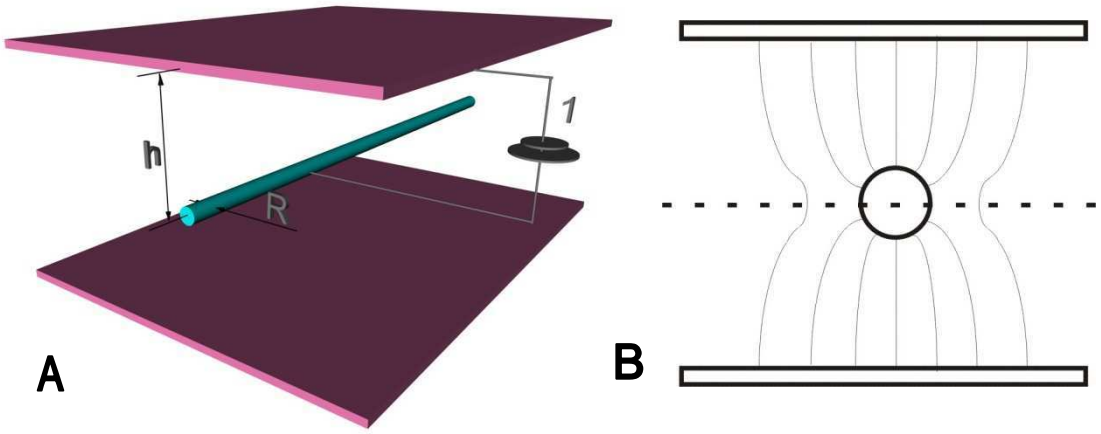

Figure E1: Two plan parallel plates with electric field and an infinite ideally conductive cylinder, heaving a diameter R. The distance h from the cylinder is the same to the upper as well as lower plate. (A) Three dimensional sketch; (B) Cross-section with the schematic view of electrostatic field lines.

Laplace of electrostatic potential in cylindrical coordinates has a form (see Fig.: E2B)

$$\Delta\varphi = \frac{1}{r}\frac{1}{\partial r}\left(r\frac{\partial\varphi}{\partial r}\right) + \frac{1}{r^2}\frac{\partial^2\varphi}{\partial^2\Theta} + \frac{\partial^2\varphi}{\partial^2 z}. \qquad \text{(E1.1)}$$

The cylinder as assumed has infinity length and therefore $\partial^2\varphi\big/\partial z^2$ is equal to zero. For more details about cylindrical and spherical coordinate systems see Appendix A1,A2.

Electric potential is constant everywhere on the surface of the cylinder, because it is equal to the potential on the surface of the conductive cylinder induced by the external electric field $\vec{E}$

$$\varphi = const\cdot\frac{\vec{E}\vec{r}\cdot\cos\theta}{r^2}. \qquad \text{(E1.2)}$$

The Laplace's equation $\Delta\varphi = 0$ has to be valid for places without any charge. It proves that potential is constant everywhere on the surface of conductive cylinder and is zero for $r\to\infty$: $\lim_{r\to\infty}\varphi = 0$. Potential everywhere outside the cylinder is a function of the distance from the center of the cylinder only: $\varphi_2 = -\vec{E}\vec{r}$. A joint intensity of electric filed will be a sum of its contribution from the surface charge of the cylinder and its external part: $\vec{E} = \vec{E}_{cylinder} + \vec{E}_{external}$. The Maxwell equation can be now rewritten as a potential difference

$$\Delta\varphi = const\frac{\vec{E}\vec{r}}{r^2}\bigg|_{r=R} - \vec{E}\vec{r}\big|_{r=R} = const\cdot\frac{ER\cos\Theta}{R^2} - ER\cos\Theta = 0, \qquad \text{(E1.3)}$$

where first part is equal to φ_1 and second part is equal to φ_2 for both sides. It is obvious from equation (E1.3) that $const = R^2$ and therefore one can find following result:

$$\varphi = -\vec{E}\vec{r}\cos\Theta\left(1-\frac{R^2}{r^2}\right). \qquad \text{(E1.4)}$$

So the general intensity of electric filed on the surface of ideally conductive cylinder can be found:

$$\vec{E}_{general} = -\frac{\partial\varphi}{\partial r}\bigg|_{r=R} = -\frac{\partial}{\partial r}\left[-\vec{E}r\cos\Theta\left(1-\frac{R^2}{r^2}\right)\right]\bigg|_{r=R} = 2\vec{E}\cos\Theta \qquad \text{(E1.5)}$$

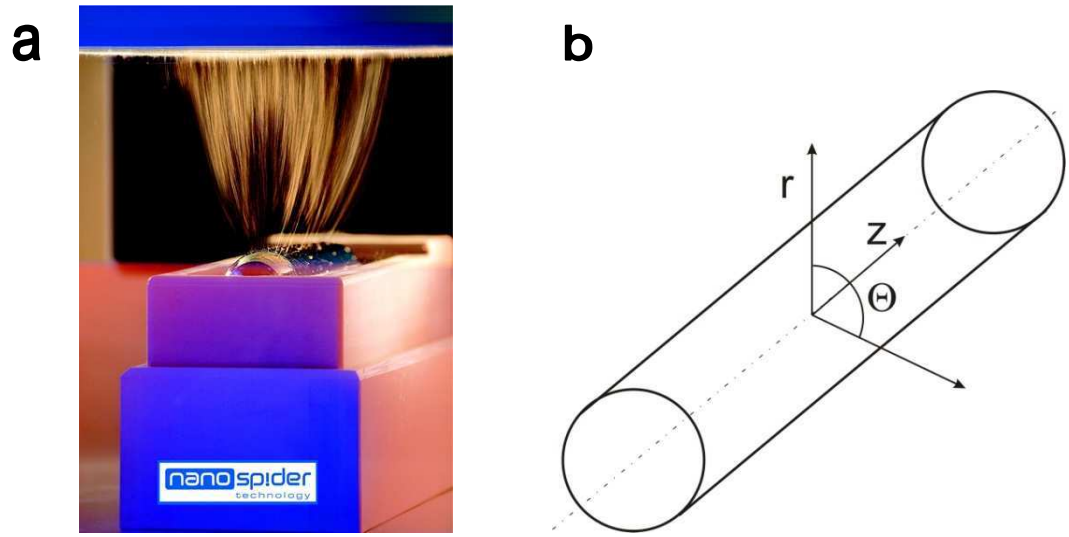

Figure E2: (a) Nanospider technology. One can see the wide area where Taylor cones are created (figure by Elmarco Company), (b) cylindrical coordinates of cylinder (fiber).

The equation (E1.5) plays a crucial role for the explanation of needleless electrospinner based on the cylinder and called Nanospider technology introduced by Jirsak et.al. (2005). Its picture can be seen in Fig E2a. This theory is in a good agreement with the experimental observations. It predicts existence of very small variations of intensity of electric field on the top of the cylinder and its independency on the radius of the cylinder. Example is solved with the presumption that the cylinder is in its half dived in the liquid. A qualitative demonstration of theory/experiment conformation can be seen on Fig E2a where one can observe the creation of Taylor cones in quite wide surface area of the cylinder.

Example E2: Electric field between two plan parallel tubes

This example demonstrates the electric field between two parallel cylinders. Such situation is sketched in Fig. E3 with all geometries. This example is important for an understating of whipping zone in electrospinning and electric field between deposited pairs of nanofibres. However there are more deposited nanofibres in a real situation. It will be necessary to use some numerical methods to solve such an general situation. This example is useful for knowledge of charge distribution between a pair of parallel fibers.

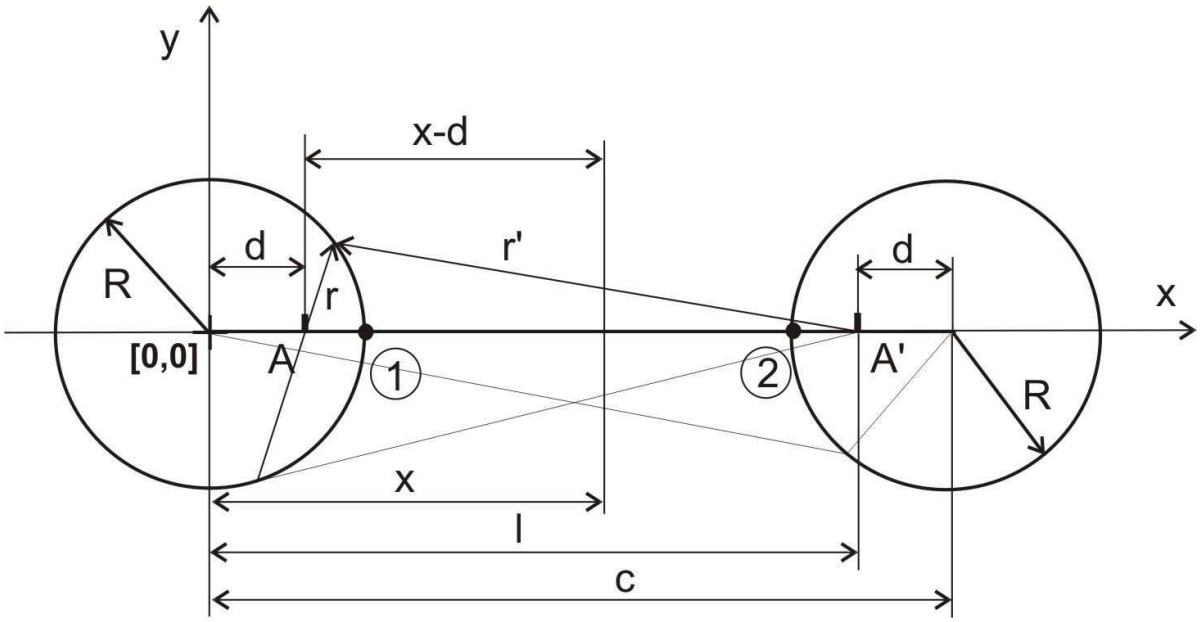

Figure E3: Two parallel nanofibres in the distance c heaving radii R and infinite lengths as a Apollonian circles.

Electric potential of these two cylinders has to be constant on their surfaces and they can be approximated as conducted "threads" heaving positions in points A and A'. These threads are unbalanced by Coulombic force from their centers when an external electric field is applied. The distance between unbalanced positions is here denoted as *d*. These "threads" are sketched as points A and A' in Fig.: E3. Electric potential of infinitely long cylinder can be calculated by Gauss-Ostrogradsky theorem of electrostatics: $\oint \vec{E} d\vec{f} = Q/\varepsilon_0$, where electric field is orthogonal to the surface of the cylinder. Therefore $\oint \vec{E} d\vec{f} = E 2\pi r L = eL/\varepsilon_0$, where L is the length of the cylinder. General electric potential φ is then sum of contributions form points A and A':

$$\varphi = \frac{e}{\varepsilon_0 2\pi}(\ln r - \ln r') = \frac{e}{\varepsilon_0 2\pi}\ln\frac{r}{r'} \quad . \qquad \text{(E2.1)}$$

We have to find a points where the ratio of r/r' is constant. It can be represented by Apollonius circles (fig.: E3). One can find that the radius of the cylinder R can be expressed as a function of the distance of charge from the center of the cylinder d and the distance from the centre of the next cylinder to the charge l as: $R^2 = d \cdot l = d \cdot (c - d)$ and the distance d is:

$$d = \frac{c - \sqrt{c^2 - 4R^2}}{R} \qquad \text{(E2.2)}$$

For simplicity we choose points (1) and (2).

$$U = \varphi\big|_{x=R} - \varphi\big|_{x=c-R} = \frac{e}{2\pi\varepsilon_0}\left[\ln\frac{R-d}{c-r-d} - \ln\frac{c-R-d}{R-d}\right] = \\ = \frac{e}{2\pi\varepsilon_0}\ln\left[\frac{R-d}{c-r-d}\right]^2 \tag{E2.3}$$

The scope of our interest is not the voltage, but the electric field. Firstly we have to find a formula for charge *e* on the cylinder:

$$e = 2\pi\varepsilon_0 U \cdot \ln\left[\frac{(c-R-d)}{(R-d)}\right]^{-2} \tag{E2.4}$$

After some mathematical manipulations one can find result for the field strength on the cylinder surface

$$E = -\frac{\partial\varphi}{\partial x}\bigg|_{x=R} = \frac{U}{2R}\cdot\sqrt{\frac{1+2\beta}{1-2\beta}}\cdot\left[\ln\left(\frac{2\beta-1+\sqrt{1-4\beta^2}}{1-2\beta+\sqrt{1-4\beta^2}}\right)\right]^{-1} \tag{E2.5}$$

where $\beta = R/c$.

Example E3: Asymmetric capacitor consisting of a large plate and a plan parallel cylinder.

Our next example is important for the explanation of a radiation phenomenon occurred during electrospinning. It is the first step how to explain extremely high values of intensity of electrostatic field in a vicinity of nanofibres. To solve such an example, it is convenient to use the method of mirror charges. This simply means to imagine another infinite cylinder with the same radius placed in the same distance on the other side of the plate. (see Fig. E4 and E5). Electric field lines have to be orthogonal to the central plate.

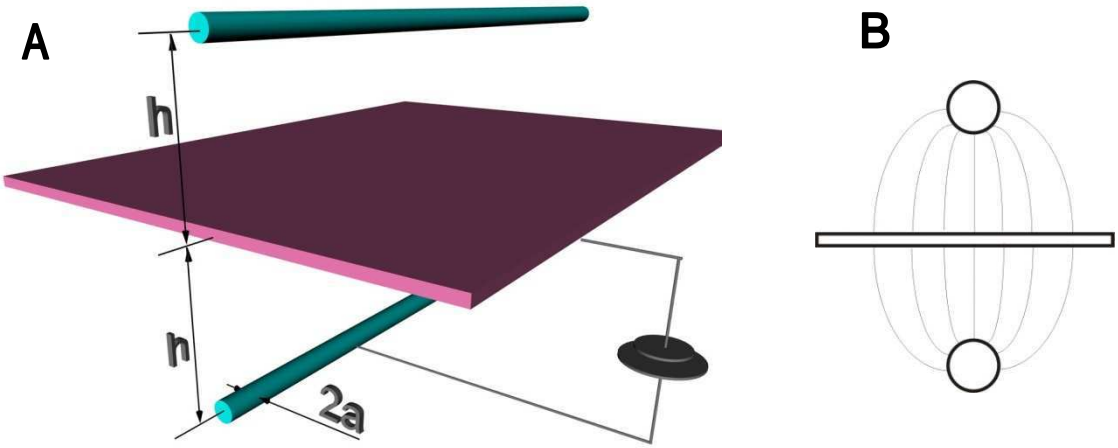

Figure E4: (A) The ideally conductive infinite cylinder and plan parallel plate forming an asymmetric capacitor. The upper cylinder represents method of mirror charges; (B) Electric field lines between two parallel cylinders after the application of the method of mirror charges.

Electric potential on the surface of the cylinder is constant. One can use Gauss formula of electrostatics: $\oint \vec{E} d\vec{f} = Q / \varepsilon_0$, where Q is a charge on the cylinder and ε_0 is the permittivity of vacuum. The intensity of electric field in the distance *R* from the fiber axis of such example is: $E = \tau / 2\varepsilon_0 \pi R$, where τ is the linear charge density. Electric potential can be simply calculated by the integration of intensity of electric field:

$$\varphi = -\frac{\tau}{2\varepsilon_0 \pi} \ln R . \qquad \text{(E3.1)}$$

Mathematical operations to get formula E3.1 are the same as for formula E2.1 in previous example. The simplest example of charge distribution along the fiber is homogenous when the fiber is infinite. So it is convenient to use the linear charge density as $-\tau$ or $+\tau$. Both fibers have the same radius a and they are separated by the distance $2h$. Electric charges are supposed to be localized along fiber axes, since we suppose that $h >> a$. A sketch of such an example can be clearly seen in Fig E5.

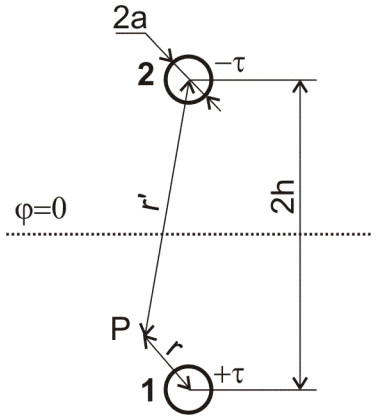

Figure. E5: A cross-section of two parallel perfectly cylindrical fibres of equal radii a: The distance between fibres is 2h. Fibres are uniformly charged with linear charge densities $+\tau$ and $-\tau$.

According to this example, the joint potential $\varphi = \varphi_1 + \varphi_2$ heaving zero value on the plane, has a shape:

$$\varphi(r) = \varphi_1(r) + \varphi_2(r') = \frac{\tau}{2\pi\varepsilon_0}\ln\left(\frac{r'}{r}\right). \tag{E3.2}$$

The potential difference between fibers is:

$$U = \varphi_1(a) - \varphi_2(2h) = \frac{\tau}{2\pi\varepsilon_0}\left[\ln\left(\frac{2h}{a}\right) - \ln\left(\frac{a}{2h}\right)\right] = \frac{\tau}{\pi\varepsilon_0}\ln\left(\frac{2h}{a}\right). \tag{E3.3}$$

The field strength on the surface of the cylinder can be simply calculated as

$$\vec{E}(r)\Big|_{r=a} = -\nabla\varphi(r)\Big|_{r=a} \cong \frac{\tau}{2\pi\varepsilon_0}\frac{\partial}{\partial r}\ln\left(\frac{2h}{r}\right)\Big|_{r=a} = \frac{\tau}{2\pi\varepsilon_0}\frac{1}{a}. \tag{E3.4}$$

It is easy to find the expression for linear charge density from (E3.3) and to combine it with (E3.4). One can simply find the dependence of $\vec{E}$ on U and a

$$E(a) = \frac{U}{2\ln(2h/a)}\frac{1}{a}. \tag{E3.5}$$

Denoting E_0 as the field intensity inside a plate capacitor with voltage $U' = U/2$ and distance *h* between plates, i.e. $E_0 = U'/h = U/2h$, the Equation (E3.5) can be rewritten as

$$\frac{E(a)}{E_0} = \frac{h/a}{\ln(2h/a)} = \frac{\xi}{\ln 2\xi} = Z_1 \tag{E3.6}$$

Where $\xi = h/a$ is a dimensionless distance between the tube and the plate and Z_1 is the amplifying factor. This field strength estimation has validity for $a << h$ only.

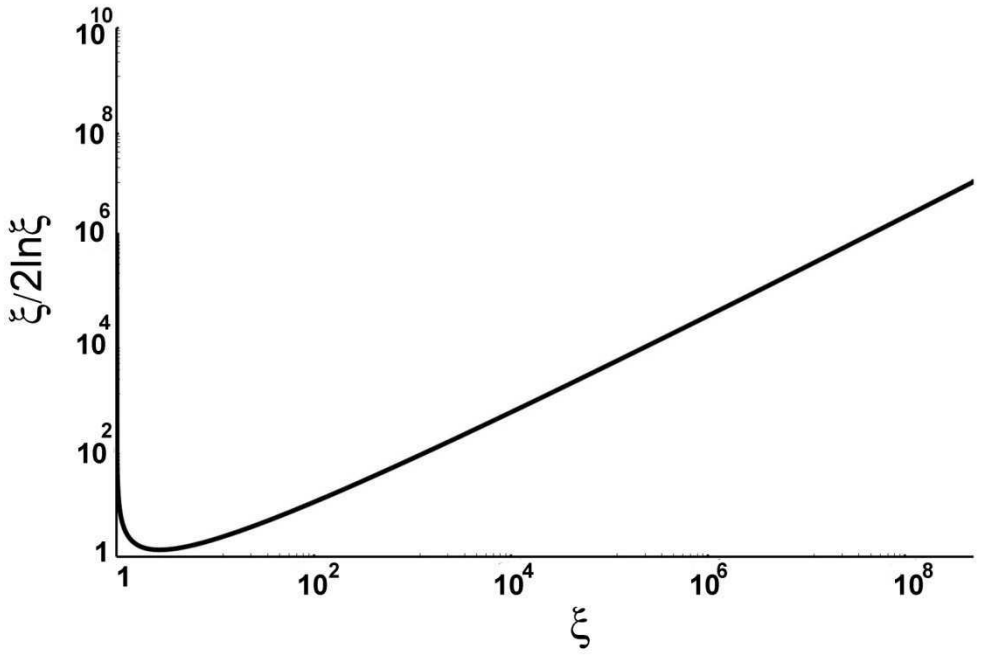

Figure E6: The logarithmic plot of the 'amplifying factor' $\xi / 2\ln\xi$ on the dimensionless distance ξ between the fibre and the plate.

Analysis of (E3.6) shows us an increase of the field strength with increasing amplifying factor Z_1. This is an important result for our nanofibre's applications, because typical diameter of nanofibres is in interval from 10^{-7} to 10^{-9} m. For classical electrospinning setup as it is sketched in Fig. E31, the distance between electrodes h is usually $10^{-1}m$ and the diameter of the nanofibre a can go down to $5\cdot10^{-8}m$. The amplifying factor Z_1 for this setup is $1.3\cdot10^5$. The reference field strength value E_0, for the used voltage of 3×10^4 V, is 3×10^5 V/m. Therefore the maximum field strength E_1 is estimated as 39 GV/m, which corresponds to the theoretical local surface charge density σ reaching the value $\sigma_1 = \varepsilon_0 E_1 =$ 0.35 Cm^{-2} and linear charge density $\tau_1 = \pi\varepsilon_0 U / \ln(2\xi) = 5.5\times10^{-8}$ C/m for conductive fibers. This calculation is valid only for single ideally conductive parallel fiber. In real situation there is not only single fiber but bunches of them. It is therefore important to find the solution for several parallel fibers.

Example E4 Asymmetric capacitor composed of a plate and a warp of parallel and equidistant fibers

The last example, which will be solved here is a warp-like pattern of fibers with constant neighbor to neighbor distance and equal diameters forming one electrode of an asymmetric capacitor having a plate as a counter electrode. It is the more general case of the example E3. Schematic view of such capacitor can be seen in Fig. E7.

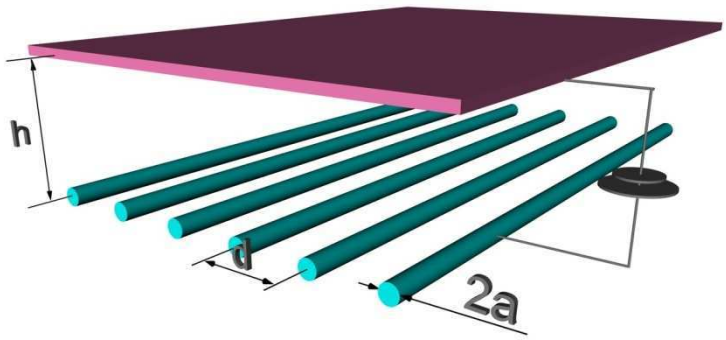

Figure E7. The asymmetric capacitor composed of a warp of parallel and equidistant nanofibres with a spacing d between neighbouring ones.

This example has to be solved by the same method as the previous one (method of charge mirroring) see Fig E8.

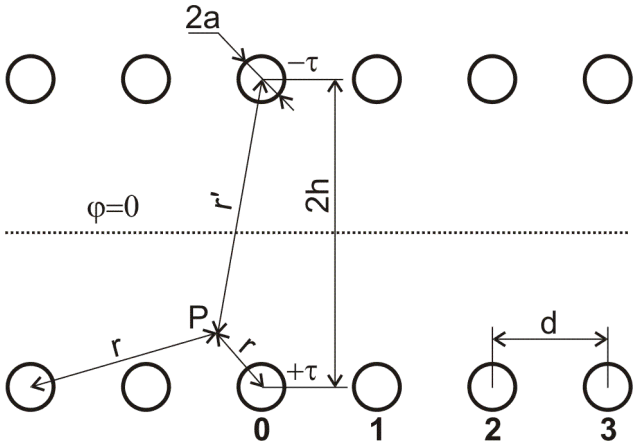

Figure E8: Two parallel and equidistant warps of cylindrical fibres: Each warp is planar with distance d between neighbouring fibres. The distance between planar warps is 2h. Fibres in the upper warp have a linear charge density $-\tau$ while lower warp fibres are charged to a charge density $+\tau$. Fibres are assigned to subsequent integer numbers with the origin of their counting in the "0" fibre.

It is not so trivial and one can find the way of solution in appendix A4 and only the solution will be sowed here. The amplifying factor Z_w is governed by a dimensionless distance $\rho = d/a$ in the case that $h >> d >> a$, and is approximately independent on h

$$\frac{E_w}{E_0} \cong \frac{\rho}{2\pi} = Z_w, \qquad \text{(E4.1)}$$

where E_W is the maximal field strength value on a surface of one of the warp fibers and E_0 is the field strength in a plate capacitor with distance between plates *h* and with voltage $U' = U/2$. Estimating the maximal inter-fiber distance *d* in a real electrospinning jet as 0.1 mm, one obtains $\rho = 2\times10^3$ and amplifying factor as $Z_W \cong 3.2\times10^2$. The maximum field strength E_W is estimated as 0.095 GV/m and linear charge density as $\tau_W \cong \pi\varepsilon_0 U/(2\pi\zeta) = 1.3\times10^{-9}$ C/m for conductive fibers, where $\zeta = h/d$. The predicted field strength enables electrons and ions, having the elementary charge *e*, to reach over the distance of 100 nm a kinetic energy W_W about 0.0095 keV, which is about three orders less than the maximal X-ray energy in measured spectra. The dependence of the amplifying factor Z_W for a warp on *a* and previously chosen *d* value is plotted in Fig. E9. This effect of neighboring fibers completely erases the decay of field potential caused by grouping of nanofibers into warps.

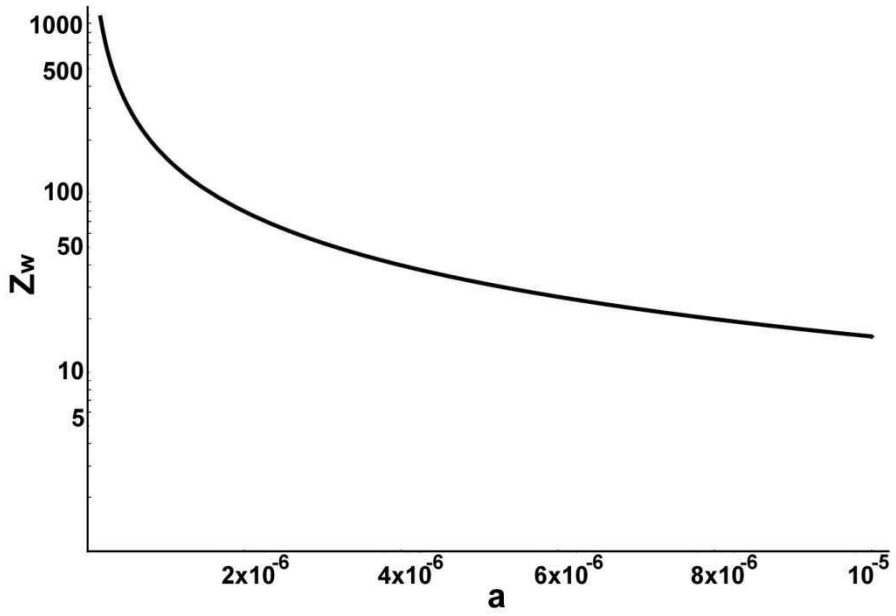

Figure E9: The Relationship between a field strength amplifying factor Z_W and a fibre radius a: Field strength E on a fibre surface is calculated for the following parameter values: $a=10^{-7}$m, $h=10^{-1}$m, $U=3\ 10^4$V, $d=10^{-3}$m.

3. Basics of hydrodynamics

There is another important part of physics for development of the theory of electrospinning. Due to the reason that nanofibers are made of polymeric solutions forming jets, it is necessary to have a basic knowledge of hydrodynamics. This part is based mainly on Landau's (1959a) course of fluid dynamics. Another introduction to hydrodynamics was done by Feynman (1971) in his Lectures on Physics or by Kundu and Cohen (2002). Here, some basic ideas, necessary for the understanding of electrospinning phenomena description, will be explained.

3.1 The equation of continuity

The problem of explanation of fluids movement by the standard way is in impossibility of using of macroscopic (Newton's) description as well as the corpuscular one. One has to use the theory of continuity which was first advanced by Georg Cantor (1877). Cantor was a mathematician and his description of a continuum was: "*There is no set whose cardinality is strictly between that of the integers and that of the real numbers.*"
In fluid dynamics, the molecules of the fluid collide with each other's and with solid objects. One way to look at fluids is to use the particle description. Fluids are consisted from many small molecules. Their description by particular movements of all these small molecules will be impossible without powerful computers. Due to the effort of finding a fundamental description of fluid dynamics, the theory of continuity was implemented. The theory describes fluids as small elementary volumes which still are consisted of many elementary particles. But the drift speed of the fluid does not belong to these elementary volumes but to the movement of their molecules/particles. To make the calculation of the drift speed of the fluid possible by analytical way, the movement of molecules has not to be considered. One can see an example of this volume and its flow in Fig.3.1.
A modern discipline how to consider individual molecules in the calculations is called computational fluid dynamics. It uses numerical methods and algorithms to solve and analyze problems by usage of modern computers. But in this chapter the classical analytical theory of continuum is used.

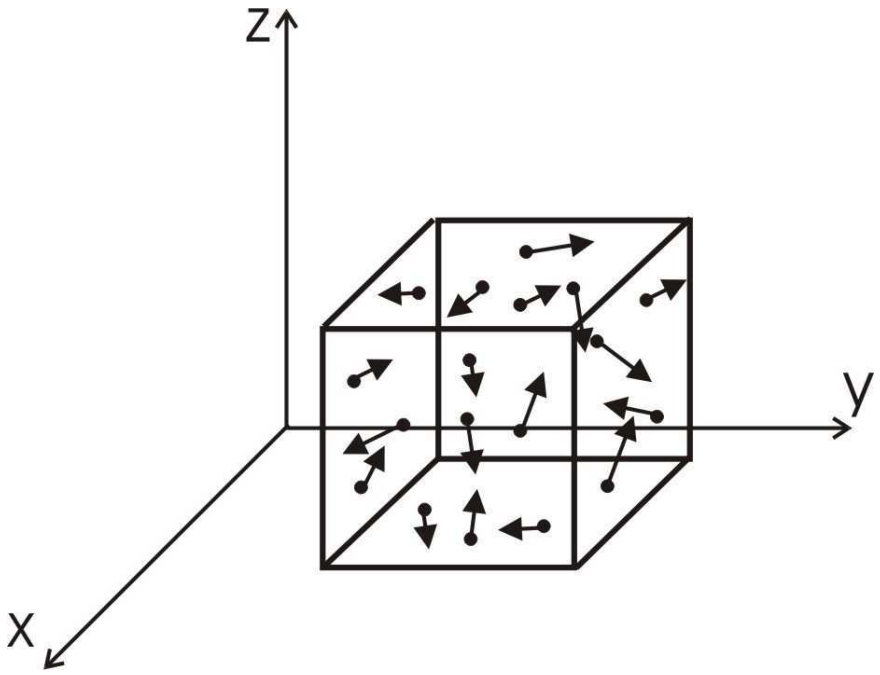

Fig. 3.1: Elementary volume V_0 containing constantly moving particles. This volume is infinitesimally small but still much bigger compare to the size of the particles. There are many particles inside the elementary volume.

A total fluid flux from boundaries of a volume V_0, is equal to the change of the fluid mass inside the volume V_0. This can be expressed by the formula:

$$\frac{\partial}{\partial t}\int_V \rho_m \vec{v}\, dV - \oint \rho_m \vec{v}\, d\vec{f}\,, \tag{3.1}$$

where ρ_m is a mass density, $\vec{v}$ is a velocity of the fluid and $d\vec{f}$ is vector of the surface area element. By applying of known Green's / Gauss formula $\oint \rho_m \vec{v} d\vec{f} = \int div(\rho_m \vec{v}) dV$, one obtains

$$\int [\frac{\partial \rho_m}{\partial t} + div(\rho_m \vec{v})] dV = 0 \tag{3.2}$$

From which follows

$$\frac{\partial \rho_m}{\partial t} + div(\rho_m \vec{v}) = 0 \tag{3.3}$$

as the equation of continuity. For incompressible fluids where $\rho_m = const$, formula (3.3) can be simplified to

$$div(\vec{v}) = 0\,. \tag{3.4}$$

3.2. Euler's equation

Transformation of total force $-\oint p d\vec{f}$ acting on the volume V_0, to the volume integral by Gauss/Green formula can get :

$$-\oint p d\vec{f} = -\int \vec{\nabla} p dV \tag{3.5}$$

where p is Pascal's omnidirectional pressure. By the introduction of this force into the classical Newton's formula $\vec{F} = m \cdot d\vec{v}/dt = \rho_m \cdot dV \cdot d\vec{v}/dt$, and after its integration we obtain the following equation

$$\frac{d\vec{v}}{dt} = -\frac{1}{\rho_m}\vec{\nabla} p \cdot \tag{3.6}$$

Positions of the liquid elements are function of the time and therefore this total derivation of $\vec{v}[x(t), y(t), z(t), t]$ has a complex form: $\frac{d\vec{v}}{dt} = \frac{\partial \vec{v}}{\partial t} + \frac{\partial \vec{v}}{\partial \vec{r}} \cdot \frac{\partial \vec{r}}{\partial t} = \frac{\partial \vec{v}}{\partial t} + (\vec{v} \cdot \vec{\nabla})\vec{v}$. Formula (3.6) can be now rewritten to

$$\frac{\partial \vec{v}}{\partial t} + (\vec{v} \cdot \vec{\nabla})\vec{v} + \frac{1}{\rho_m}\vec{\nabla} p = 0, \tag{3.7}$$

which is the known Euler's equation. But very small amplitudes of surface waves are considered for the beginning of electrospinning process, what can be expressed as $A << \lambda$, where A is amplitude of the wave and λ is its wavelength (see Fig. 3.2). The horizontal phase velocity of the wave can now be estimated as $v \cong A/T$, where T is a period of the wave. The comparison of first two terms of the Euler's equation gives following relations where the first term is equal to $\partial v/\partial t \cong A/T^2$ and second element is $\partial v/\partial r \cdot \partial r/\partial t \cong A^2/T^2\lambda$. And now the comparison of both of them is $A/T^2 >> A^2/T^2\lambda \Rightarrow \partial v/\partial t >> \partial v/\partial r \cdot \partial r/\partial t$. One can see, that second element is much smaller than first one and therefore it can be neglected. Euler's equation for small deflections of the surface of the liquid, such as in the case of electrospinning, can be simplified

$$\frac{\partial \vec{v}}{\partial t} + \frac{1}{\rho_m}\vec{\nabla} p = 0 \cdot \tag{3.8}$$

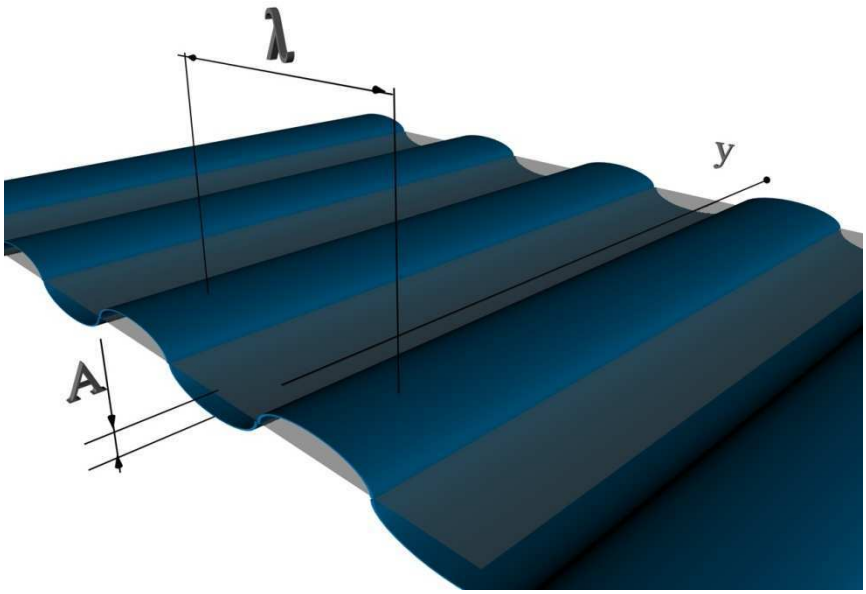

Figure 3.2. A schematic view of liquid's surface with main parameters of the wave

Another simplification is the application of curl on the both sides of equation (3.8):

$$\vec{\nabla}\times\frac{\partial\vec{v}}{\partial t}+\frac{1}{\rho_m}\vec{\nabla}\times(\vec{\nabla}p)=0, \tag{3.9}$$

where by the identity $\vec{\nabla}\times(\vec{\nabla}p)\equiv 0$. Therefore also the first term in (3.9) is zero

$\vec{\nabla}\times\frac{\partial\vec{v}}{\partial t}=0$ and so $\vec{\nabla}\times\vec{v}=const$. The constant should be taken as zero, which is the condition for the implementation of the velocity potential $\boldsymbol{\Phi}$ as $\vec{v}=\vec{\nabla}\boldsymbol{\Phi}$. Assignment of definition of velocity potential to the formula (3.4) gives the known Laplace's formula:

$$\Delta\Phi = 0. \tag{3.10}$$

Laplace's formula is very important result. Detailed explanation can be found in Landau's (1959a) book. This velocity potential plays an important role in solution of Euler's equation for many examples. Formula (3.8) can now be expressed in a more familiar form:

$$\vec{\nabla}(\frac{\partial}{\partial t}\Phi+\frac{1}{\rho_m}p)=0, \tag{3.11}$$

and its solution will be found in following chapter 4.

3.3 Capillary pressure

The curved liquid surface introduced in Fig. 3.2 is studied in this chapter. It is necessary to include capillary pressure $p_c = F_c/S = \gamma_0 L/S$ when considering a real liquid; where γ_0 is a surface tension and L is the length of the wave (see Fig. 3.3 A). The term of the surface tension will be described in detail in the next part of this chapter. The vertical component of capillary pressure p_c is important for electrospinning process due to the vertical orientation of electrostatic field strength.

One can see in Fig.3.3 B that $\gamma_0 = \gamma \cdot \sin(d\varphi)$ and $S = L \cdot 2d\varphi \cdot R$. For very small angles can be $\sin(d\varphi)$ approximated as $d\varphi$. The well known formula for capillary pressure for cylinder:

$$\frac{F_n}{S} = p_c = \frac{2\gamma d\varphi L}{2Ld\varphi R} = \frac{\gamma}{R}, \tag{3.12}$$

and for sphere it has the form: $p_c = 2\gamma/R$ and for an surface with two radiuses of curvature: $p_c = \gamma(1/R_1 + 1/R_2)$. But the capillary pressure as a function of surface deflection $\zeta(x)$ instead a function of radius of curvature, is important for electrospinning. A harmonic planar wave can be approximated by series of circles (see in Fig. 3.3 C) Radius of the curvature can be expressed as extended formula:

$$\frac{1}{R} \equiv \lim_{ds \to 0} \frac{d\alpha}{R \cdot d\alpha}. \tag{3.13}$$

Now we can implement: $d\zeta / dx = tg(\alpha)$ and approximation for small angles: $tg(\alpha) \cong \alpha$. The interest is only in the change of this angle in x direction, $d\zeta / dx = \alpha$ so the formula is

$$\frac{1}{R} = \lim_{ds \to 0} \frac{\alpha(x+dx) - \alpha(x)}{(x+dx) - x} = \frac{d\alpha}{dx} = -\frac{\partial^2 \zeta}{\partial x^2}. \tag{3.14}$$

One can obtain from (3.13) and (3.14) the important approximation: $\frac{1}{R} \cong \frac{\partial^2 \zeta}{\partial x^2}$. So finally capillary pressure has an important form useful for the description of electrospinning process:

$$p_c = -\gamma \frac{\partial^2 \zeta}{\partial x^2}, \tag{3.15}$$

When second derivation is negative, the surface of the function has concave shape, but the capillary pressure acts always against the surface's deflection and vice versa. Therefore the formula (3.15) has negative sign. This is important to keep liquid surface stabilized.

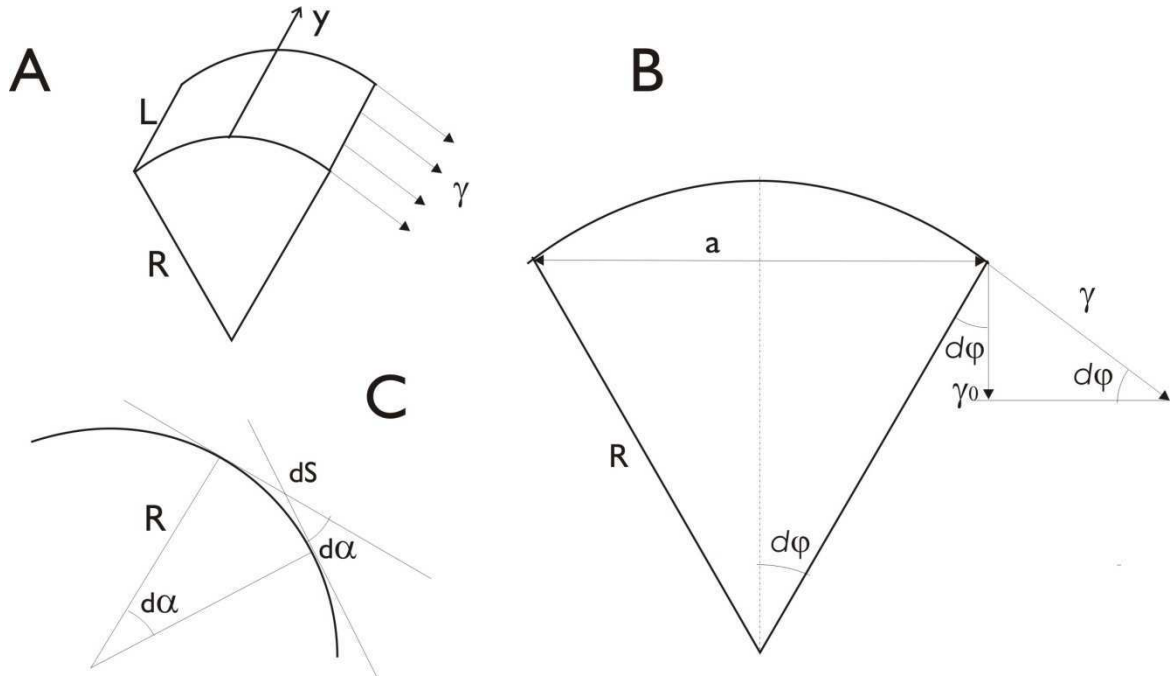

Fig. 3.3: An element of a liquid surface with cylindrical symmetry.

3.4 Surface tension

The notion of surface tension was already used in previous chapter describing the capillary pressure (formulas 3.12 and 3.15). It is an important parameter for electrospinning process. The unit of the surface tension is according to (3.12) the force per unit length or the energy per unit area. Surface tension can be explained as the excess of free energy at an interface. The molecules in a liquid bulk attract each other and all attractions are balanced by the attractive force in all directions. But the molecules on the surface of the liquid are unbalanced due to the state transition of the liquid and the air as indicated in Fig. 3.4.

The liquid surface must remain flat, if no force acts on it. But if there is some pressure on one side which is different from pressure on the other side, some normal force has to be acting on it. This surface will then be unstable and instability creates the curved surface of the liquid. When all forces are balanced, the pressure difference could be written by known Young-Laplace equation

$$\Delta p = \gamma\left(\frac{1}{R_x}+\frac{1}{R_y}\right), \tag{3.16}$$

which is the general formula (3.12) for two dimensions and where Δp is the pressure difference, γ is the surface tension and R_x and R_y are radii of curvatures.

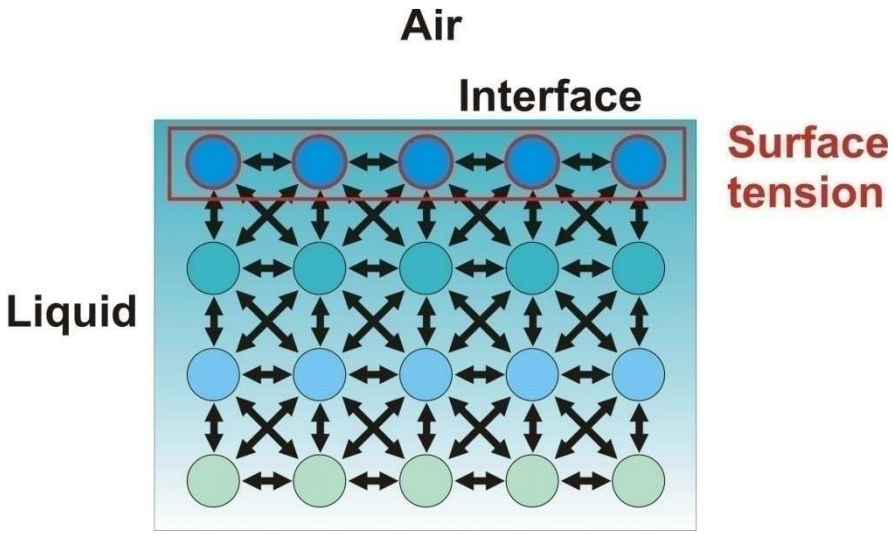

Figure 3.4: Schematic view of liquid's molecules attraction. In the interface between the liquid and air the interactions are unbalanced and create the surface tension

More precise and detailed explanation of surface tension was done by Bush (2004) in his MIT lectures which can be freely downloaded from internet. There is detailed explanation of Ryleigh-Plateau instability, which is as well important phenomenon for electrospinning theory.

3.5 Viscosity

Viscosity is another important parameter which affects the process of electrospinning. The influence of viscosity on the electrospinning is still not known in detail but some first analytical studies had been already done by Shiryaeva (1998) (2000). At the beginning it is necessary to get some basic ideas about viscosity. Basic ideas can be found also in Feynman (1971) in the chapter 41 entitled as: The Flow of Wet Water, where Feynman highlighted that it is "funny" to talk about liquids without inclusion of viscosity. Another more detailed and precise explanation of viscous fluids was written by Landau (1959a) or Levich (1962). Everything what was determined until now in this chapter is valid for ideal fluids only. For real fluids, it is necessary to include viscosity into the analytical description. The viscosity is the internal friction of the fluid. Every real fluid which is deformed by the tensile or shear

stress puts a resistance against it. The general definition of viscosity based on imagining the fluid as a "sandwich" that contains different layers and all layers move by different velocities see Fig. 3.4.

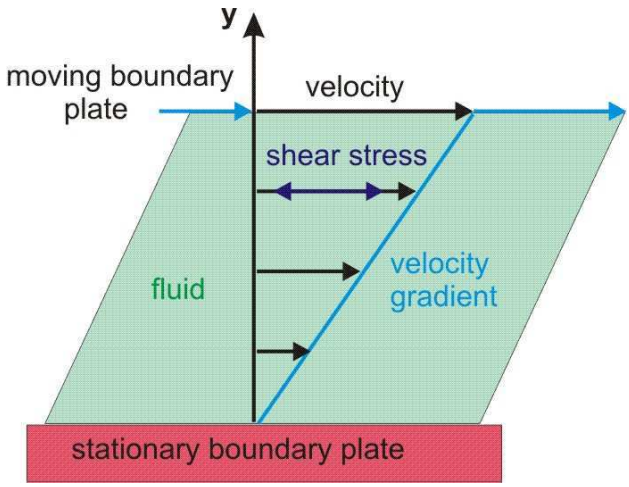

Figure 3.5: Drifting of the fluid between two boundary plates.

To speak about the real fluids, it is necessary to modify the previously determined Euler's equation by adding the stress tensor τ_{ij} which gives the irreversible transfer of momentum in ideal fluid. The viscous stress tensor τ_{ij} between the layers is proportional to the $\partial \vec{v}_i / \partial x_k + \partial \vec{v}_k / \partial x_i$.

As is known, the process of internal friction occurs only when neighboring particles move with various velocities in the fluid. As it is shown in Fig 3.5, the viscous stress tensor τ_{ij} depends on the space derivatives of velocity components. Its components for incompressible fluids $\vec{\nabla}\vec{v} = 0$ are:

$$\tau_{ij} = \eta\left(\frac{\partial v_i}{\partial x_j} + \frac{\partial v_j}{\partial x_i}\right) \tag{3.17}$$

where η is called as *dynamic viscosity*. To find the formula for stress tensor of compressible fluids, it is necessary to add another term called *second viscosity.* It is possible to find its determination in the Landau (1959a). But for our purpose, incompressible viscous fluids are assumed and the equation of motion can be written in the form:

$$\frac{\partial \vec{v}}{\partial t} + (\vec{v}\cdot\vec{\nabla})\vec{v} = -\frac{1}{\rho}\vec{\nabla}p + \upsilon\Delta\vec{v} \tag{3.18}$$

where $$\upsilon = \eta / \rho_m , \tag{3.19}$$

is the *kinematic viscosity*. Equation (3.18) is often called as Navier-Stokes equation and it should be for nonturbulent flows lienarized into the form:

$$\frac{\partial \vec{v}}{\partial t} = -\frac{1}{\rho}\vec{\nabla} p + \upsilon \Delta \vec{v} \tag{3.20}$$

Taking the curl on both sides one obtains a diffusion equation for velocity field:

$$\frac{\partial}{\partial t}\left(\vec{\nabla}\times\vec{v}\right) = \nu\Delta\left(\vec{\nabla}\times\vec{v}\right), \tag{3.21}$$

where the kinematic viscosity plays the role of the diffusion coefficient. It is possible to implement two dimensional (x,z) velocity field $\vec{v}$ by decomposing into two parts: $\vec{v} = \vec{v}_0 + \vec{u}$, where $\vec{v}_0$ represents the potential part of the liquid flow, for which holds $\vec{\nabla}\times\vec{v} = 0$. It is therefore possible to implement velocity potential Φ which holds to Laplace equation (3.10). This velocity potential fulfils the Euler part of the lienarized NS equation (3.20), i.e.: $\partial\Phi/\partial t = -p/\rho_m$. There are the normal components of of the pressure tensor that are not caused by viscosity effects. The solution of Laplace equation (3.10) should be written in exponential form $\Phi = A\cdot\exp(kz)\cdot\exp[i(kr-\omega t)]$ (explained in following chapter).

The rotational parts of the velocity field can be determined by scalar field ψ which holds to the non-potential part of the liquid velocity $\vec{u} = (-\partial\psi/\partial z, 0, \partial\psi/\partial x)$ and the continuity equation. Obviously, for ψ holds the same diffusion equation as for the curl of $\vec{v}$

$$\frac{\partial \psi}{\partial t} = \nu\Delta\psi . \tag{3.22}$$

It has the solution $\psi = C\cdot\exp(lz)\cdot\exp[i(kr-\omega t)]$ with decay *l* along the axis *z* that differs from the decay parameter *k*, that is identical to the wave number, for Φ. The relationship between both parameters should be written as $l^2 = k^2 + -i\omega/\nu$ (see Levich 1962). The boundary condition on the free surface of a viscose liquid should be expressed as

$$\frac{\partial \varphi}{\partial t} = -p - p_{zz} \quad , \qquad p_{xz} = 0 , \tag{3.23}$$

where $p_{zz} = 2\mu\left(\partial v_z/\partial z\right)$ is the nnormal and $p_{xz} = \mu\left(\partial v_x/\partial z + \partial v_z/\partial x\right)$ is the tangential compnents of the viscouse stress tensor, Landau (1959a), Levich (1962). The pressure *p* is consisted of gravity, capillary and electric part, Lukas (2008). The vertical liquid surface displacements $\zeta \cong 0$ forms a tiny harmonic wave, $\zeta = \int \partial v_z/\partial z \; dt = \int\left(\partial\varphi/\partial z + \partial\psi/\partial z\right) dt$.

The dispersion law of viscouse liquid should be foud by following of Levich (1962) steps in

part 117 of his book. He divided liquid into the non-viscous and viscous part where ω_0 is the angular frequency of non-viscous liquid:

$$\left(-i\omega+2\nu k^2\right)^2+\omega_0^2=4\nu^2k^4\sqrt{\frac{-i\omega}{\nu k^2}+1}\,. \tag{3.24}$$

Analytical solution of equation (3.24) is almost impossible due to biquadrate root of ω. It is only possible to find asymptotical solutions of (3.24). In the case of low viscosities, the irrational part is much larger the rotational part of the velocity: $A/C>>1$. If we follow the boundary condition for free surface of a viscous liquid (3.23) then $A/C>>-i(1-i\omega/2\nu k^2)$ which should be even simplified to $-i\omega/2\nu k^2>>1$ and $l>>k$. Under this assumption, the solution of the dispersion law (10) can be sought in the from $-i\omega=-i\omega_0+\beta$, where $\beta<<\omega_0$. By using of equality $-i\omega=-\omega_0+\beta$ the formula (3.24) will have a form:

$$-i\omega_0(-i\omega)\left(\beta+2\nu k^2\right)^2=2k^3\sqrt{\nu^3(-i\omega)} \tag{3.25}$$

and the right hand side can be according to our assumption negligible and hence

$$-i\omega=-i\omega_0+\beta\cong-i\omega_0-2\nu k^2\,. \tag{3.26}$$

The minimal value of ω_0^2 expressed from the dispersion law for a non-viscose liquid has been introduced in Lukas *et al*. (2008). It takes the form of $\omega_0^2=\frac{2g}{3a}K\left(1-K\Gamma\right)=\frac{g}{a}\Omega_0^2$, where Γ is a dimensionless electrospinning number defined as $\Gamma=a\varepsilon E_0^2/2\gamma$ and for the dimensionless wavenumber *K* holds $K=k/a$. The symbol *a* is used for the capillary number $a=\sqrt{\gamma/(\rho g)}$ and Ω_0 denotes a dimensionless angular frequency. The dimensionless electrospinning relaxation time *T* is then defined as

$$T=\frac{1}{-i\omega}\sqrt{g/a}\,. \tag{3.27}$$

The substitutions from Equations (11) and (12) into the formula for *T* provides with the relationship for the dimensionless relaxation time of low-viscosity liquids

$$T_{Low}=\frac{1}{\sqrt{\frac{2}{3}K\left(K\Gamma-1\right)}-2O_hK^2}=\frac{1}{\Omega_0-2O_hK^2}\,. \tag{3.28}$$

The symbol O_h is used the Ohnesorge number defined as $O_h=\sqrt{\nu^2/ga^3}$.

There is another way how to get some basic description of viscous fluids via the characteristic hydrodynamic time of capillary waves of a flat charged surface of a polymeric solution of the The second asymptotical solution of (3.24) for highly viscous liquids holds $-i\omega/\left(\nu k^2\right)>>1$ and it reforems the dispersion law to a simple quadratic equation for the angular frequency:

$$\left(-i\omega\right)^2+2\nu k^2\left(-i\omega\right)+\omega_0\cong 0 \tag{3.29}$$

from which follows:

$$-i\omega=-2\nu k^2\pm\sqrt{\nu^2k^4-\omega_0^4}\cong-\frac{\omega_0^2}{\nu k^2} \tag{3.30}$$

where we have done a choice for which $-i\omega$ has a real positive value for negative ω_0 values. The dimensionless relaxation time for highly viscose liquids is then derived from Equation (13) as

$$T_{High}=\frac{3O_hK}{K\Gamma-1}=\frac{2O_hK^2}{\Omega_0^2}. \tag{3.31}$$

4. Electric forces in fluids

Both previously mentioned chapters about electrostatics and hydrodynamics will be joined into one theory which will describe electrospinning process. This interconnection of two different theories is sometimes called electrohydrodynamics and includes application of electric field on the liquid surface. Ideally conductive or dielectric fluids will be considered. Various forms of pressure, straightly connected to fluids, were determined in the previous chapter. The hydrostatic one has the same importance in both forms of fluids: gases and liquids. Whereas capillary pressure has the main importance only in liquids due to the surface tension γ. Only liquids will be considered in this work. Both pressures mentioned above keep liquids in the as most stabilized status as possible, they actuate against its upward movements in the case of needle less electrospinning.

The initialization of instability on the surfaces of liquids should be caused using the application of the external electric field that induces electric forces on surfaces of liquids. To include this phenomenon, it is necessary to find formula for electrostatic pressure and add it to the dispersion law. Electrostatic pressure for ideally conductive liquids was determined in chapter 2.4 and for dielectric ones in chapter 2.6. It is convenient to start with the study of the ideally conductive liquids. The description of the wave's instabilities is expressed by equations called dispersion laws.

4.1 Application of the electric force on ideally conductive liquids

The simplest example is an ideally conductive liquid with infinity depth. The derivation starts with the solution of the Laplace's equation for velocity potential (determined in chapter 3).It has manifold solutions that is determined by the boundary conditions for special cases. We will consider further only uncompressible fluids: $\rho_m = const$. Boundary condition comes for infinite liquid layer depth: $\lim_{z->-\infty} \Phi = 0$. The speed potential of the liquid can be expressed as:

$$\Phi = A \cdot \exp(kz) \cdot \cos(kr - \omega t). \qquad (4.1)$$

Velocity potential introduced in relation (4.1) is a solution of Laplace's formula $\Delta\Phi = 0$, boundary condition include the hydrostatic pressure $p_h = \rho_m g h$ and capillary pressure,

$p_c = -\gamma \cdot \partial^2\zeta / \partial x^2$ (determined in chapter 3), actuating against the surface's instabilities and the electrostatic pressure $p_e = \frac{1}{2}\varepsilon_0 \vec{E}_0^{\,2} + \varepsilon_0 k \cdot \vec{E}_0^{\,2} \cdot \zeta$ (determined in chapter 2) creating the surface's deflections.

Inclusion of all above mentioned pressures, one can get following boundary condition:

$$\frac{\partial \Phi}{\partial t} + g\zeta - \gamma \frac{\partial^2 \zeta}{\partial x^2} - [\frac{1}{2}\varepsilon_0 \vec{E}_0^{\,2} + \varepsilon_0 k \cdot \vec{E}_0^{\,2} \cdot \zeta] = 0 \qquad (4.2)$$

where ζ is the vertical displacement of the surface's oscillations. The derivative $\partial\zeta/\partial t$ is the vertical component of the velocity v_z, therefore:

$$\frac{\partial \zeta}{\partial t} = \frac{\partial \Phi}{\partial z} \qquad (4.3)$$

After the derivation of the formula (4.2) with respect to time and using (4.3), one obtains:

$$\frac{\partial^2 \Phi}{\partial t^2} + g\frac{\partial \Phi}{\partial z} - \gamma \frac{\partial}{\partial z}\frac{\partial^2 \Phi}{\partial x^2} - \varepsilon_0 k \cdot \vec{E}_0^{\,2} \cdot \frac{\partial \Phi}{\partial z} = 0 \qquad (4.4)$$

This differential equation is solved with the proposed velocity potential (4.1) and the searched dispersion law for infinity depth is now written as:

$$\omega^2 = (\rho_m g + \gamma k^2 - \varepsilon_0 E_0^{\,2} k)\frac{k}{\rho}. \qquad (4.5)$$

The more detailed analysis of this law will be done in the paragraph 4.3.

The bottom of the liquid must be zero in the situation with tiny liquid layers, as for example is case of the Nanospider:

$$v_z = \left.\frac{\partial \Phi}{\partial z}\right|_{z=-h} = 0. \qquad (4.6)$$

General solution of the Laplace's equation of such system is:

$$\Phi = [A \cdot \exp(kz) + B \cdot \exp(-kz)] \cdot \exp[i(kx - \omega t)]. \qquad (4.7)$$

With boundary condition (4.6), it is easy to find the ratio between constants A and B:

$$\Phi = A \cdot \cosh[k(z + h)] \cdot \exp[i(kx - \omega t)]. \qquad (4.8)$$

The deflection of the wave is:

$$\zeta = C \cdot \exp[i(kx - \omega t)], \qquad (4.9)$$

and another condition is that the velocity in the *z* dimension must be equal to the time change of the deflection $\partial\zeta/\partial t$, equation (4.3).

After constitution of (4.8) and (4.9) to (4.3) the searched ratio between constants A and C will be:

$$A = \frac{-iC\omega}{k \cdot \sinh(kh)}, \tag{4.10}$$

The using of Euler's formula it is now possible to write the dispersion law for thin films as:

$$\omega^2 = (\rho g \cdot + \gamma k^2 - \varepsilon_0 E_0^2 k)\frac{k}{\rho}\tanh(kh) \tag{4.11}$$

This form of dispersion law for thin films was firstly presented in International Nanofiber Conference in Prague on March 2009 by prof. David Lukáš, Petr Mikeš and Pavel Pokorný and later published by Miloh (2009) and colleagues.

It is now possible to have a look into the detailed analysis of achieved results of both dispersion laws.

4.2 Analysis of dispersion law for ideally conductive liquids

An analysis of the dispersion law for infinite depths of liquid layers was done by Lukáš (2008), the analysis of thin layers is firstly presented here. Our main focus is concentrated on finding of negative values of square root of angular frequency. Negative ω^2 violates the stability of liquid surface. The critical position of the value of the electrostatic field is independent to the depth of the liquid (Fig. 4.1a), but the minimal value of ω^2 is a little bit shifted on the *k* axis for the different depths and values of the electric field (Fig. 4.1b). The dependence of wavelength on the surface tension γ is almost linear and the wavelengths between jets are a little bit smaller for lower depths (Fig. 4.1c). Dependency of wavelength on electric field strength is exponential.

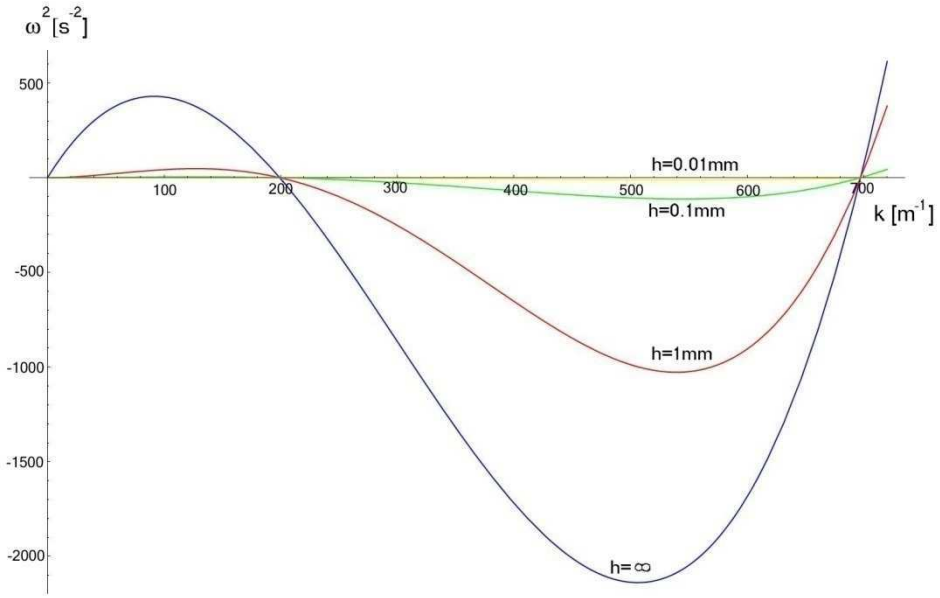

Fig. 4.1 (a) Square root of angular frequency vs. wavelength number for $E_0 = 2.7 \cdot 10^6 V/m$, $\rho = 1000 kg/m^3$, $g = 10 m/s^2$, $\gamma = 72 \cdot 10^{-3} N/m$.

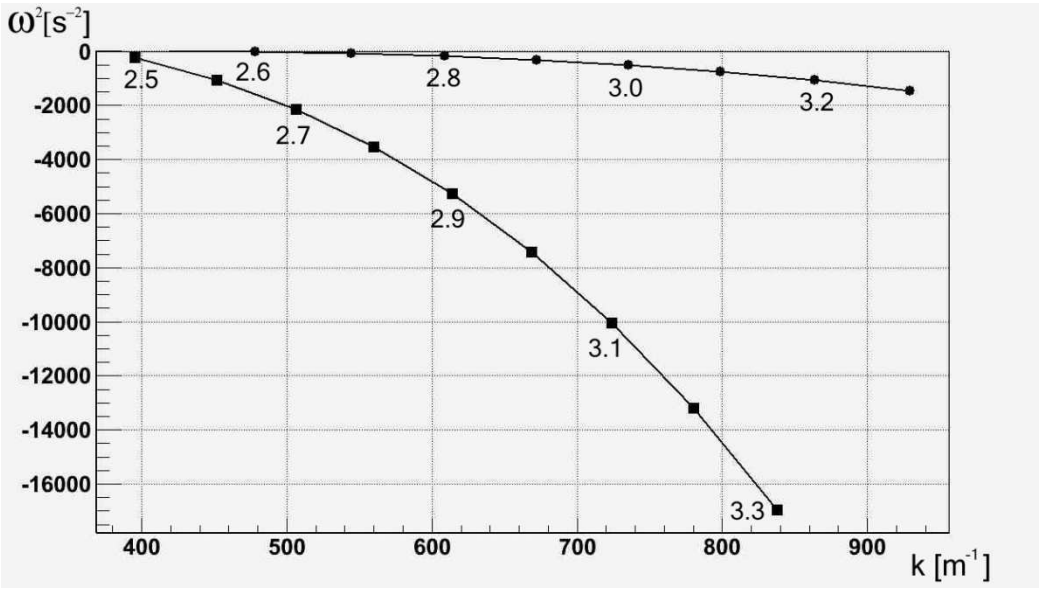

Fig. 4.1 (b) Minima of ω^2 *vs. wavelength number for several values of intensities of electric field* E_0 *(values by the points in multiplicands of* $10^6 [V/m]$*) and for infinity depth (bottom) and depth h=0.1mm (up),* $\rho = 1000 kg/m^3$, $g = 10 m/s^2$, $\gamma = 72 \cdot 10^{-3} N/m$.

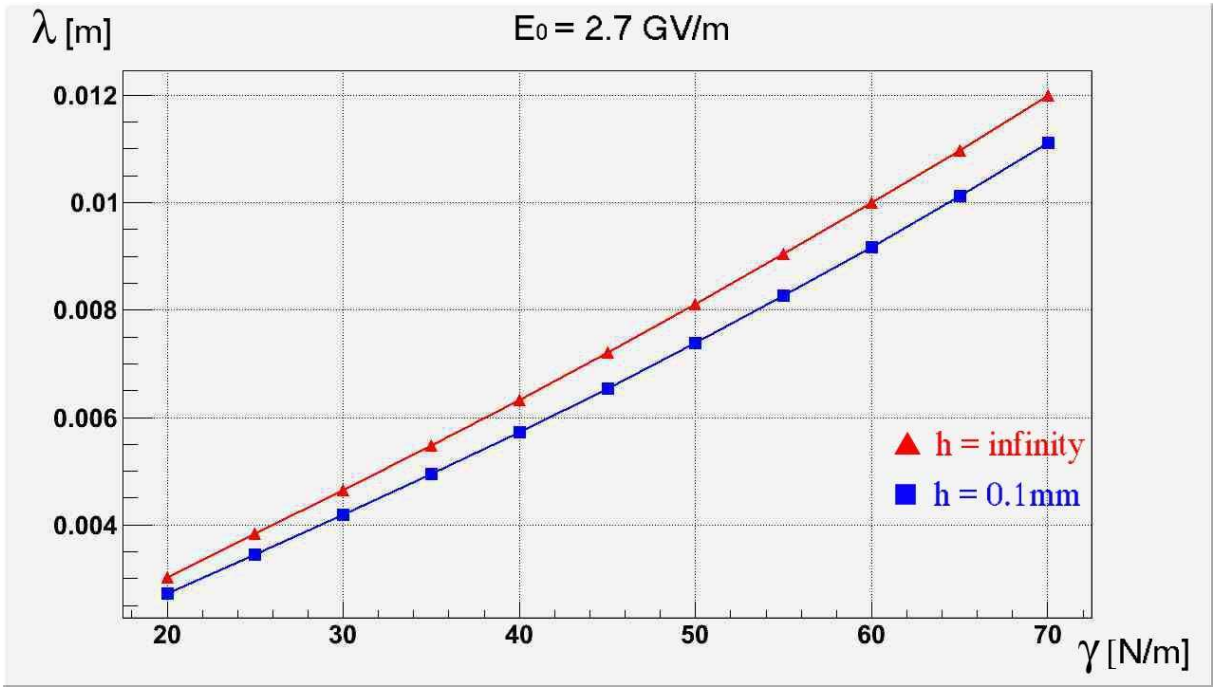

Fig. 4.1 (c) Wavelength λ as a function of surface tension γ for two different depths, $E = 2.7 \cdot 10^6 V/m$, $\rho = 1000 kg/m^3$, $g = 10 m/s^2$.

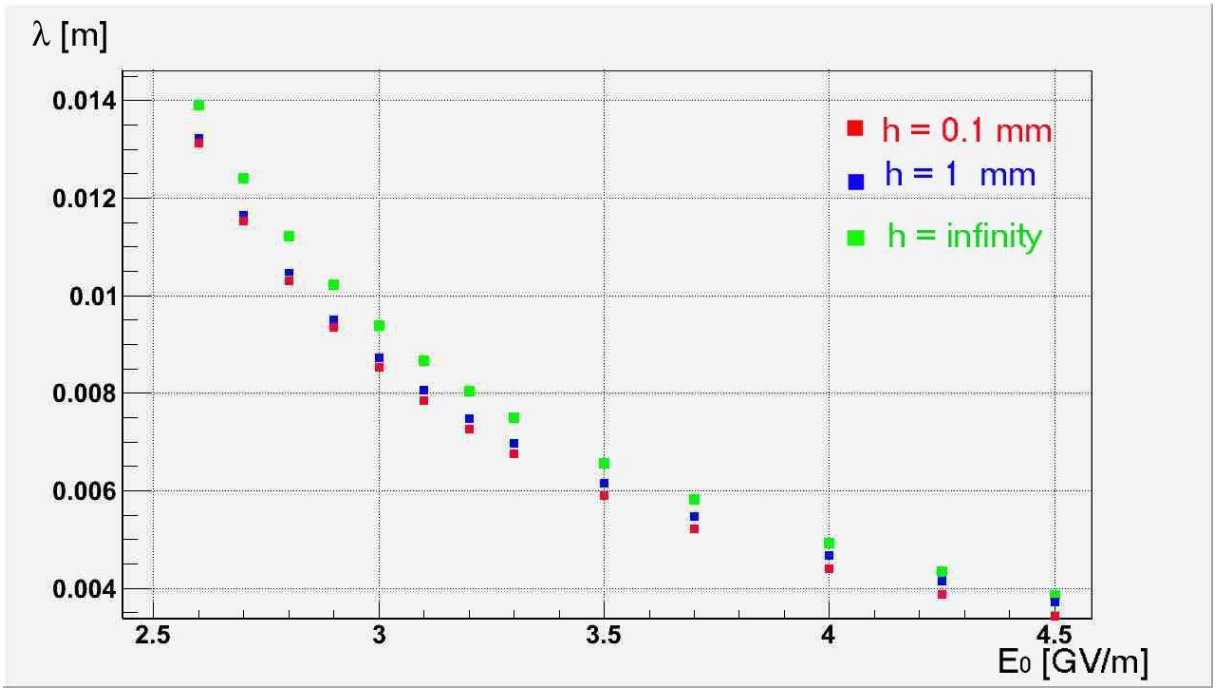

Fig. 4.1 (d) Wavelength λ for three different depths as a function of intensity of electrostatic field E_0, $\rho = 1000 kg/m^3$, $g = 10 m/s^2$, $\gamma = 72 \cdot 10^{-3} N/m$.

4.3 Application of the electric force on the dielectric liquids

Only ideally conductive liquids were mentioned in previous part of this chapter and dielectric properties were neglected. Two electrostatic pressures for non-polar and weakly polar dielectric liquids were determined in the chapter 2.6.

It is time now to find the dispersion laws for liquid dielectrics with using of Clausius-Mossotti and Onsager's relations. To do so, one can follow the same steps as for ideally conductive liquids (see formulas 4.2 -4.5) obtaining following formulas:

1) For nonpolar liquids with infinite depths:

$$\omega^2 = \left(\rho g + \gamma k^2 - \varepsilon_0 \frac{(\varepsilon_r - 1)(\varepsilon_r + 2)}{3} E_0^{\ 2} k \right) \frac{k}{\rho} \tag{4.12}$$

2) for nonpolar liquids with finite depths:

$$\omega^2 = \left(\rho g + \gamma k^2 - \varepsilon_0 \frac{(\varepsilon_r - 1)(\varepsilon_r + 2)}{3} E_0^{\ 2} k \right) \frac{k}{\rho} \tanh(kh) \tag{4.13}$$

3) for weakly polar liquids with infinite depths:

$$\omega^2 = \left(\rho g + \gamma k^2 - \varepsilon_0 \frac{\varepsilon_r (\varepsilon_r - n^2)(2\varepsilon_r + n^2)}{2(\varepsilon_r)^2 + n^4} E_0^{\ 2} k \right) \frac{k}{\rho} \tag{4.14}$$

4) for weakly polar liquids with finite depths:

$$\omega^2 = \left(\rho g + \gamma k^2 - \varepsilon_0 \frac{\varepsilon_r (\varepsilon_r - n^2)(2\varepsilon_r + n^2)}{2(\varepsilon_r)^2 + n^4} E_0^{\ 2} k \right) \frac{k}{\rho} \tanh(kh). \tag{4.15}$$

4.4. Analysis of dispersion laws for dielectric liquids

A brief analysis of dispersion laws for nonpolar and weakly polar liquids with infinity depths according to relations (4.12) and (4.14) follows analysis of thin layers already made in previous part of this chapter for ideal liquids. Example of dependency of square root of angular frequency on wavenumber for both Clausius-Mossotti and Onsager relations is introduced in Fig. 4.2.

Main influence of relative permittivity on dispersion law is the decreasing critical value of E_c with increasing of ε_r. This is dominant for value of ε_r between 1 - 3.5, but this

critical value starts to stabilize for $\varepsilon_r > 4$. With increase of refractive index *n* which is important for inclusion of polarity to the liquids, this decrease is shifted to the higher values of ε_r. Detailed analysis of influence of ε_r on the critical value of ω^2 can be seen in Fig. 4.3.

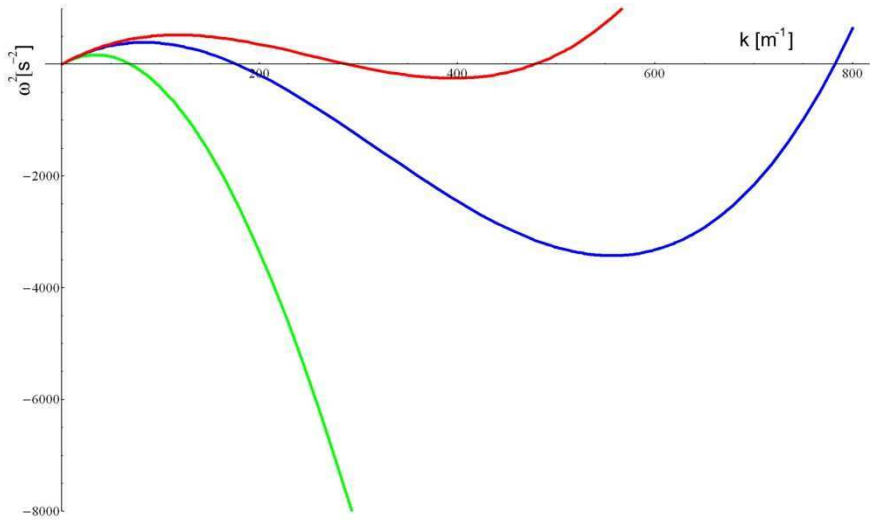

*Figure 4.2: Square of angular frequency ω vs. wavelength number k for ideal liquids (red), nonpolar liquids according to Clausius-Mossotti relation (blue) and for weakly polar liquids (green) (E_0= 2,5 10^6 V/m; ε_r=2.2, n=1.4; γ =32*10^{-3} N/m; ρ=10^3 kg/m^3;g=10 m/s^2).*

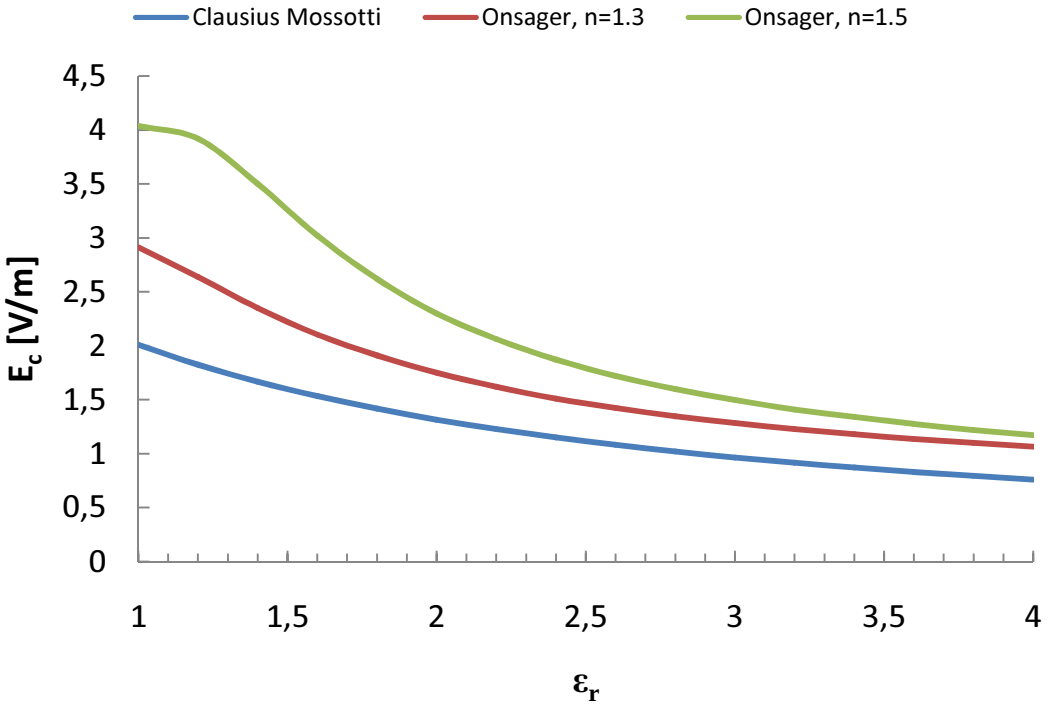

*Figure 4.3: Influence of relative permittivity ε_r on the critical value electric field E_c for nonpolar and weakly polar liquids (γ =32*10^{-3} N/m; ρ=10^3 kg/m^3;g=10 m/s^2).*

Another important parameter for electrospinning process is the minimal value of ω^2. The wavenumber where ω^2 is minimal and the minimal value of ω^2 was plotted as function of relative permittivity and in the case of polar liquids for different values of refractive index.

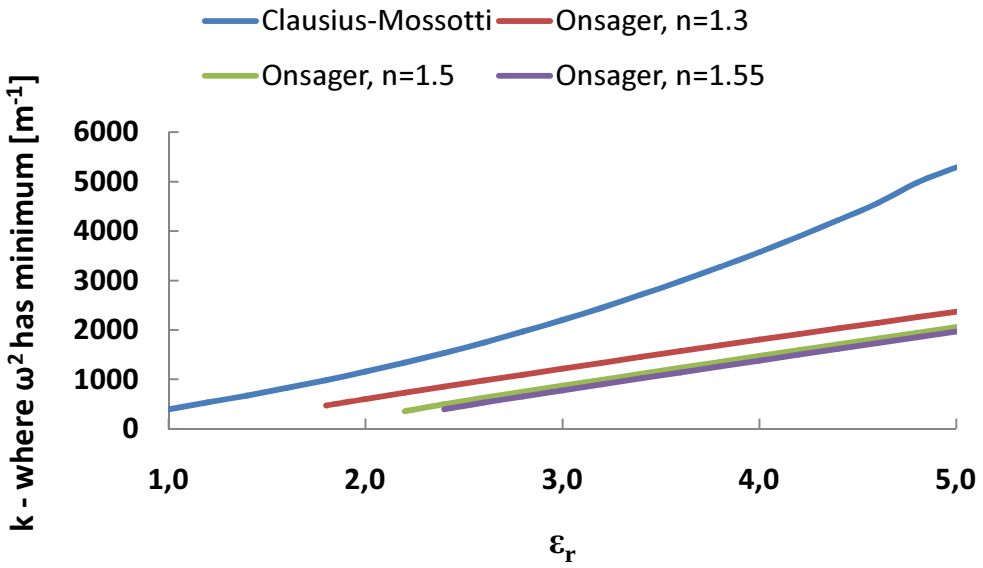

*Figure 4.4: Influence of relative permittivity on the position of mimimal value of ω^2 (E_0= 2,5 10^6 V/m; γ =32*10^{-3} N/m; ρ=10^3 kg/m^3;g=10 m/s^2).*

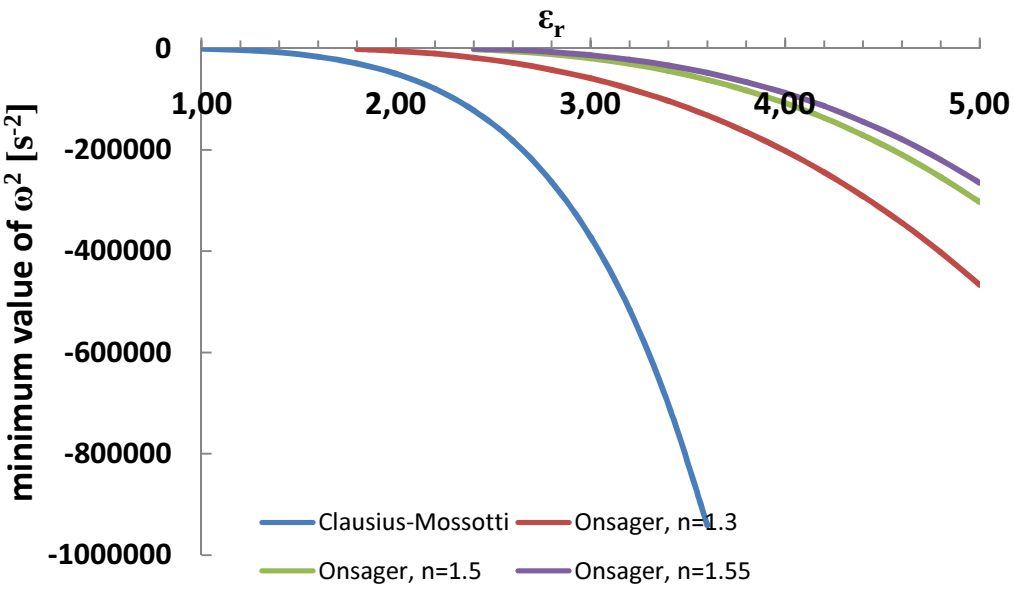

*Figure 4.5: Minimal value of ω^2 for different values of relative permittivity (E_0= 2,5 10^6 V/m; γ =32*10^{-3} N/m; ρ=10^3 kg/m^3;g=10 m/s^2).*

The shift of wavenumber of minimal value of ω^2 is rising with increase of relative permittivity for weakly polar liquids. The question is still the changing of refractive index with changing of relative permittivity of the liquid such is in the case of evaporation of solvent. In the case of nonpolar liquids the rising of ω^2 with rising of ε_r is slightly increasing for higher values of relative permittivity. Some values of relative permittivity and refractive indexes of few chosen materials can be seen in tab. 4.1.

material	**Relative permittivity**	**Refractive index**
air	~1	~1
water	80.1 (20°C), 55.3 (100°C)	1.33
ethanol	24	1.36
PVA	1.9-2.0	1.49 – 1.55
Electroactive polymers	2 - 12	-

Tab 4.1: Relative permittivity and refractive indexes for some materials.

Relative permittivity is also a function of the temperature for liquids. Some deeper analysis of influence of relative permittivity has to be done. There is a massive evaporation of solvent during electrospinning jet path from a spinning electrode to a collector and therefore the relative permittivity dramatically changes its value as well.

5. Observation of St. Elmo's fire in laboratory conditions

One of the unexpected radiation phenomena accompanying electrospinning process has been already known for many decades by the sailors. This chapter deals with the observation of St Elmo's fire in laboratory conditions.

Zeleny (1914) already referred about the intensity and range of luminosity that depends on the prevailing type of a discharge realized by a spray in the nearby Taylor cones vide, Taylor (1964). Zeleny distinguished negative and positive discharges depending on the net charge involved in the spray. According to him positive discharge is the one which transports positive net charge through a spinning zone and vice versa. Positive discharges provide fibrous "brushes" of light that reach out further away from the electrode towards the collector than those of the negative discharges. The process was observed using solution of poly-vinyl-alcohol in distilled water. The solution was not viscous enough to produce nanofibres instead of nanodroplets, but it was viscous enough to keep the mother and daughter droplet connected for the same potential before the daughter droplet is pulled-out. This process is sketched in Fig. 5.1a and picture of observed St. Elmo's fire during electrospraying can be seen in Fig. 5.1b.

A mechanism of St. Elmo's fire was described by Grigor'ev and Sinkevich (1984) and Grigor'ev et.al. (1991). Small charged droplets, so called mother droplets, of residual solution have been ejected from charged liquid bodies by applying strong electric field. Smaller daughter droplets can be created due to their electric disintegration from these mother droplets as described by Grigor'ev (1985) and Shchukin (2000). The daughter droplet is about twenty times smaller than the mother one and can usually reach a diameter of units of micrometers and then extract great portion of all charge from its mother droplet, as described by Landau (1960). Tiny daughter droplets emit high energy photons after collision with external ions accelerated by strong fields in ambient gas.

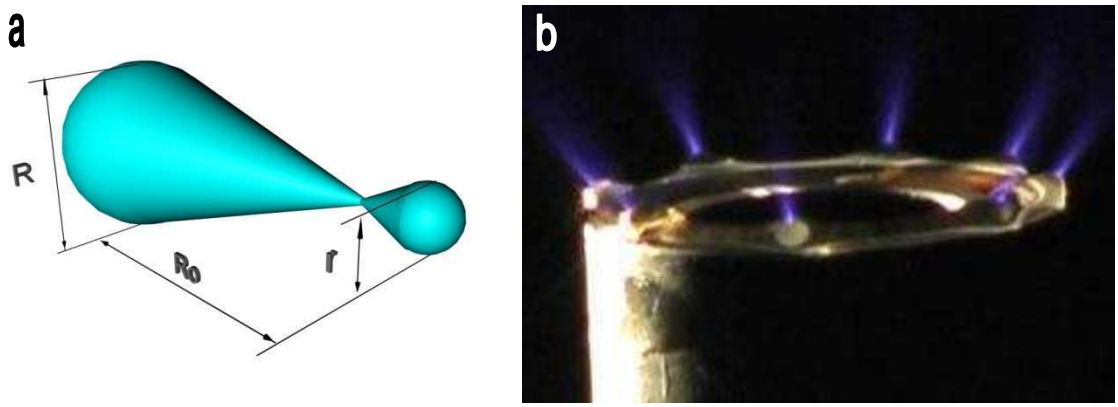

Figure 5.1. (a) Sketch of separation of a daughter droplet with diameter r from a mother droplet with diameter R. The distance between them is denoted as R_0 measured from centers of both droplets. (b) St. Elmo's fire created nearby Taylor cones during electrospraying of demineralized water.

5.1 Numerical analysis

To calculate parameters of droplets in external electric field, one has to deal with electrohydrodynamic instability, where some modes of capillary liquid become unstable. This mechanism was proposed by Tonks (1935) and Landau (1959a). Some theoretical explanation of St. Elmo's fire generation has been made by Grigor'ev (1984,1991). He used Landau's (1960) calculation of Coulomb repulsion between two charged drops interconnected by a thin wire; similar example was calculated by Feynman (1971). Landau assumed the same potential for both drops and the radius of the small drop r much smaller than the radius R of mother drop, R is not large compared with distance between centers of both drops R_0. Electrostatic force *F* between both drops is according to Landau's (1960) § 5, problem 1:

$$F = 4\pi\varepsilon_0\varepsilon_r \frac{\varphi^2 rR}{R_0^{\,2}}\left(1-\frac{R}{R_0}\right), \qquad (5.1)$$

where φ is the potential of both droplets. Grigor'ev used Landau's equation and modified it under different conditions including some external forces. He solved more complex problem closer to the real situation of St. Elmo's fire. He considered drops with different potentials, because they are not supposed to be conductively connected. His result of free energy change is:

$$\Delta F = 4\pi r^2\gamma + \frac{q^2}{2r} - 4\pi\varepsilon_0\varepsilon_r \frac{\varphi^2 r^2}{2R_0}\frac{1}{(R_0^{\,2}/R^2-1)} + q\varphi, \qquad (5.2)$$

Where φ is the potential of the external field plus the field of the large drop at the point where the small droplet separates from the large drop. The fiirst right-hand term of equation (5.2) is the energy of surface tension; the second is the drop's own electrostatic energy with charge *q*.

The third and the fourth addends are variations of the energy of external field, of the field of the induced charge in the drop *q*, and the energy of interaction of the drop's own charge *q* with the external field

Let's now make some basic numerical analysis of both approaches made by Landau and Grigor'ev. To do so, one has to integrate Landau's repulsion force

$\Delta F = \int \frac{1}{4\pi\varepsilon_0\varepsilon_r} \frac{\varphi^2 rR}{R_0^{\,2}} \left(1 - \frac{R}{R_0}\right) dR_0$ to get energy of both drops. Then it has to be compared with Grigor'ev third addend of equation (5.2) and plotted with dimensionless radius $\nu = R_0/R$

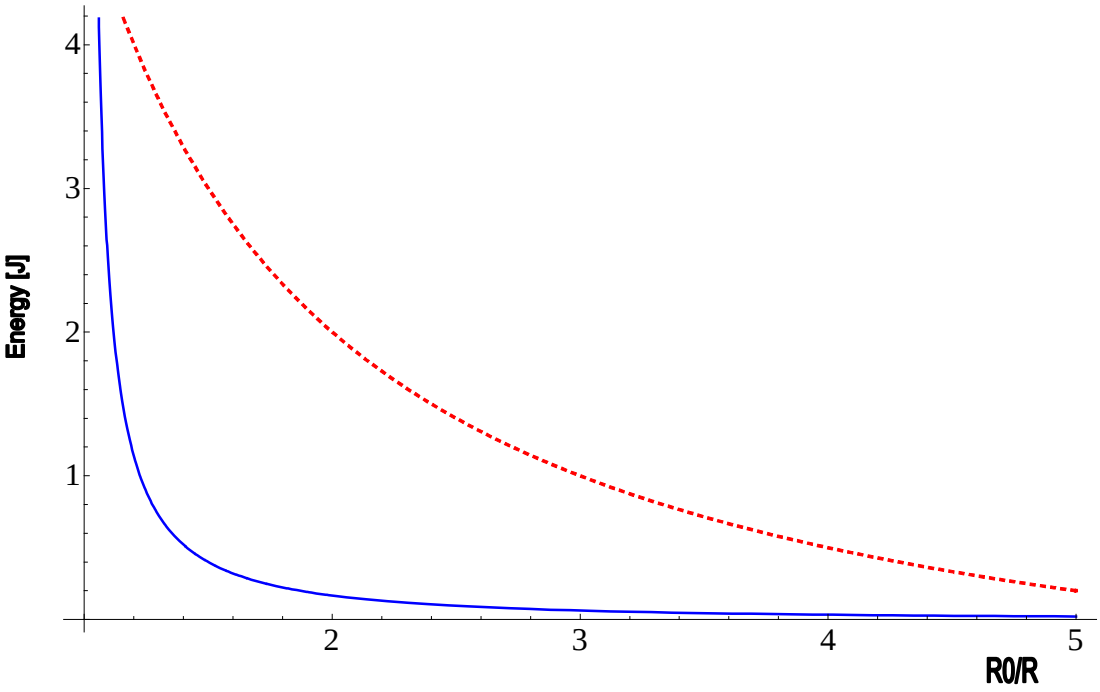

Figure 5.2 Numerical analysis of Landau's (red, dashed) and Grigorev's (blue) results of Electrostatic energy of two charged drops.

One can see the difference between both results when the small drop is close to the mother's one. Energy of non-connected drops decreases much faster, but with increasing distance both results has been showing similar results.

By following of Grigorev's steps and calculation of ratio of mother's and daughter's drop's diameters r/R by the minimalisation of free energy $\partial(\Delta F)/\partial r = 0$, there will be very small difference between both approaches. Grigor'ev (1991) found that $r/R = 0.018425$ and using Landau's result and the same Grigor'ev (1991) approach $r/R = 0.01778$. A relative derivation of small and big droplets radii r/R is, according to Grigor'ev, and Landau about

0.018. Main difference between both approaches is that Landau considered electric contact of both drops for all time, it means the same potential φ of both drops. But Grigor'ev didn't consider the same potential on the both spheres. Smaller drop start to "still" electrostatic charge from its mother one and become more and more charged until the electric contact is lost completely by the electrostatic repulsion. Landau didn't mention St Elmo's fire, in his exercise, but his consideration was a very helpful step for theoretical description of St Elmo's fire.

To observe St Elmo's fire in a laboratory during electrospraying it is necessary to find the border between electrospaying and electrospinning process. A polymeric solution has to be viscous enough to create adequate charged droplets but not so viscous to make fibers. The ideal concentration was found to be 4-5% for aqueous PVA solution. Polymer had predominant molecular weight of 60,000 g/mol. The temperature during the experiments was $21^{o}C \pm 2^{o}C$ and the air relative humidity was $40 \pm 5\%$. The distance between electrodes was 10 cm and voltage of 25 kV was applied. The schematic picture of this experiment can be seen in Fig. 5.3. To observe this phenomenon circular cleft was used as sketched in fig. 5.1b.

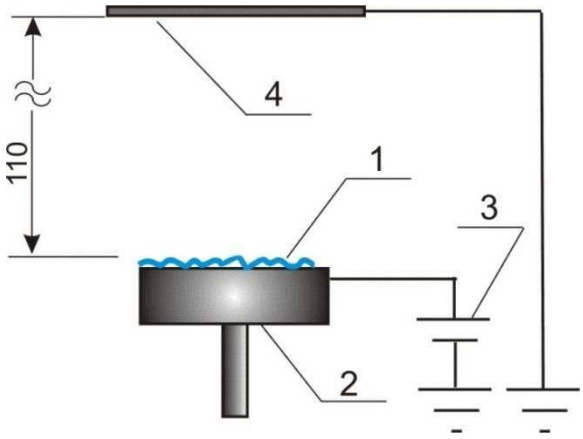

Figure 5.3: A scheme of the experiment for the observation of St Elmo's fire, (1) polymeric solution, (2) circular cleft, (3) high voltage source, (4) collector.

St. Elmo's fire is an electrical weather phenomenon of luminous plasma generated during thunderstorms. Electro-spinning/spraying process can be used for observing and studying of this, still not fully known natural phenomenon. We describe here the conditions necessary to generate St. Elmo's fire. Some theoretical approach done by Landau and Grigor'ev et.al was provided and basic comparison of two different theoretical approaches had been made. Anyway, observations of St Elmo's fire moved us to some new ideas about electrospinning and detection of unexpected phenomena connected straightly to that.

6. Detection and measurement X-rays generated by electrospinning.

Unexpected phenomenon of electrospinning will be explained in this chapter. It was proved by a series of experiments, that electrospinning generates X-rays radiation which will be described later in this chapter. Next three chapters will be the keynote of this work.

6.1 Detection by radiographic film

The first detection of X-rays produced by nanofiber deposition was observed using radiographic film MEDIX XBU manufactured by FOMA Czech Republic. The primal goal of using of radiographic film was to need of understanding of Taylor cone creation. A similar phenomenon was observed for field emission from carbon nanotubes by Bonard (2000) or in the form of St Elmo's fire (see chapter 5). We started with X-rays detection called radiography at that time. Radiographic films were packed in original paper boxes and placed perpendicularly to the running electrospinning so the nanofibres were collected even on these boxes. Films shoved several black traces in the places, where silver lines were painted on the box and most of the nanofibers were collected here. The measurement of conductivity of these lines showed slightly higher value then the rest of the box. Radiographic recording of this first observation can be seen in Fig. 6.1.

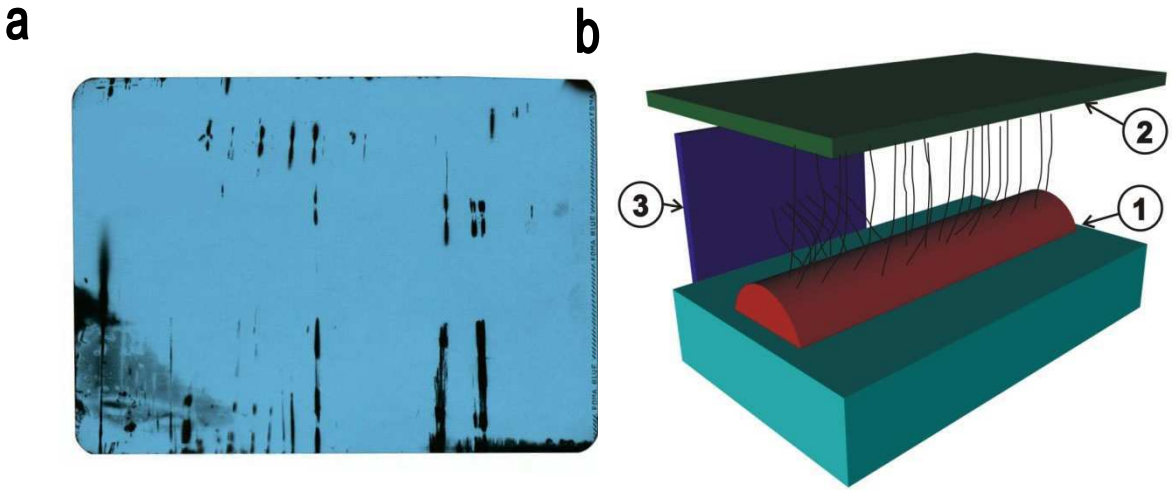

Figure 6.1: (a) First black traces produced by electrospinning and recorded by radiographic film MEDIX XBU.The film was packed in original polyethylene (PE) foil. (b) A Sketch of experimental setup of first observation of blackening of radiographic film consisted of nanospider (1), collector (2) and radiographic film (3).

It was necessary to make more precise observations for deeper understanding of this phenomenon. Several experiments with different polarities of electrospinners and with various materials used as shields of films were carried out. Radiographic film INDUX R7, produced by FOMA Czech Republic, was chosen instead of MEDIX XBU, because of its main usage for X-ray/gamma spectrometry. But as was discovered later, MEDIX XBU seems to be more sensitive for lower energetic part of X-ray spectra then INDUX R7. Out of hand MEDIX XBU is more sensitive to the parasite electrostatic effects, for more details see chapter 6.1.3.

6.1.1 Characteristics of radiographic film

Some basic details about MEDIX XBU and INDUX R7 radiographic films produced by FOMA Czech Republic are written in this part.

MEDIX XBU

MEDIX XBU is a blue-sensitive, double emulsion high-speed medical radiographic film featuring uniform and reasonable high contrast over the whole exposure area. MEDIX XBU is manufactured on a bluish 0.18 mm thick polyester base. That ensures dimensional stability. The building up of electrostatic charges prevents an antistatic supercoat.

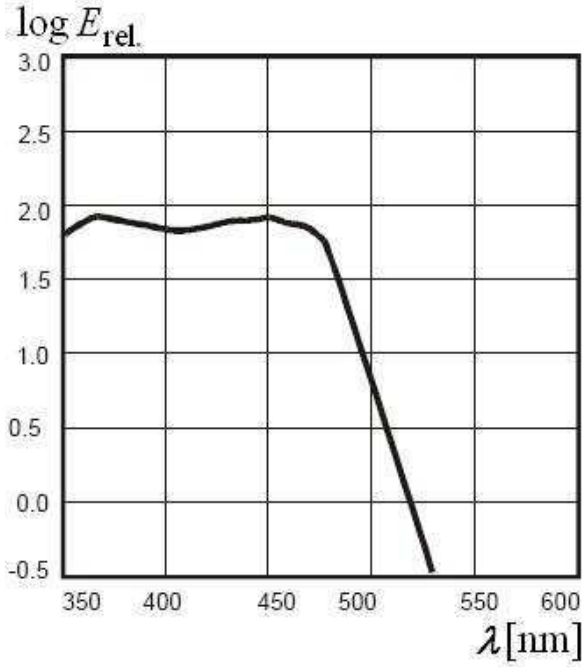

Fig. 6.2. Relative spectral sensitivity: Logarithms of MEDIX XBU spectral sensitivity is plotted against a light wavelength. Original picture of FOMA Company.

INDUX R7

INDUX R7 is an industrial radiographic film intended for non - destructive material testing using X-rays or gamma radiation. INDUX R7 is a high-speed, high-contrast, fine-grain film suitable for radiography with or without lead screens. INDUX R7 corresponds with the class C5 classification according to EN 584-1 standard and according to ASTM E 1815 standard with class II. INDUX R7 is manufactured on a dimensionally stable bluish polyester base of 0.175 mm thickness. The data were taken from FOMA Czech Republic.

6.1.2 Detection of radiation during electrospinning process using various film shielding

We decided to shield radiographic films by three various materials. First of them was PE foil in which these films were originally packed, second material was black paper having the thickness of 0.2 mm and area density 160 g m^{-2} and the last one was aluminum foil with a thickness of 0.01 mm and area density of 25 gm^{-2}. All materials were for five minutes tested by exposure of Deuterium lamp, HERAEUS D200F, 300W, providing UV light of wavelength interval 160 nm- 400 nm, i.e. 50 eV -120 eV, to prove their attenuation of UV radiation. All samples proved nearby absolute shielding of UV radiation. Detection of electrospinning was as well done for different polarities using 300 Watt High Voltage DC Power Supply with regulators; model number PS/ER50N06.0-22; manufactured by Glassman High Voltage, INC. with output parameters: 0-50 kV, 6mA.

The fresh 12% wt aqueous poly-vinyl-alcohol (PVA) solution was prepared by dissolving the polymer in distilled water. Polyvinyl-alcohol Sloviol-R was purchased from Novácké chemické závody, Nováky, Slovakia, having a predominant molecular weight of 60,000 g/mol and the dynamic viscosity of 10.4 mPa s for 4% original aqueous solution. The temperature during the experiments was $21^{o}C \pm 2^{o}C$ and the air relative humidity was $40 \pm 5\%$. This experimental setup for chosen polarity can be seen in Fig. 6.2. Used polarity of all setups can be seen in Table 6.1.

B1, C1, D1	B2, C2, D2	B3, C3, D3	B4, C4, D4
collector - grounded	collector – pos. HV	collector - grounded	collector – neg. HV
rod - positive HV	rod grounded	rod – negative HV	rod - grounded

Table 6.1: Table of different polarities used for different electrospinning setups, where B is signification for PE foil, C for aluminium foil and D for black paper shielding. Indexes 1,2,3,4 mean used polarity.

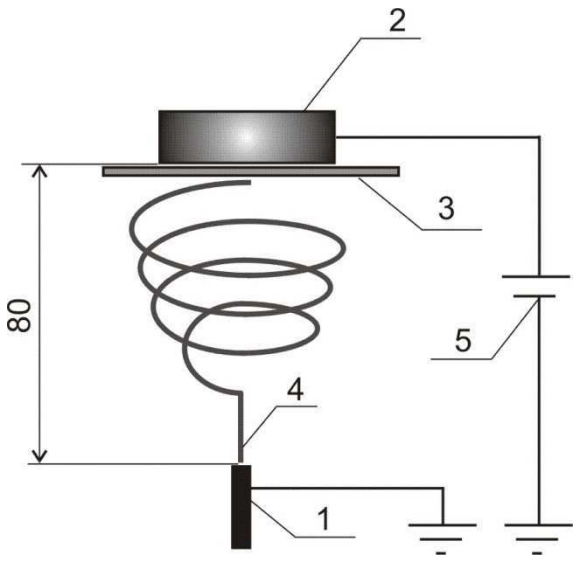

Figure 6.3: *An apparatus for studying high-energy emission from electrospinning. Electrospinner for production of fibrous electrospun materials consists of a rod (1), a collector (2), shielded radiographic film (3), a polymeric solution transported from the charged rod (4) and a high voltage source(5). The distance between the needle tip and the collector is given in millimetres.*

Poly-ethylene shielding

The first shielding was the original PE foil, in which the radiographic films were packed. This foil is a very good dielectric and it was placed inside the asymmetric capacitor as sketched in (Fig. 6.3). It is very difficult to decide which tracks on radiographic films had been made by X-rays and which are simply Kirlian effect or corona discharge (both these efects will be explained later in chapter 6.1.3), but there is strong believe that most of the blackening of the film was done by luminescence of free electrons generated from the PE foil. Due to these difficulties, we decided not to use this shielding for future experiments. The record of film's blackening can be seen in fig. 6.4. Some detailed calculation of electron's energy losses in polyethylene was done by Ashley (1982).

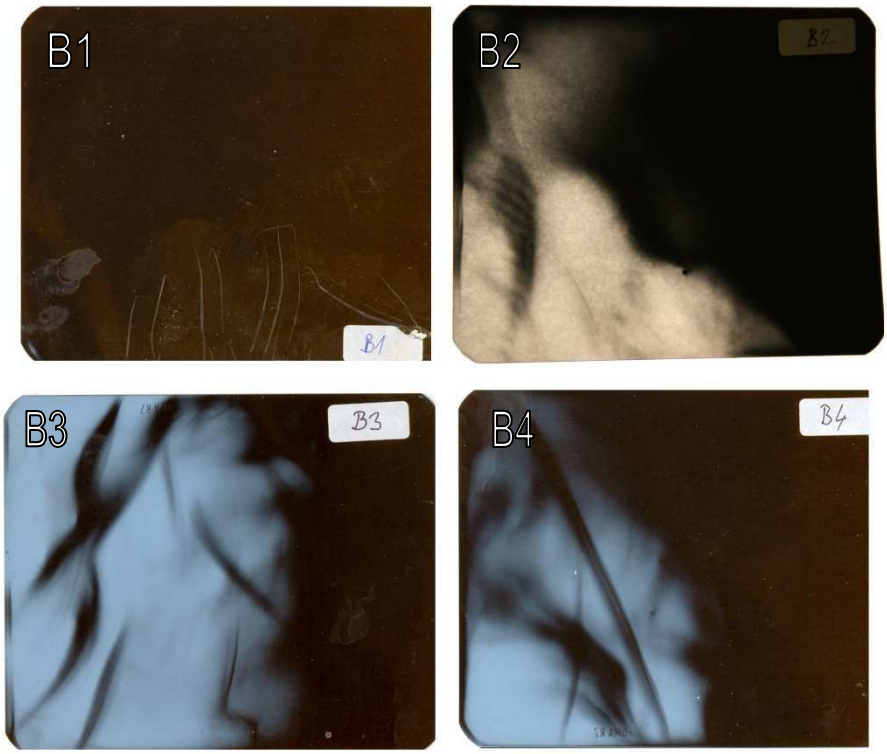

Figure 6.4: Radiographic films shielded by PE foil radiated by electrospinning apparatus with various polarities introduced in Tab. 6.1.

Black paper shielding

Another shielding of radiographic film was black paper. It was proved that this shield at least filters out all ultraviolet radiations up to 160 nm (120 eV) which were produced by the deuterium lamp (see specifications above). But we cannot be sure about the Kirlian effect and some blackening of radiographic film by processes of electron luminescence. This paper is not a conductor and therefore it doesn't filter out all electromagnetic spectrum which can expose the radiographic, film wrapped in the black paper, via discharges that penetrate to it. Anyway one can see that deposited fibers correspond to the records on radiographic films (see Fig. 6.5). There is a correlation between spots of deposited fibers and radiographic records. The rest clean area of radiographic film around the black traces can be used as a reference area without any radiation record. But it is hard to be sure about X-rays produced around spinned fibers due to the accompanying parasite effects, which are in more detail described in chapter 6.1.3. Kirlian effects and Lichtenberg's figures can be clearly seen on the both top corners of the film. Some observations of luminescence during the nanofibers deposition was observed in dark room. This is probably due to the discharging around the fiber when it hits an oppositely charged collector. Due to the very low intensity of produced light by the fiber's deposition, it was impossible to record it by standard camera.

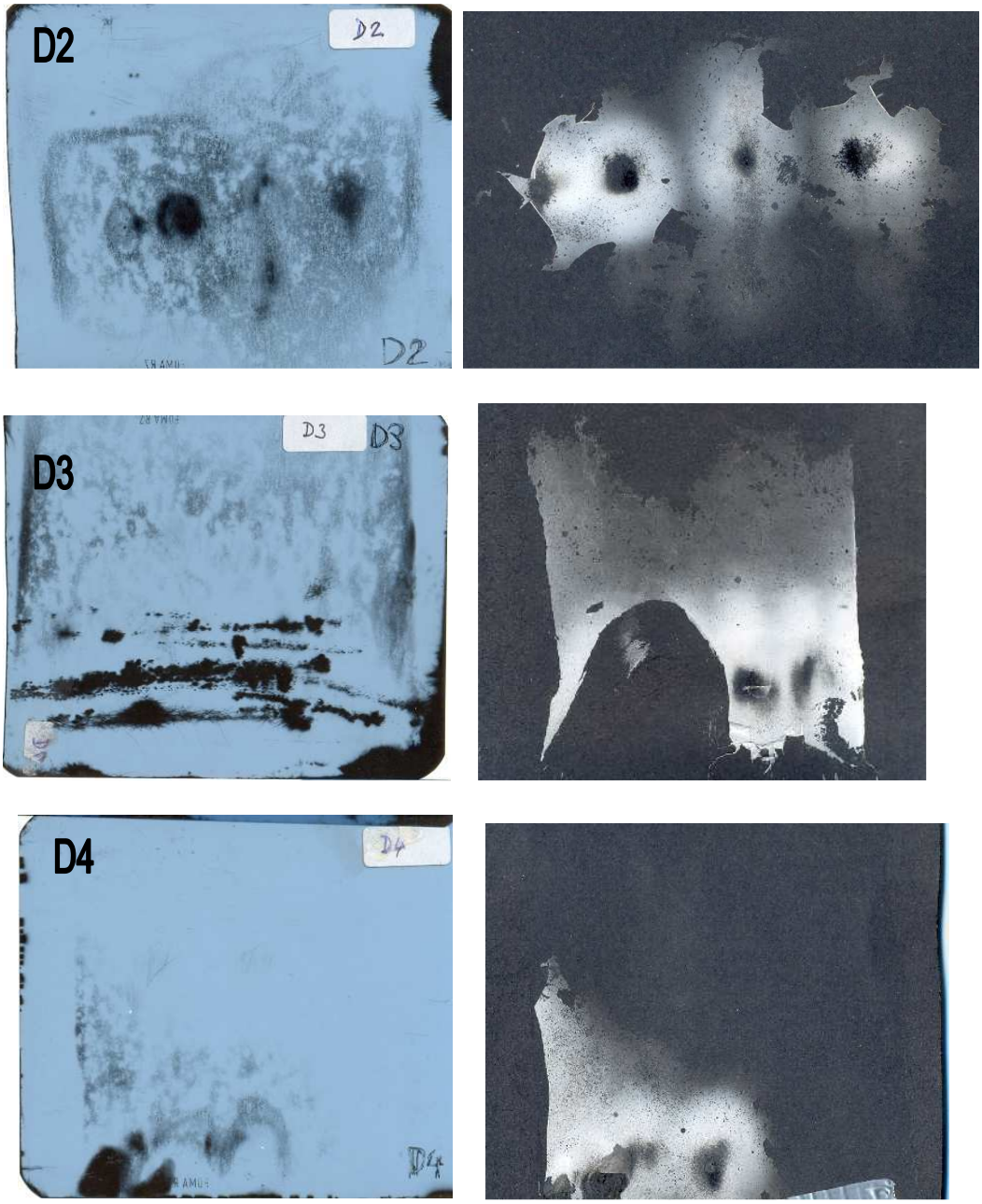

Figure 6.5: Comparison of radiated radiographic film shielded by black paper. Radiographic records (left) and deposited nanofibrous layers corresponding to the traces on the radiographic films (right). Indexes D2,D3 and D4 are introduced in Tab. 6.1.

Aluminum shielding

Another series of films C1-C4 (Fig 6.6) were shielded by 0.02 mm thick aluminum foil. One can assume aluminum foil as Faraday's cage, because it is a good conductor. It means that the charge should stay only on the surface of the aluminum and cannot penetrate inside the aluminum envelope. Therefore the experiment without electrospinning so called "blind experiments" was carried out as a reference to prove the quality of the Faraday's cage.

But “blind” sample exhibited same black traces too. These black traces are most probably not made by X-ray radiation but by secondary electrons which passed through the aluminum foil creating some currents that cause radiographic film records. This experiment therefore cannot be imagined as an electrostatic phenomenon (Fig. 6.6 and Fig. 6.7).

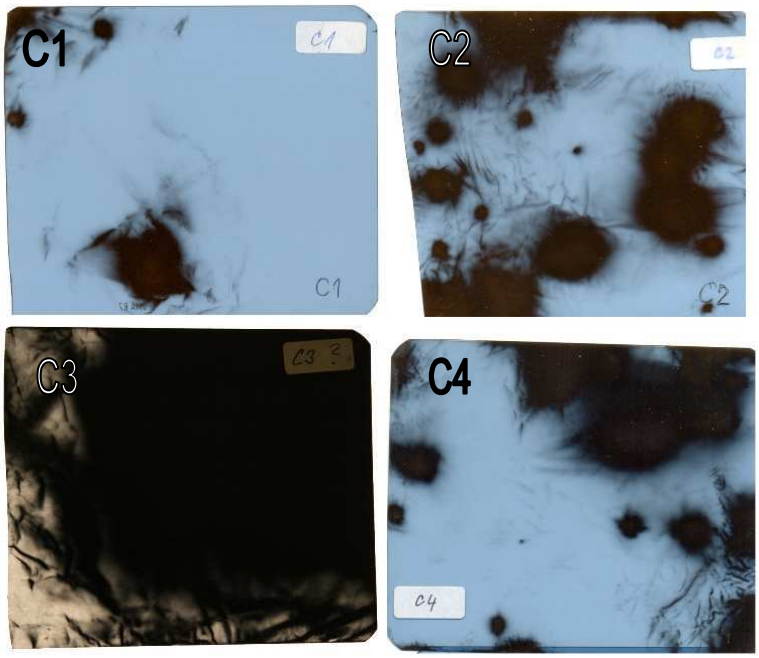

Figure 6.6 Radiographic films INDUX R7 shielded by aluminum foil radiated by electrospinning apparatus with different polarities. Shielding of sample C3 was partly broken. Indexes C1, C2, C3 and C4 are introduced in Tab. 6.1.

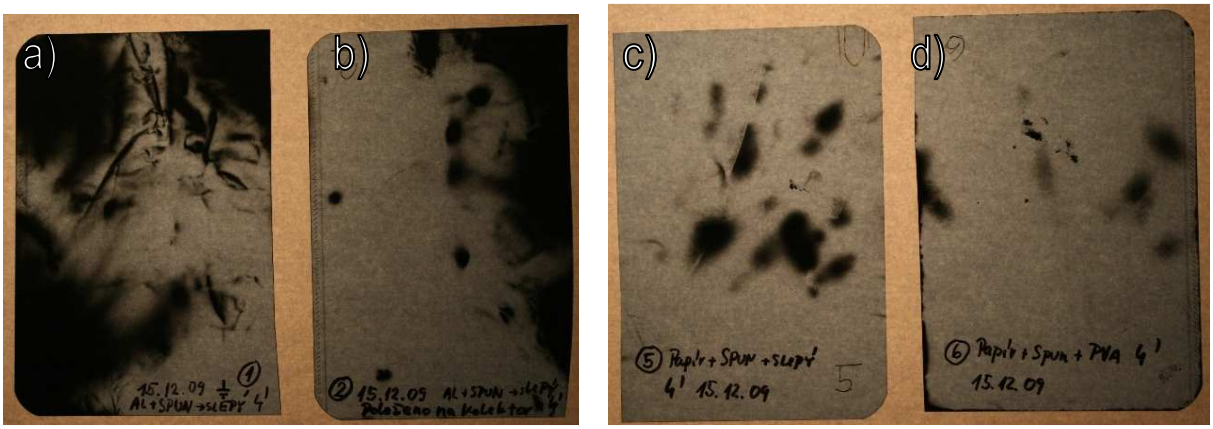

Figure 6.7: Radiographic films packed in different shielding and placed in asymmetric capacitor depicter in Fig. 6.3 for four minutes. (a) Al + spunbond, the sample was grounded, no el.spinning; (b) Al + spunbond, the sample was placed on charged collector, no el.spinning; (c) black paper + spunbond (carrying textile),sample, the sample was grounded, no el.spinning; (d) black paper + spunbond, sample, the sample was grounded, el. spinning process.

Similar current occurs even for black paper shielding, but it will be discussed later. As can be clearly seen in Fig. 6.7a, the blackening of the film is in the places, where aluminum foil was in contact with the radiographic film, so the current can pass through.

6.1.3 Effects that might mimic X-rays

Two parasite effects which can mimic X-ray records are explained in this part. First of them is called Lichtenberg figure. It can be expressed as branching electric discharges that sometimes appear on the surface or the interior of insulating materials. Second one mentioned here is so called Kirlian photography or Kirlian effect. If an object on a photographic plate is connected to a source of high voltage, small corona discharges (created by the strong electric field at the edges of the object) create an image on the photographic plate.

Electric discharge

Pictures 6.5 and 6.6 are different from pictures of electric breakdown of the aluminum foil by electric dicharge. This was done by using very high voltage around 150 kV accompanied by a spark. Such an example of electric breakdown record can be seen in Fig. 6.8.

Figure 6.8: Electric breakdown of the aluminum foil produced by high electric source and accompanied by a spark.

It is impossible to create classic Lichtenberg figure by creating an electric discharge between a needle and collector of the electrospinner with a radiographic film shielded by the aluminum foil. Much higher voltage then what is used for electrospinning process has to be used.

Kirlian effect

When conductive object is placed on a metallic plate which is connected to the high voltage source, the small corona discharges will appear on the edges of the object. It is called as aura or Kirlian (1939) photography. It can be clearly seen and photographed in dark rooms. So due to the dielectric features, the electric field can pass through the film shield and affect the film's blackening. It was decided not to use PE foil shield for the next experiments due to this parasite effects. Detailed explanation of Kirlian photography was done for example by Boyers and Tiller (1973). Sample of Kirlian effect can be seen in Fig. 6.9. Picture was observed by radiographic film during electrospinning process with black paper shielding.

Figure 6.9: Sample of Kirlian effect observed by radiographic film during electrospinning process with black paper shielding.

So it is almost impossible to decide which electrostatic process or electromagnetic radiation is responsible for the radiographic film's blackening. It is therefore necessary to filter out all parasite effects mentioned above.

6.1.4 Experiment with carton frame

First main goal is to cancel impact of discharges on blackening of the radiographic film. To do so, one has to prevent contact of Aluminum foil with radiographic film. The carton frame was used for this purpose. A piece of spunbod (carrying textile) textile was placed in between the Aluminum foil and radiographic film. Setup can seen in Fig. 6.10.

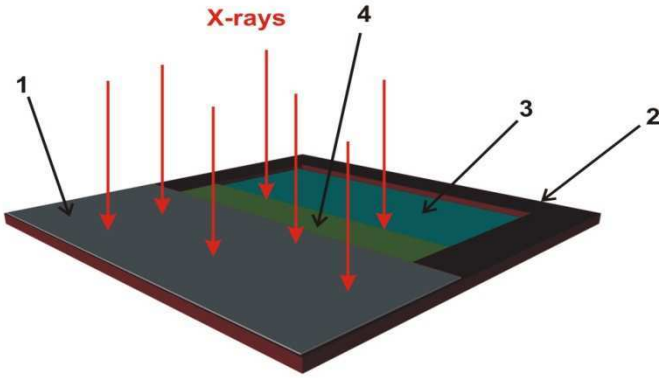

Figure 6.10: Schematic view of experiment with carton frame. (1) aluminum foil; (2) carton frame; (3) radiographic film; (4) spunbond or other material.

This alignment was then placed in between the charged needle spinning electrode and the collector of asymmetric capacitor and left there for ten minutes to prove its prevention against electron's luminescence. Experiment proved complete prevention against parasite electrostatic effects and any blackening occurred on the radiographic film (see Fig 6.11b). Another experiment was done to prove X-rays during electrospinning. So the same alignment was placed in between same electrodes of the same spinner, but this time electrospinning process was running. There was some blackening on the radiographic film after its elicitation (see Fig 6.11a). It is possible to see structure of spunbod placed between the aluminum foil and radiographic film on this record. These black traces have to be caused by outer radiation and this radiation has to be in X-ray region of electromagnetic spectrum.

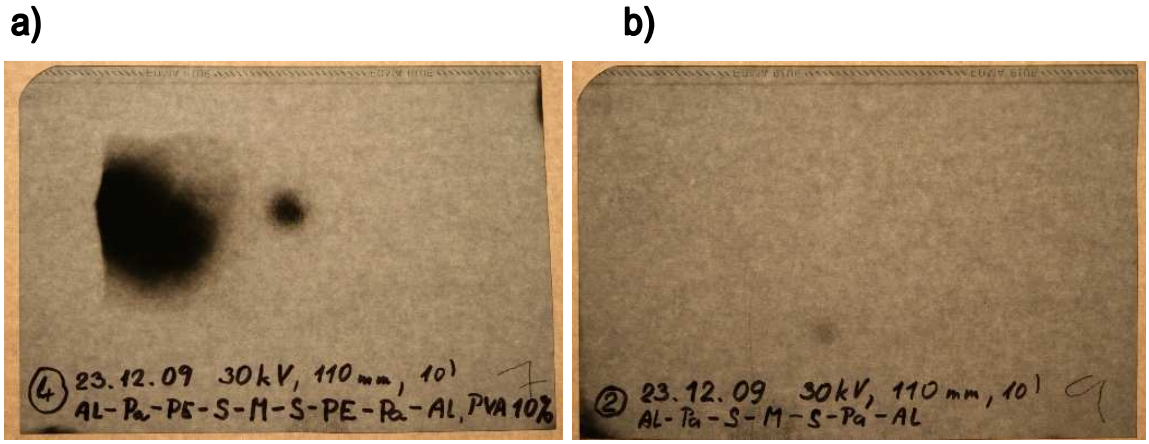

Figure 6.11: Irradiated radiographic films a) with running electrospinning process and b) without electrospinning process but with high voltage applied.

6.1.5 Experiments carried out in a photographic laboratory

The last experiments were done in a photographic laboratory illuminated only by the green light source specially designed for developing of photographic/radiographic films. This setup is very useful for observation of all corona discharges around all sharp edges of equipments or made by imperfect high voltage connection plugs. The intensity of corona discharge depends on the flow-rate of the polymeric solution as well as on the concentration and viscosity of the polymeric solution. It will be described later in this chapter, that the X-ray generation is probably dependent on diameters of the nanofibers that are affected by the flow rate and viscosity. So it is important to find the ideal concentration (viscosity) of polymeric solutions and flow rate to spin nanofibers as thin as possible. For some polymeric solutions such as for example aqueous solution of PVA, it is important to control the air humidity. Thinner PVA nanofibers are created at lower humidity.

It is handy to work in dark room since there is no need to shield radiographic films against day light and it is therefore more effective for observation of several effects which cannot be seen under day light. Some of these effects are for example corona discharge or sometimes the corona accompied deposition of nanofibers on the collector (regular grid made of 0.35 mm thin bronze wires with average inner distance 2.3 mm), it was occupied by the illumination of small “flashes” probably due to depolarization. The sketch of the experimental setup in photographic room is depicted in Fig. 6.12. The shielding against the parasite discharging effects was tested and proved by this setup.

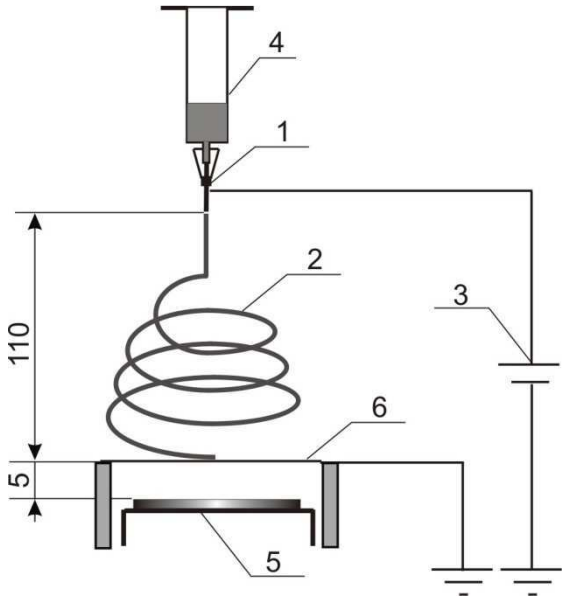

Fig. 6.12: *Apparatus for studying high-energy emission from electrospinning in the photographic room. Electrospinner consists of a hypodermic needle (1), from which a jet (2) is ejected, a high voltage source (3) and a syringe (4) supplying the needle with polymeric solution. Radiographic film (5) is positioned just behind the grounded aluminium foil (6). The distances are given in millimetres.*

The shielding against parasite electrodynamics effects mentioned in paragraph 6.1.3 was tested and proved by this setup. Each series of radiographic films during one experiment consist of a sample with high voltage applied but without polymeric solution, sample with electrospinning process running and reference sample. A reference sample was developed without any outer electromagnetic radiation (high voltage and electrospinning). Second sample was left for five minutes in between the electrodes of spinner with high voltage applied to prove resistance against parasite effects mentioned in chapter 6.1.3. The last sample was developed after five minutes of electrospinning process running. Any blackening of radiographic film wasn’t observed with the absence of nanofibrous production. So one can be almost sure, that these black traces had been made by outer radiation, generated by nanofibers

and the radiation has to be in the X-ray region of electromagnetic spectra, because the radiation of lower energy is absorbed by the Aluminum foil. One of these pictures can be seen in Fig 6.13, where the blackening of the film can be clearly seen in the places of absence of carton frame holding the aluminum foil.

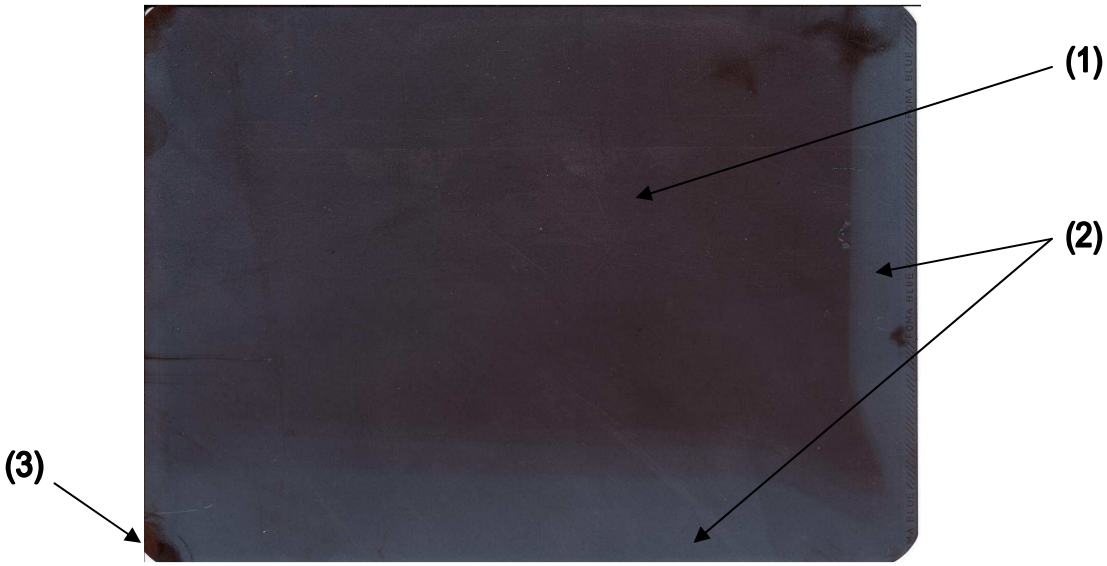

Figure 6.13: Radiographic films irradiated by electrospinning in dark room. (1) place irradiated by outer radiation, (2) edges of carton frame on which the radiographic film was placed, (3) parasite effects.

For detailed study of electron's energy looses in the matter one can see the table of X-rays absorption coefficients calculated by Hubell and Seltzer (1989).

6.1.6 Static samples

Another experiment was done with static nanofibrous structure. Fibers were parallelized in between two parallel wires used as a collector (see Fig. 6.15a) and then for 2 minutes coated in vacuum by BELTZER BU which creates 10 - 15 nm layer of gold. This sample was then placed with radiographic film shielded by black paper between electrodes of asymmetric capacitor. See Fig 6.14:

As can be clearly seen in Fig 6.15b, this gold coated nanofibrous layer can concentrate electrostatic field up to high values and probably generate X-rays. Blackening of the radiographic film occurs only in places where nanofibers were positioned. Other experiments with various materials were done too. These experiments proved that it is necessary to have nanofibrous material with average diameter below 200 nm. But it wasn't possible to measure spectrum of these X-rays due the possibility of harming the Silicon Lithium detector (see

chapter 6.2). As it was calculated in example E4 in chapter 2, that electrons cannot reach such kinetic energy over the distance 100 nm for nanofibers grouped into the warp.

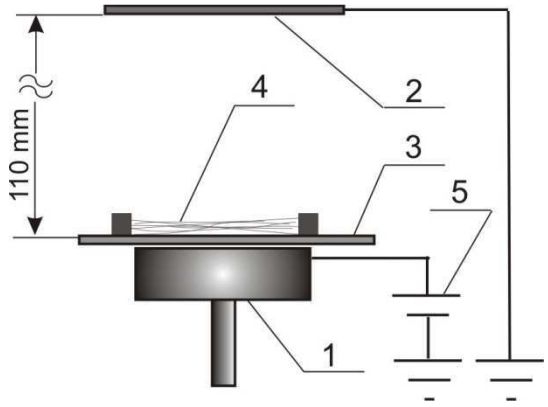

Figure 6.14: Apparatus for studying of high-energy emission from asymmetric capacitor: Asymmetric capacitor consist of: a collector (1), counter electrode (2), radiographic film (3), gold coated nanofibrous layer (4) and a high voltage source (5).

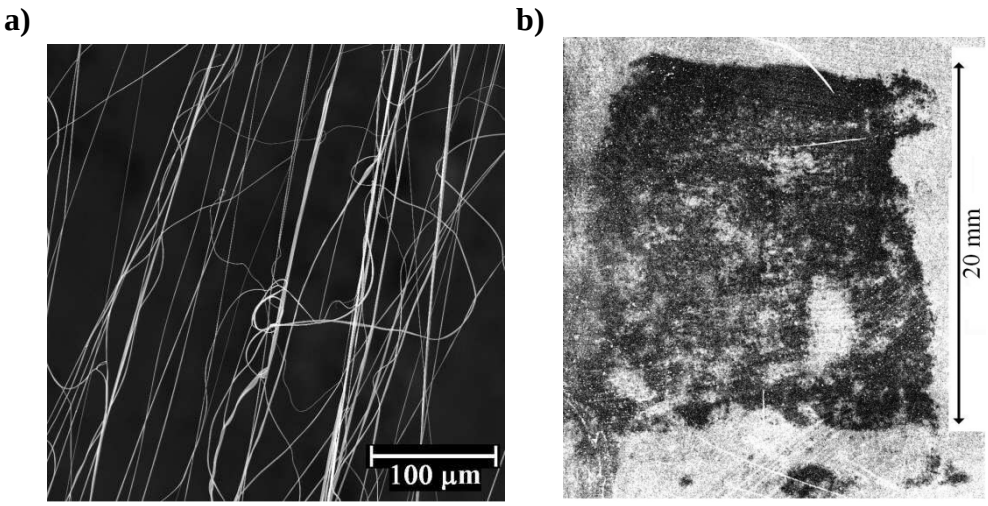

Figure 6.15: Microphotography of the electrospun nanofibrous layer and radiographic film records: (a) Scanning Electron Microscope image of the thin gold coated electrospun nanofibrous layer used as the nano-electrode in the asymmetric capacitor, (b) Radiographic records exposed by the nanofibrous layer in the asymmetric capacitor.

Radiographic method of X-ray detection is efficient and sensitive. It is obvious that this method didn't tell us anything about its spectrum, but it can clearly show its space distribution. To measure the spectrum of X-rays generation by the electrospinning process one has to use another method, which will be described in following part of this chapter.

6.2 Spectral measurement

An energetic spectrum of X-rays emitted during electrospinning process is its substantial feature. This is fundamental experiment to prove the existence of X-rays. The estimation of energy was above 1 keV, because it was recorded by the radiographic film after shielding by the 0.02 mm Aluminum foil. No tracks were observed after passage through doubled layer of Aluminum foil. Aluminum attenuation data were taken from Hübell and Seltzer (1989).

It is a common problem to detect electromagnetic radiation with lower energy then 1 keV at atmospheric conditions due to its high absorption by air molecules. For detection of energy lower than 1 keV it is necessary to use vacuum system, which brings many complications to the measurement. Photons with energy higher than 1 keV should be measured by SLP Silicon Lithium-drifted [Si(Li)] Planar Low-Energy X-ray Detector (SLP). Such a detector seem to be the only reasonable option how to measure spectrum of our radiation. One of the closest laboratories having such equipment is at the Czech Technical University in Prague, Faculty of Nuclear Science and Physical Engineering in the Department of Dosimetry and Ionizing Radiation leaded by Prof. Tomáš Čechák.

Specifications of lithium-drifted silicon detector

The detector used for spectrum measurement was manufactured by ORTEC and the particular type of the detector used was SLP-10180P. The SLP series has become an important tool in soft x-ray spectroscopy in fusion research. This detector doesn't have the same detection efficiency in its energy range. There is an almost zero efficiency to detect photon with energy lower than 1 keV and high detection efficiency between 2 – 30 keV, see in Fig. 6.16. The energy range of this detector is from 30 keV down to 1 keV, depending on the thickness of the beryllium window (Fig. 6.16). The detector was occupied by 25 μm, Beryllium window and its energy resolution is about 35 eV. The X-ray detector consists of a lithium-drifted silicon crystal and cryogenically cooled FET (field-effect transistor), a high-gain, low-noise hybridized preamplifier in a PopTop capsule.

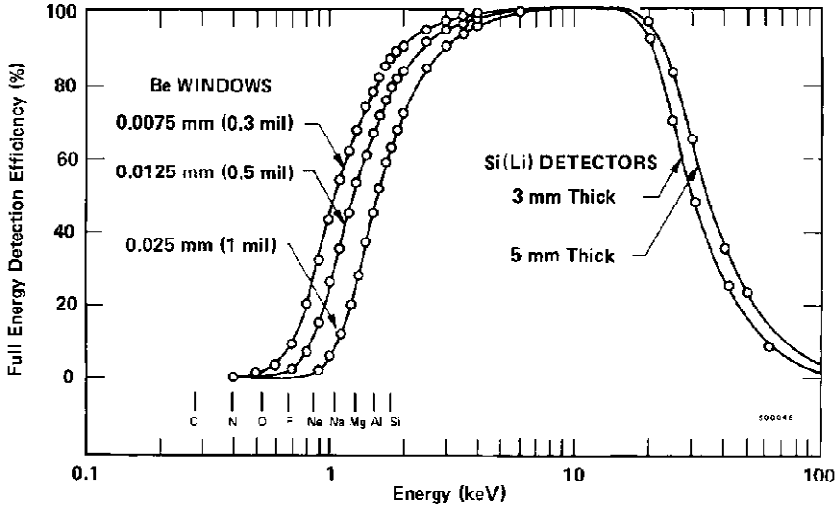

Figure 6.16: Detection Efficiency vs. Be Window Thickness on Low-Energy Curve and vs. Crystal Thickness on High-Energy Curve. Original picture of ORTEC.

Two independent experiments were done, both with the same setup. The syringe with a hypodermic needle was used as a spinning electrode. The 12% wt fresh aquous solution of PVA was used (see specifications in the part 6.1.2). Grounded bronze grid was used as a collector. Beryllium window of the detector was shielded by a thin paper towel to protect it against the polymer leakage. The coat of the detector was grounded too to protect it against high voltage discharge. The distance between Be window and bronze grid was kept at 10 mm. The schematic view of this experiment is sketched and documented in Fig. 6.17. The distance between the hypodermic needle and bronze grid was changed to prove amplifying factor mentioned in chapter 2, example E3. As will be explained in chapter 8, there is an extended theory independent to this amplifying factor called Counterion condensation which explains the mechanism of X-rays generation during electrospinning. Some influence, caused by changing the distance between the needle and the collector on X-rays energy was observed.

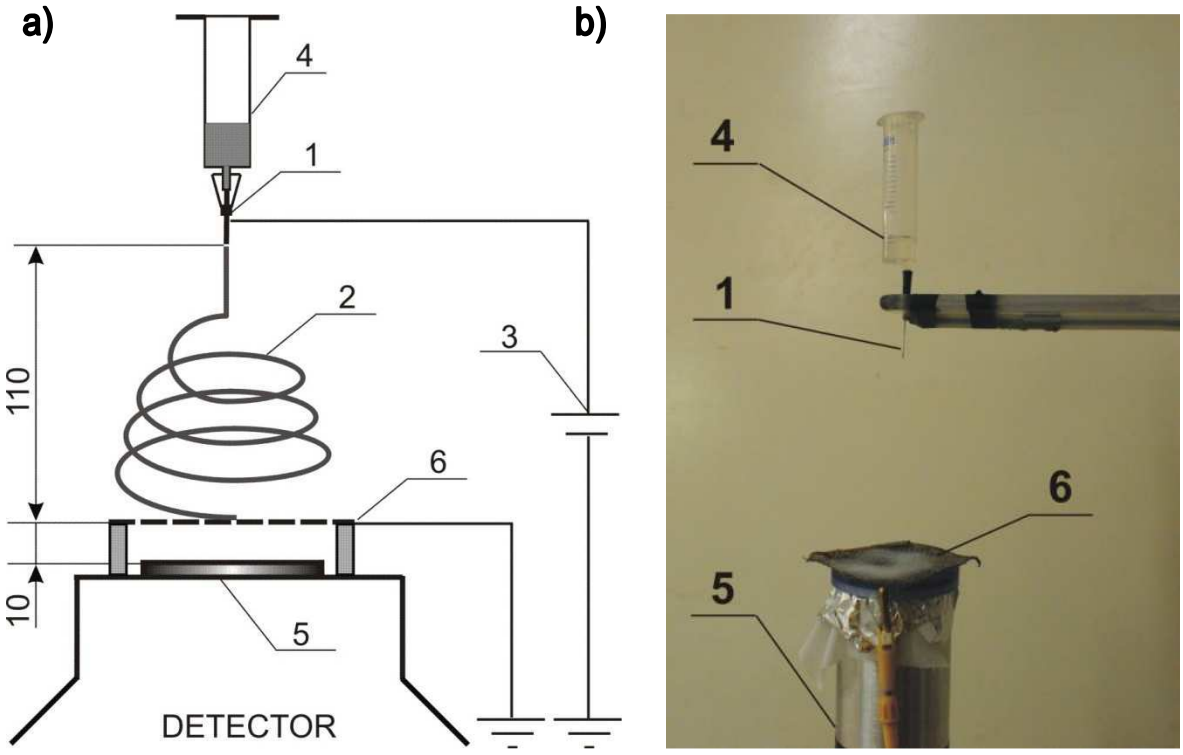

Figure 6.17: *Apparatus for a study of high-energy emission from electrospinning. (a), (b), Electrospinner consists of a hypodermic needle (1), from which a jet (2) is ejected, a high voltage source (3) and a syringe (4) supplying the needle with a polymeric solution. The SLP Detector (5) is positioned just behind the grounded screen collector (6). The distance between the needle tip and the collector is given in millimetres.*

Seven spectra were measured during the first experiment with variable distances between the hypodermic needle and bronze grid. Temperature during measurement was 25 ± 3°C, humidity 40 ± 3 % and time of each electrospinning measurement was 5 min. This was done to prove the existence of the amplifying factor mentioned in chapter 2 (example E3). The deposited nanofibrous layer during the experiment was captured on the grid and it therefore created another shield for X-rays.

The amplifying factor explanation for X-rays generation by nanofibre's deposition is not quite obvious, because another analysis (example E4) for a warp of parallel fibers disproved the possibility of reaching sufficiently high values of electrostatic field strength. It should be used for explanation of the deposition of one fiber. Generation of X-rays by the static sample wasn't proved experimentally by the spectral measurement due to the risk of harming the detector.

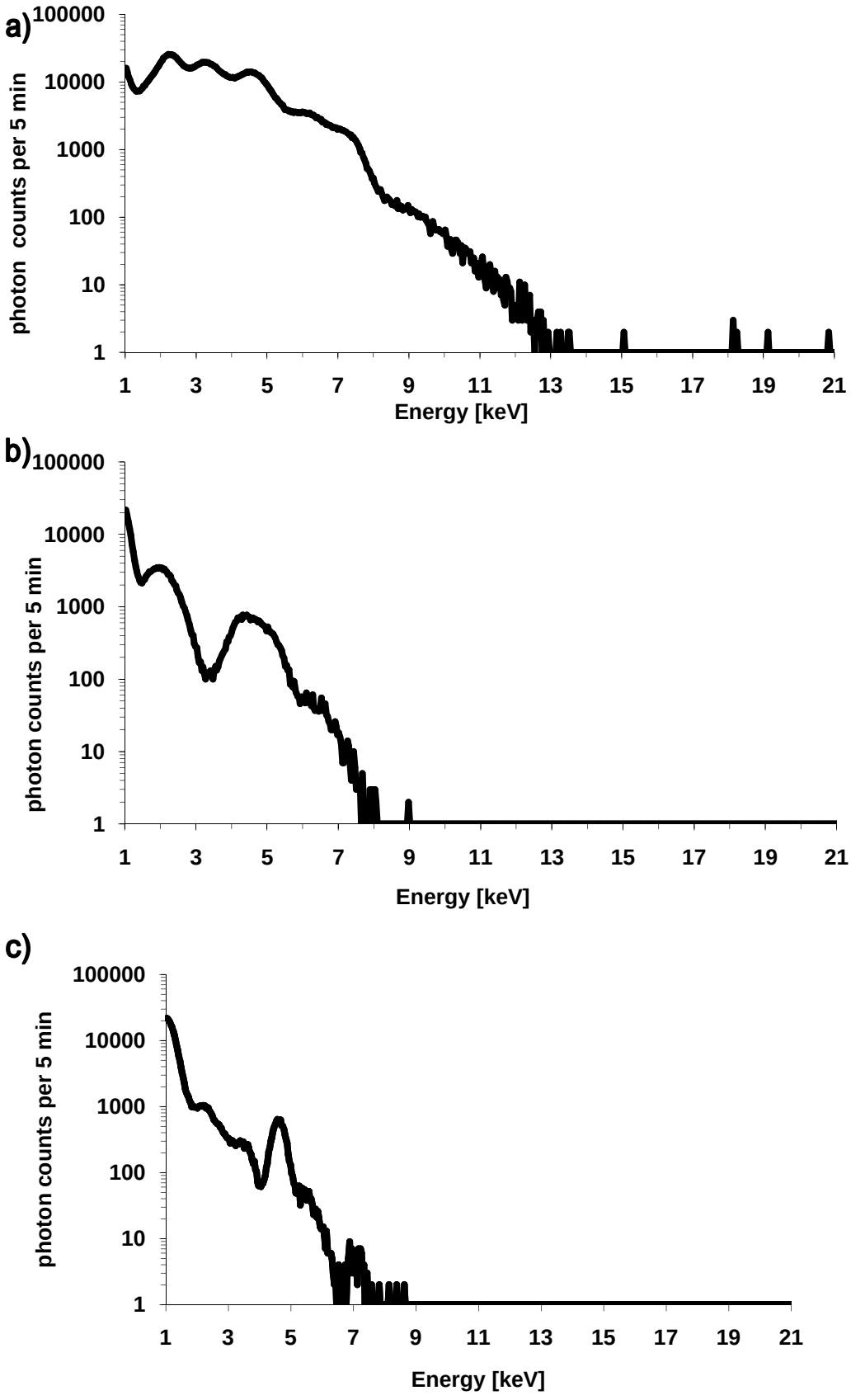
a)
photon counts per 5 min
100000
10000
1000
100
10
1
1 3 5 7 9 11 13 15 17 19 21
Energy [keV]
b)
photon counts per 5 min
100000
10000
1000
100
10
1
1 3 5 7 9 11 13 15 17 19 21
Energy [keV]
c)
photon counts per 5 min
100000
10000
1000
100
10
1
1 3 5 7 9 11 13 15 17 19 21
Energy [keV]

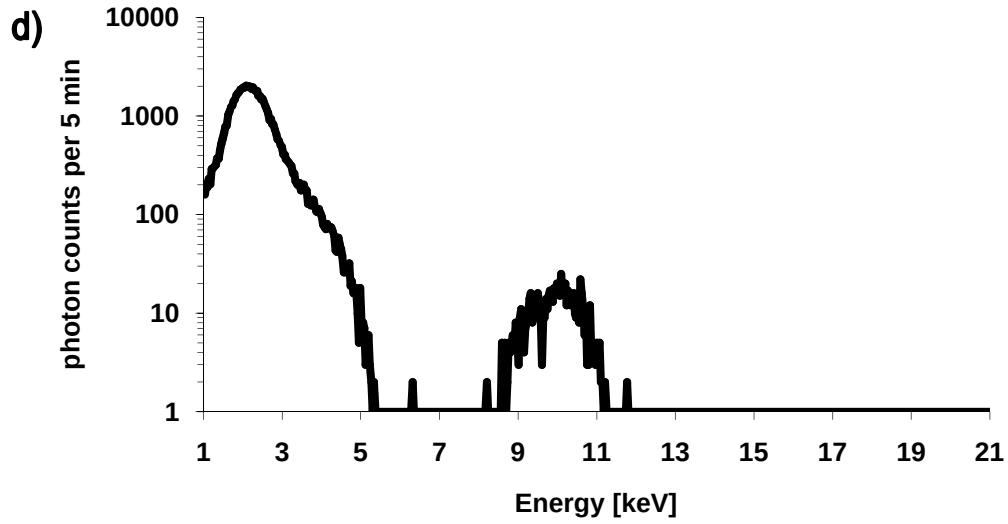
d)
10000
1000
100
10
1
photon counts per 5 min
1 3 5 7 9 11 13 15 17 19 21
Energy [keV]

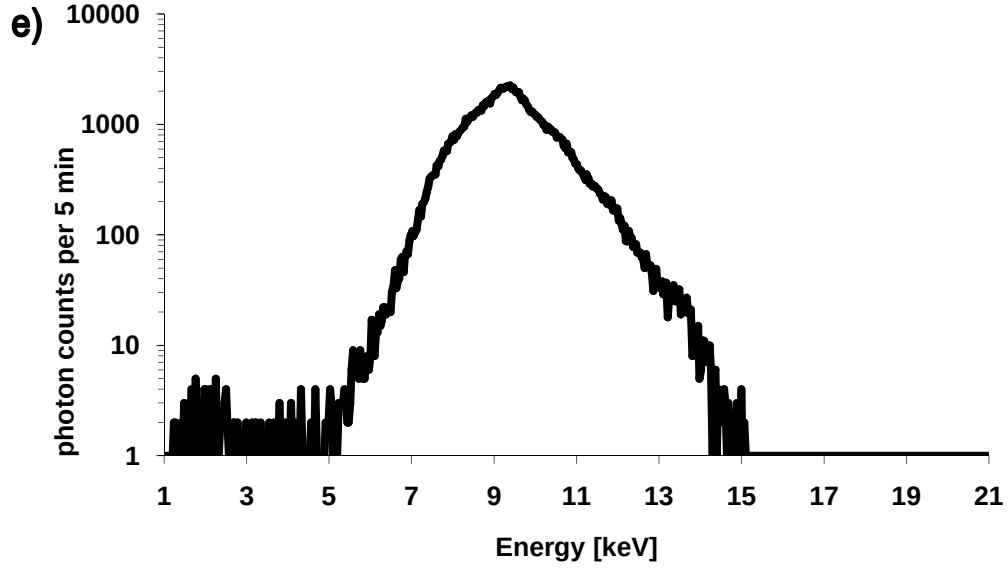
e)
10000
1000
100
10
1
photon counts per 5 min
1 3 5 7 9 11 13 15 17 19 21
Energy [keV]

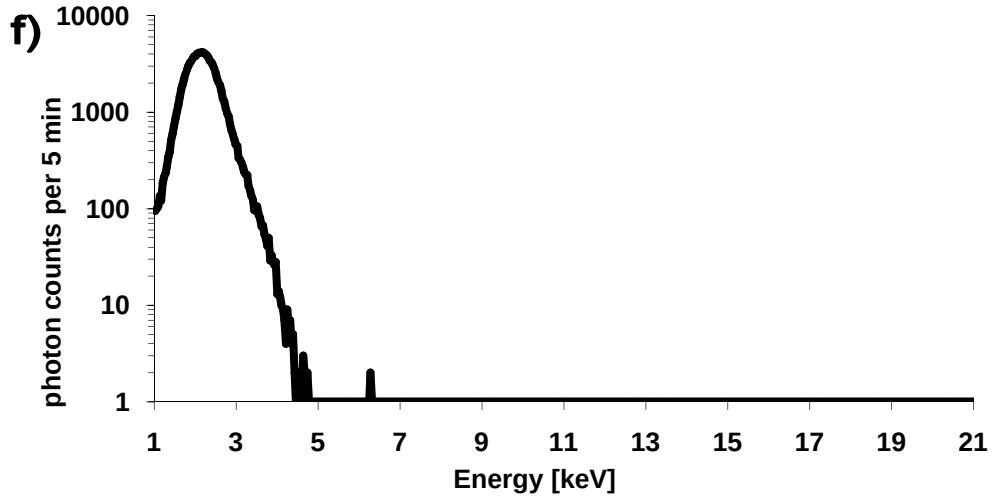
f)
10000
1000
100
10
1
photon counts per 5 min
1 3 5 7 9 11 13 15 17 19 21
Energy [keV]

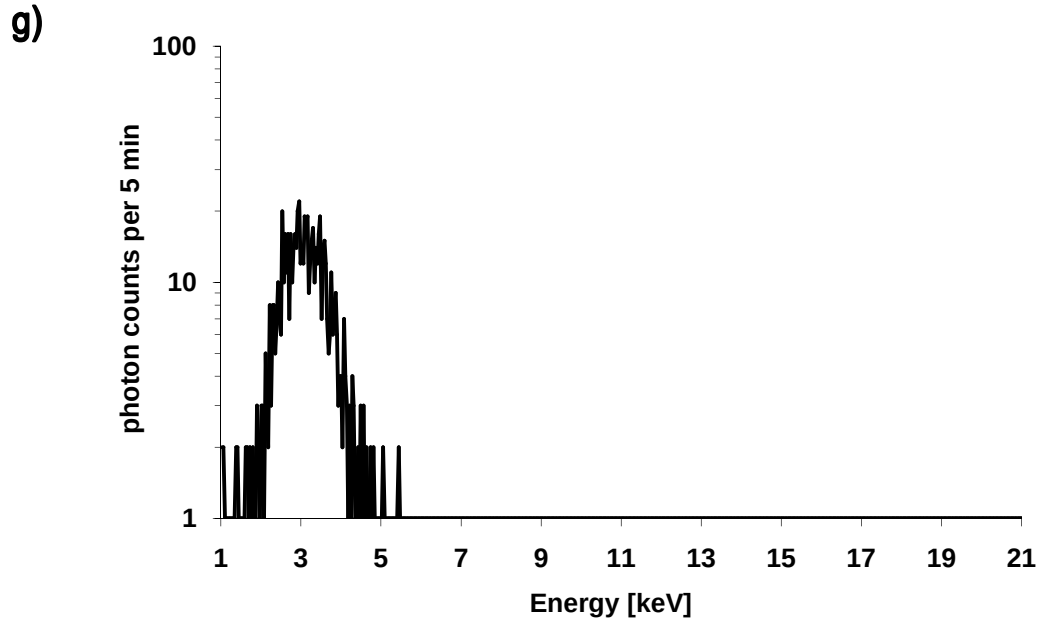

Figure 6.18: First spectral measurements of X-rays generated by the electrospinning process and testing of validity of amplifying factor: a), b), c), d), e) distance from Be window 10 cm, voltage 30 kV f) distance 7.5 cm, voltage 22.5 kV, g) distance 5 cm and 15 kV.

Second spectral measurement was done several months later with the accent on the spectroscopy evidence of the existence of the X-rays generation during the nanofiber's deposition and elimination of all possible parasite effects. Several parameters were controlled such as temperature, humidity, flow rate of the polymeric solution and some rheological properties of the polymeric solution. As was mentioned above in this chapter, many experiments with radiographic films were done before and it was proved, that the process of X-rays generation is affected by many parameters. That's why many experiments were done without any signal of X-rays. The only one spectrum was obtained and recorded. There was an Aluminum foil placed in between the Beryllium window and bronze grid to measure K-absorption line of aluminum. The bronze grid was at this time coated on one side by thin layer of gold. As can be clearly seen in Fig. 6.19, the non-destructive physical evidence of existence of X-rays generation by the electrospinning process was made. K absorption line measured here is slightly wider due to using of Aluminum foil which is alloyed by other elements instead of pure Aluminum.

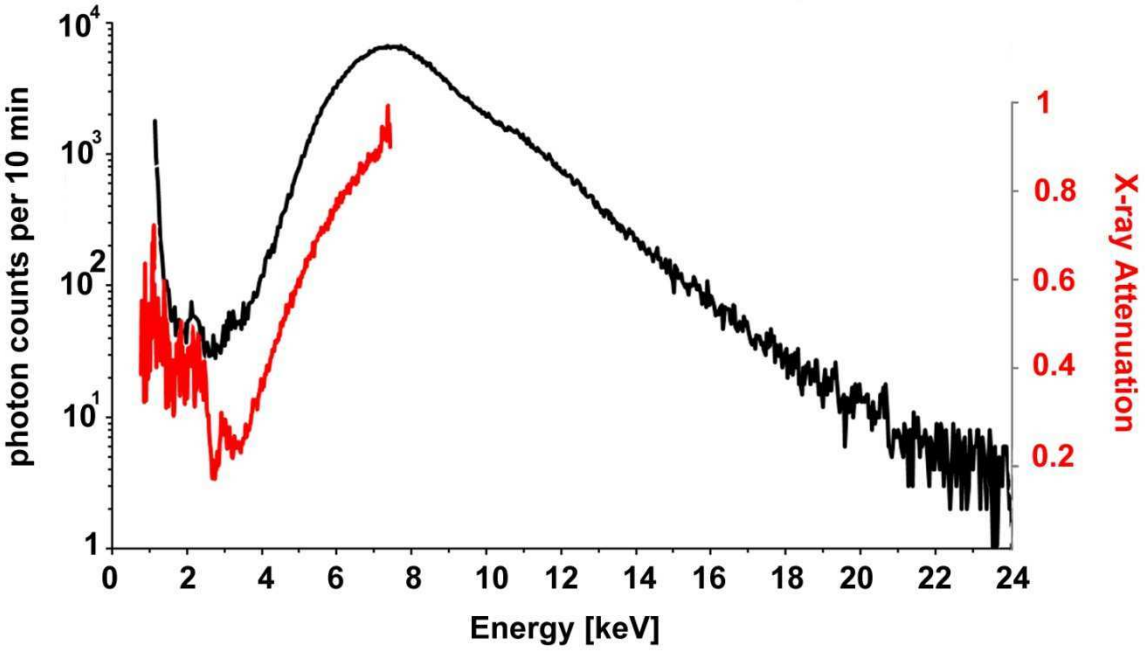

Figure 6.19: Spectral measurement of X-rays produced by electrospinning (black) and comparation spectral K-line absorption of Aluminum foil measured using X-ray tube TF 3005/Mo (red).

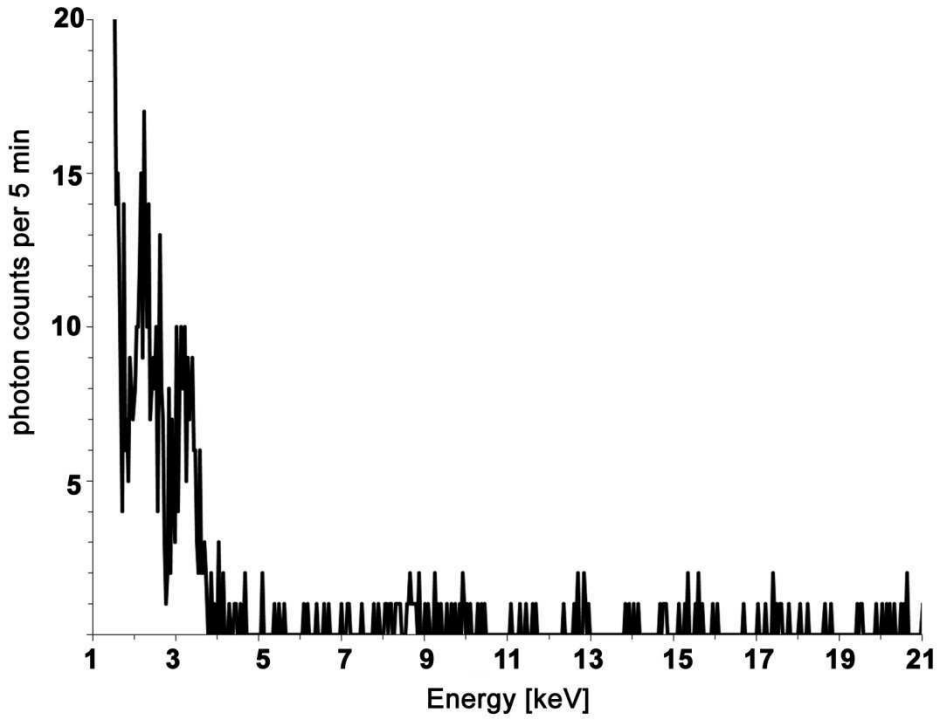

Figure 6.20: Measurement of background noise created by high voltage applied in between electrodes without electrospinning process running.

Measurement of spectral K-line was made using X-ray tube TF 3005/Mo and by the comparison of spectrum with and without Aluminum foils shielding of the Beryllium window. Measurement of noise created by application of high voltage between electrodes without electrospinning process running for five minutes was made too (see Fig. 6.20). There wasn't any signal above range of tens of events detected during this measurement.

Now emerges another important question which has to be answered. Why the repetability of spectral measurement of X-rays of the electrospinning process is so difficult and which parameters are responsible for that? Only every eighteenth experiment of detection of X-rays was successful. The 12% wt water solution of PVA was the same as for all previous examples and the used hypodermic needle has outer diameter 8.5 mm and an inner diameter of 0.55 mm pointing downwards. The humidity at the laboratory was 45 ±5% and the temperature was around 20°C. It is very difficult to control the flow rate through the needle because it depends on many rheological parameters of the polymer. There is a serious suspicion that the X-rays generation depends on the diameter of the deposited fiber, because thinner fiber concentrates higher electric field. Therefore it is important to analyze the morphology of the sample with deposited nanofibers and measure their diameters.

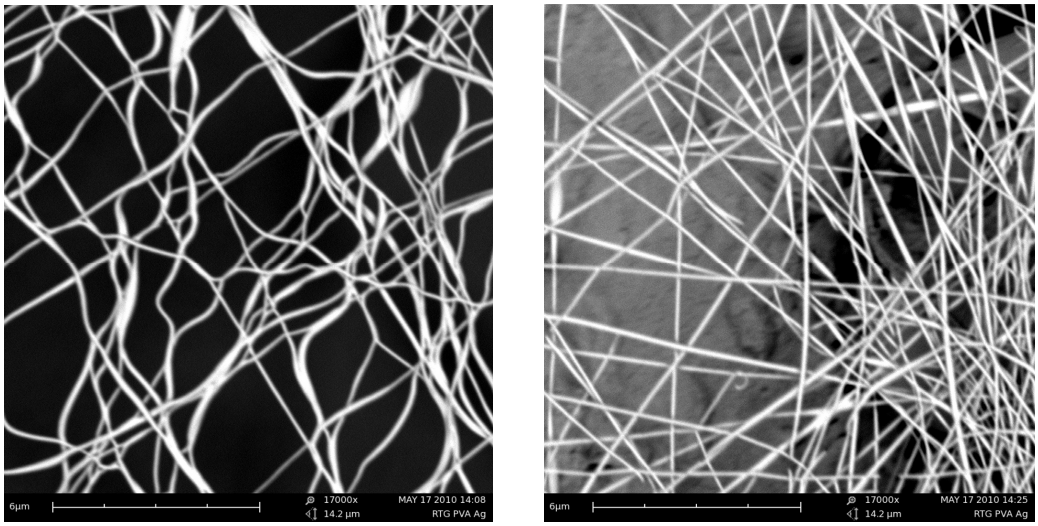

Figure 6.21: Micrographs of deposited nanofibers taken from the SLP detector made by scanning electron microscopy PHENOM. Fibers are around 100 nm in diameter.

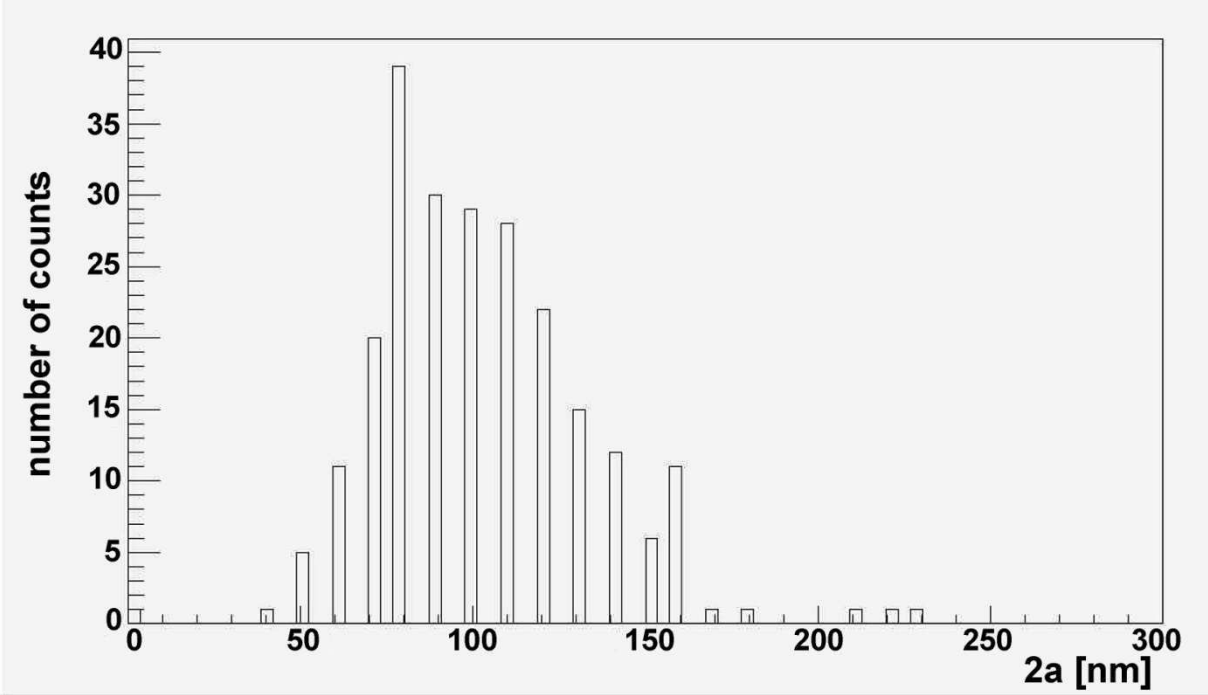

Figure 6.22: Analysis of nanofiber's diameters deposited on the bronze grid of the collector during the spectral measurement of the X-rays generation.

Analysis of deposited nanofibrous layer during the experiment was done by scanning electron table top microscope PHENOM and measurement of fiber's diameter was carried out by Lucia software. As obvious from Fig 6.21 and 6.22, the diameters of fibers are very small. Average diameters are in the range from 40 – 150 nm and the most fibers have a diameter around 80 nm. Quite many of them have diameter even smaller than 80 nm. So there is a strong believe that the X-ray generation is somehow connected with the diameters of produced fibers. Some theoretical explanation will be done in following chapters, mainly in the chapter 8 entitled as Counterion condensation theory.

7. Electromagnetic radiation with main focus on X-rays

Electromagnetic radiation is usually created by an accelerated motion of electrically charged particles. This radiation travels through vacuum as well as through air and other substances. A source of electromagnetic radiation as a form of energy should be explained as waves or as particles. It is called as Wave-Particle Duality. It exhibits both particle and wave properties. Some experiments prove the description of light as waves such for example double-split experiment. On the other hand the photoelectric effect introduced firm evidence of a particle nature as well. The particle properties of electrons were well documented when the DeBroglie hypothesis and the subsequent experiments by Davisson and Germer established the wave nature of the electron. Main classification of a wave is based on its wavelength λ As was found by Max Planck (1901) both characterizations are joined into one simple formula.

$$E = hf = hc/\lambda, \tag{7.1}$$

where E is energy of photon, $h = 6.626068 \times 10^{-34}\ \mathrm{m^2\ kg/s}$ is the Planck's constant, f is the frequency, c is speed of light in vacuum and λ denotes wavelength. There are many regions in electromagnetic radiation's scale. The visible light is one of them. One can have a look into detailed characterization of electromagnetic radiation clases in Tab. 7.1.

As is obvious from Table 7.1, electromagnetic waves are subdivided into six main regions. The lowest energetic and with the longest wavelengths are the radio waves. They are followed by infrared waves (IR), visible light with frequencies between 720 – 400 nm, ultraviolet waves (UV), X-rays and Gamma rays. Our main focus will be for waves with energies higher than 100 eV. This is the border of Extreme ultraviolet (EUV) and soft X-rays waves. Both regions are not precisely defined. There isn't also any exact limit which will divide soft/hard x-rays. But one has to determine some division of these regions. So let classify all waves (photons) with higher energies than 124 eV be already soft X-rays and with energy higher than 12.4 keV be hard X-rays as can be for example seen in Tipler (2004). This work will not focus on gamma rays, because their energies are much higher than what we measured (see chapter 6).

Class	frequency	wavelength	energy
γ rays	300 EHz	1pm	1.24 MeV
Hard X-rays	**30 EHz**	**10 pm**	**124 keV**
Soft X-rays	**3 EHz**	**100 pm**	**12.4 keV**
Extreme UV	**30 PHz**	**10 nm**	**124 eV**
Near Ultra Violet	300 THz	1μm	1.24 eV
Near Infra red	30 THz	10 μm	124 meV
Moderate infrared	3 THz	100μm	12.4 meV
Extreme high freq.	300 GHz	1 cm	1.24 meV
Super high freq.	30 GHz	10 cm	124 μeV
Ultra light freq.	3 GHz	100 cm	12.4 μeV
Very high freq.	300 MHz	1 m	1.24 μeV
High frequency	30 MHz	10 m	124 neV
Medium freq.	3 MHz	100 m	12.4 neV
Low freq	300 kHz	1 km	1.24 neV
Very low freq	30 kHz	10 km	124 peV

Table 7.1: Characterization of electromagnetic radiation subdivided by its wavelength and energy into classes. All values (i.e. frequency, wavelength and energy) represent here the upper limit of the subdivision of the el.mag. spectrum.

7.1 Energy levels

To understand mechanism of generation of X-rays and even lower energetic subdivisions of electromagnetic spectra, one has to explain basic principles of quantum mechanics of our system. A quantum mechanical system can reach only discrete values of energy (formula 7.1), as opposed to the classical mechanical system which can reach any energy. These discrete values of energy are called energy levels and are commonly used for electrons orbiting the nucleus or for the atoms or molecules. Every energy level is strictly quantized. The wave function of an electron in the atom has the form of standing waves. Only electrons with no time dependance probability density can occupy energy levels wiyh corresponding integral numbers of wavelengths. These states are called stationary and other states have zero probability density.

Excitation/de-excitation of electron to the higher/lower energy can be done by the absorption/emission of the quantum of energy when the probability density of the electron has been vibrating. It is grossly represented by the accelerated movement of electric charge. This is very complicated resonant process when electron passes through non-stationary states.

Electrons always tend to occupy levels with the lowest energy to keep system stabilized and energetically optimal. Bigger difference between levels means higher energy of absorption/emission is needed or released. Some more details were introduced for example by French (1978). If the magnetic field is affecting the movement of the charged particle, cyclotron radiation is emitted. But there is no any magnetic field observed during electrospinning process.

7.2 Characterization of selected subdivisions of electromagnetic spectrum

Three main clases of electromagnetic spectrum important for detection of radiation generated by electrospinning process will be introduced in this article.

7.2.1 Extreme ultraviolet region

Extreme ultraviolet subtype of electromagnetic radiation is the most energetic part of UV spectrum. It has wavelengths between 1μm – 10 nm and energies from 1.24 eV up to 124 eV. EUV is naturally generated by solar corona and significantly by plasma sources. To emit EUV radiation, we have to primarily ionize atoms. It is typically emitted by electrons which are bound to the charged positive ions. Bonds between electrons and charged positive ions are weaker then bonds of typical valence electrons. Primarily ionized particle has to be energetic enough to cause bound electrons to be excited to the conduction band in the case of solids or free electron state. As these freed electrons return to the parent ion they accelerate and emit high energetic photons. Absorption of these energetic photons (EUV or X-ray) lead to the creation of electron-hole pairs with time of life in femtoseconds or microseconds, depending on the band structure. This cascade of electron-hole pairs leads to the excitation of high energetic photoelectrons or Auger's electrons and holes which can produce secondary electrons. Absorption of high energetic photon in EUV or X-ray region generates other photoelectrons or secondary electrons which can later accelerate other electrons by the process of impact ionization or emission of Auger's electron as described by Bass (1995). Energy of absorbed EUV photon should be then lost to electron binding energy, which is the energy of unbounded electron from potential well of nucleus or to the photoelectron initial kinetic energy. Photoelectron loses its energy by ionization of the atom and by generation of secondary electrons. These secondary electrons are then usually decelerated by production of the heat, but sometimes they can continue with ionization of atoms and generate tertiary electrons. For every absorbed EUV photon, about 4 secondary electrons are generated,

Kozawa (1992). These secondary electrons have energies of few to tens of eV and can travel tens of nanometers in polymers because they have significant amounts of free volume. It is very difficult to detect EUV photons at atmospheric conditions due to their very low penetrability. One has to use vacuum systems for their detection as is used in EUV lithography which is a promising technique for future microprocessor's technology, Bakshi (2008).

7.2.2 Röentgen radiation (X-rays)

When Wilhelm Conrad Röntgen (1895), Fig. 7.1A, firstly observed for that time unknown radiation, he simply called it X-rays, for many people known now as Röentgen radiation. He get historically first Nobel prize in 1901 for this remarkable discovery. Discovery of X-rays has been voted as the most important modern discovery by the British public, in a Science Museum poll in November 5th, 2009. This fact highlights how important this discovery for modern life was.

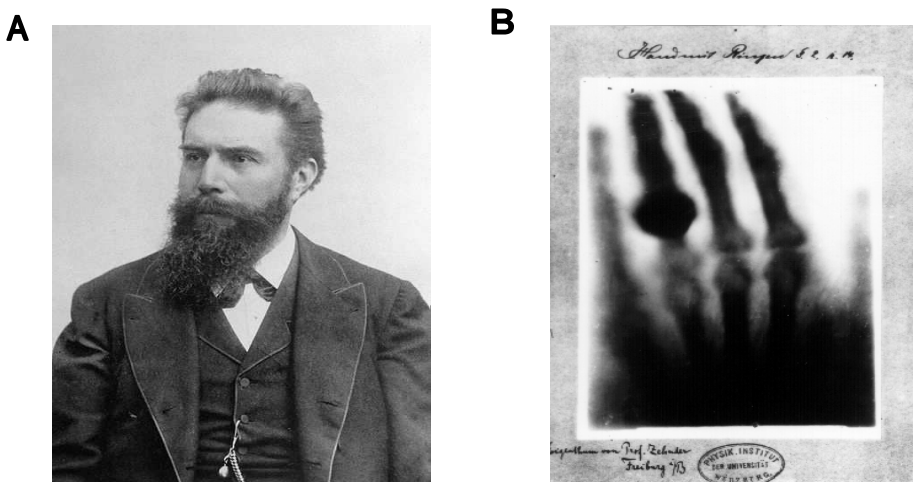

Figure 7.1: A) Wilhelm Conrad Röentgen. B) Anna Bertha's hand, first radiograph.

The first picture using X-rays was his wife's hand. This picture is very famous around all the world and known as the first radiograph (Fig 7.1 B). More details about Röntgen is available in Howard (1995).

Waves with wavelengths lower than 10 nm (energy higher than 124 eV) are usually already clasified as soft X-ray subdivision of electromagnetic spectrum. Energy of X-rays can go up to hundreds of keV, where gamma radiation starts to dominate. There isn't the clear

border between soft and hard X-rays, but one can estimate it around 12 keV , see Tipler (2004) . Due to our observations we will focus mainly on soft X-ray region.

The simplest process how to generate X-rays is to have vacuumed vessel with cathode which emits thermal electrons by high electric field. These electrons are later accelerated and after a strike are absorbed by anode, which is usually made by some material with high atomic number. These electrons collide with atoms of anode's material and create X-ray radiation. This mechanism will be described later in this chapter. The efficiency of such system is very low. Many electrons loses its energy in the form of heat as was described in the previous chapter and anode has to be cooled by water. Schema of a simple X-ray tube is introduced in Fig. 7.2.

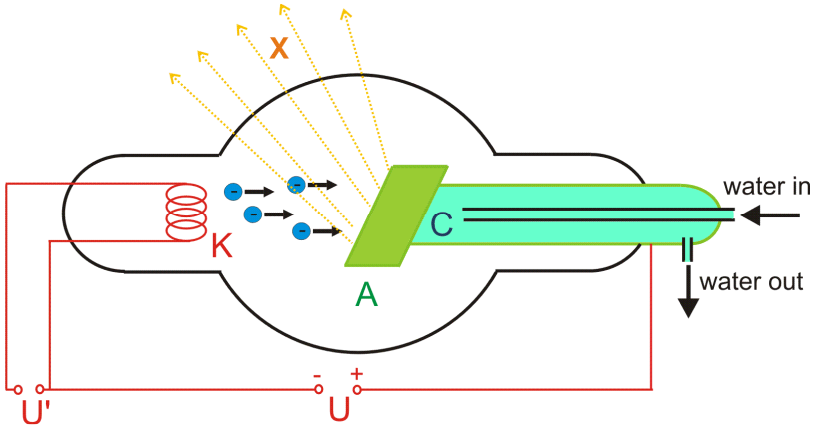

Figure 7.2: Schematic drawing of simple X-ray tube. (K) is a cathode emitting electrons, (A) is an anode made by some heavy material, (C) is cooling of anode, (U') is applied voltage on cathode and (U) is voltage of the system.

7.3 Mechanisms of generation of X-rays.

The main physical interest in following chapters will be focused on processes of X-ray generation. There are two possibilities of generation of X-rays. First is called Bremsstrahlung and second is named Characteristic radiation. Several mechanisms of X-ray generation will be explained here.

7.3.1 Bremsstrahlung

The most common process of X-ray generation is called Bremsstrahlung (i.e., braking radiation). When the freed electron or charged particle has been accelerated or decelerated an electromagnetic radiation included synchrotron radiation is emitted similarly as is described in production of EUV photons mentioned in previous chapter. It is frequently used for

radiation of electrons stopping in matter. Now we deal with higher energies of electromagnetic radiation. When freed accelerated electron travels close to the nucleus of some heavy atom it changes its direction and the electron decelerates by the Coulomb force. It is obvious that Coulombic attraction increases with higher atomic number and therefore loses of electron's kinetic energy increases too. Spectrum of this radiation has continuous distribution. Figure of bremmstrahlung can be seen in Fig 7.3.

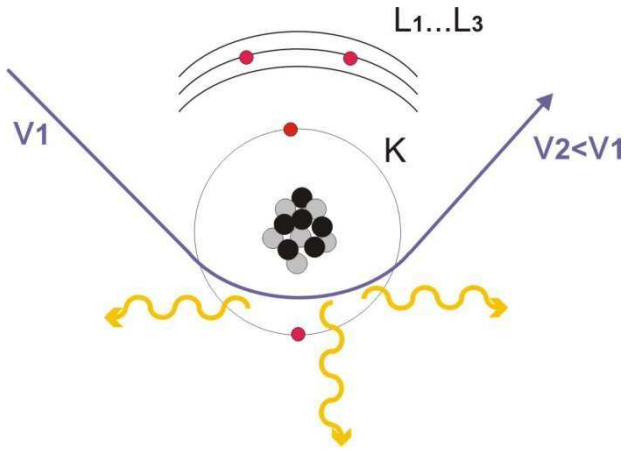

Figure 7.3: Schematic picture of Bremsstrahlung radiation

7.3.2 X-ray radiation produced by acceleration of single point charge

Consider a particle accelerated by electric field in the direction collinear to its original direction of the speed. Total radiated power R passing out through the surface (spherical shell) is according to Griffiths (1999):

$$R \cong \oint \vec{S} \cdot d\vec{a} = \frac{\mu_0}{6\pi c}\left(\frac{d^2\vec{p}}{dt^2}\right)^2 \quad , \tag{7.2}$$

where $\vec{S} = 1/\mu_0 \cdot \vec{E} \times \vec{B}$ is the Poynting vector; $\vec{a}$ is the acceleration of the particle, μ_0 is the permeability of vacuum, $\vec{p}$ is momentum of the particle, t is time and c is speed of light in vacuum. For oscillating electric dipole the dipole momentum will have form: $p = p_0 \cos(\omega t)$ and $\ddot{p} = -\omega^2 p_0 \cos(\omega t)$. Total radiated power for dipole radiation will be: $\langle P \rangle = \mu_0 p_0^2 \omega^4 / 12\pi c$. But more important example for our needs is the radiation radiated by single point charge accelerated by electrostatic field.

Charge momentum $\vec{p}(t)$ of the single point charge q is $\vec{p}(t) = q\vec{d}(t)$ with trajectory $\vec{d}$ of the charge with respect to the origin. Accordingly its second derivation will be:

$d^2\vec{p}(t)/dt^2 = q\vec{a}(t)$ since electric charge is invariant. Therefore the radiated power *R* in this case is according to Griffiths (1999) is:

$$R = \frac{\mu_0 q^2 \vec{a}^2}{6\pi c}. \tag{7.3}$$

This is the famous **Larmor formula** which tells us, that the power radiated by single point charge is proportional to square of its acceleration. More detailed explanation was done for example by Griffiths (1999). The radiation energy propagates itself to the infinity. Although this formula was found with assumption that $\vec{v} = 0$ which should be done by smart choice of reference system, it holds to good approximation as long as $\vec{v} << c$. Otherwise one has to include relativistic behavior of the charged particle. Solution of radiated power from high speed charged particles was calculated by Griffiths (1999) using **Lienard's generalization** of Larmor formula:

$$R = \frac{\mu_0 q^2 \vec{a}^2 \gamma^6}{6\pi c}\left(\vec{a}^2 - \left|\frac{\vec{v}\times\vec{a}}{c}\right|^2\right), \tag{7.4}$$

where $\gamma = 1/\sqrt{1-(v^2/c^2)}$ is the Lorentz factor and it is obvious that radiated power grows enormously when the speed of the charged particle approaches to the speed of light.

For the collinear speed $\vec{v}$ and acceleration $\vec{a}$ i.e. when $\vec{v}\times\vec{a} = 0$, of the charged particle, the Lienard formula has according to Griffiths (1999) form:

$$R = \frac{\mu_0 q^2 \vec{a}^2 \gamma^6}{6\pi c} = \frac{q^2 \vec{a}^2 \gamma^6}{6\pi\varepsilon_0 c^3}. \tag{7.5}$$

One can see that angular distribution of radiation is the same whether the particle is accelerating or decelerating due to square root of $\vec{a}$ in the simplified Lienard formula. So when the electron with high speed is decelerated by some heavy target, the lost of its energy is emitted in a form of electromagnetic radiation and it is therefore called braking radiation or **Bremsstrahlung** (in German language). When the speed of charged particle is constant, $\vec{a} = 0$, it does not emit any radiation. Only when particle is accelerated or decelerated, emission of radiation will occur. The energy lost by the particle in any given interval must be therefore equal to energy of emitted radiation. Every accelerated/decelerated particle emits electromagnetic radiation on which is then acting radiation reaction (recoil) Abraham-Lorentz

force $\vec{F}_{rad} = \frac{\mu_0 q^2}{6\pi c}\dot{a}$ and relativistic Abraham-Lorentz-Dirac force experienced by relativistic charged particle due to electromagnetic field expressed by Dirac (1938).

7.3.3 Thermal Bremsstrahlung

Every charged accelerating or decelerating particle in plasma produces microscopic electric field. In addition we apply a macroscopic electrostatic field externally to plasma. The motion of each charged particle is therefore affected by both macroscopic and microscopic electric fields. These mutual interactions between particles and electric field produce many interesting phenomena in plasma. It is important to consider processes in which particles are scattered by the fluctuating microscopic electrostatic fields and then radiate X-rays. Such processes are called Bremsstrahlung of plasma, thermal Bremsstrahlung or free-free emission. This process is done by the collision of free electrons with the ions. Analytical explanation of this phenomenon is very complicated and various approximations have to be made. For example, interaction of electron-electron is very weak compare to electron's initial energy and therefore can be neglected. Only electron-ion collisions are important, and only electrons emit radiation significantly during collisions. The mean electron kinetic energy E_T in plasma of temperature T can be calculated from well known partition theorem for one degree of freedom:

$$E_T = \frac{1}{2} k_B T \qquad (7.6)$$

So from our measured energy of X-rays up to 15 keV, the temperature of plasma has to be at least in order of 10^8 K if thermal Bremsstrahlung is responsible for X-rays observed during electrospinning.

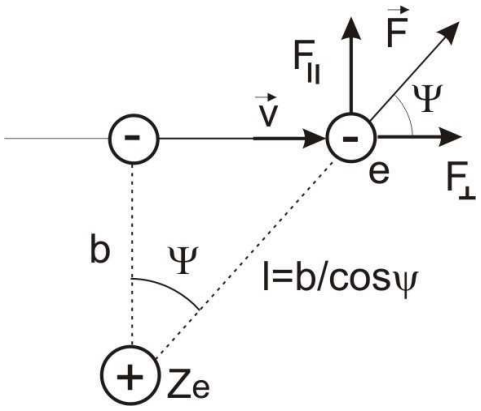

Figure 7.4: Fast electron passing a slow, heavy ion. The distance b of the closest approach of the electron to the ion is called impact factor and the interval t=b/v is called collision time.

During interaction, electron will be accelerated by electrostatic field in parallel and perpendicular to the path of the ion. But its parallel acceleration will emit much higher energetic photon, then the perpendicular one. The perpendicular acceleration emits radio frequencies which are important for studying of far away galaxies. More details were written by Rybicki (1979) or Ichimaru (1973). The force can be calculated from simple formula:

$$F_{\perp} = ma_{\perp} = \frac{1}{4\pi\varepsilon_0}\frac{Ze^2}{l^2}\cos\psi = \frac{1}{4\pi\varepsilon_0}\frac{Ze^2}{b^2}\cos^3\psi\,, \tag{7.7}$$

$$F_{\parallel} = ma_{\parallel} = \frac{1}{4\pi\varepsilon_0}\frac{Ze^2}{l^2}\sin\psi = \frac{1}{4\pi\varepsilon_0}\frac{Ze^2}{b^2}\sin\psi\cos^2\psi\,, \tag{7.8}$$

where *Z* is Atomic number (number of protons found in nucleus). One can now find Larmor formula (7.3),(7.5) for parallel acceleration in the form:

$$R_{\parallel} = \frac{e^2}{6\pi\varepsilon_0 c^3}\frac{Z^2e^4}{m_e^{\,2}}\left(\frac{\sin\psi\cos^2\psi}{b^2}\right)^2. \tag{7.9}$$

And by the comparison of all mentioned formulas (7.3),(7.5) and (7.9) it is possible to find relation for parallel acceleration of the particle

$$a_{\parallel} = \frac{Ze^2\sin\psi\cos^2\psi}{m_e b^2}\quad. \tag{7.10}$$

Another detailed explanation and calculation of Larmor's formula was done by Sarazin (1986).

7.3.4 Characteristic radiation

Another process of generation of X-rays is called characteristic radiation, a process called inner-shell ionization. When the high energy electron "knock out" by the Coulombic repulsion another electron bounded in the atom, this electron should be ejected out from the atom. Another electron from higher energy level then shift to its level due to the stability reason. Energetic difference between these levels is emitted in form of electromagnetic radiation. About 0.1% of all ejected electrons produce K-shell vacancies; most produce heat. It is obvious that higher difference between levels causes an emission of more energetic characteristic radiation. To obtain radiation in X-ray region, heavy element is needed. Spectrum of this radiation is strictly quantified, because energy levels differences are quantized. Possible energetic levels for characteristic X-rays can be K-shells, L-shells and M-shells. When electron is transferred from L-shell n=2 to K-shell n=1, K-alpha X-rays are emitted, when from n=3 to n=1, K-beta X-rays are emitted. Transitions to L-shells are called as L X-rays. When electron is transfered from n=3 to n=2, L-alpha and form n=4 to n=2, L-beta X-rays are emitted and so on.

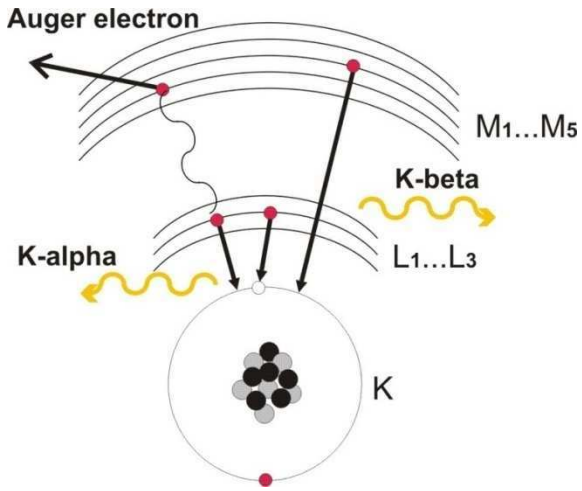

Figure 7.5: Schematic principles of generation of characteristic radiation

To find possible elements for characteristic X-rays generation, one can use Moseley (1913) formula:

$$hf_{K\alpha} = \frac{3}{4}13.6 \cdot (Z-1)^2 eV \;\; ; \;\; hf_{L\alpha} = \frac{5}{36}13.6 \cdot (Z-7.4)^2 eV \qquad (7.11)$$

Which predicts energy (frequency f) of emitted characteristic K-alpha and L-alpha X-rays for element with atomic number Z. Simple plot of Moseley's (1913) law can be seen in Fig. 7.6 .

One can see, that K-alpha X-rays are observable for elements with higher atomic number than 13 (Aluminum) and L-alpha X-rays are observable for Z > 39 (Yttrium).

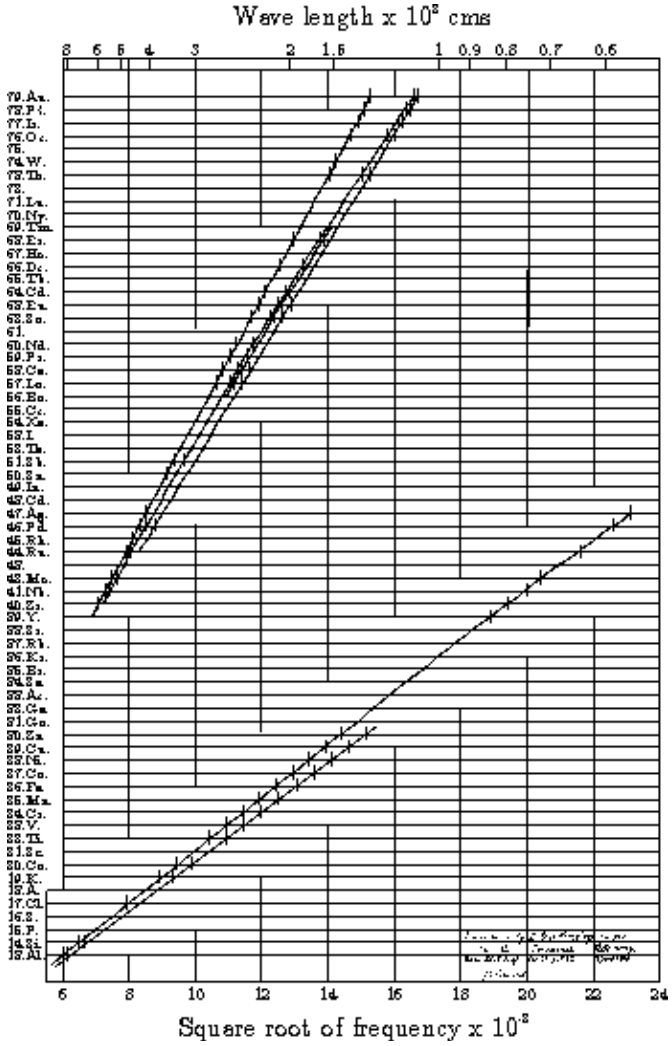

Figure 7.6: Scan of original picture from Moseley's (1913) work. Picture shows dependency of square root of frequency of characteristic X-ray radiation for elements with different atomic number. Lower line is for K-alpha X-rays and upper line is for L-alpha X-rays.

The detailed absorptions of the X-rays in different materials were calculated by Hubbell and Seltzer (1989).

7.3.5 X-ray emission by heavy ions, Particle Induced X-ray Emission (PIXE)

The phenomenon of X-ray emission by heavy ions was firstly reported by Chadwick (1912). There are elastic and non elastic collisions of ions with the atoms of the target when

ions pass through the matter. Electrons are forced to the higher energetic levels during non elastic – electron collisions. Vacations created by emitted electrons are then filled by electrons from higher energetic levels accompanying by the emission of the Auger's electron or by the radiation of X-ray photon which can be then detected. PIXE ions exploit the ionization of inner levels and the spectral lines K, L, M are emitted depending on the position of indigenous vacation.

Interaction of ions with atoms depends on the energy of an ion inside matter. Therefore braking of the ion changes its energy according to its depth inside a matter. Not all X-rays radiation is emitted in the form of characteristic radiation and bombarding of a matter by ions accompanied by emission of the continuous radiation (bremsstrahlung). Energy of electromagnetic radiation produced by Bremsstrahlung is much lower for ions than for electrons. Maximal kinetic energy lost after the collision of the stationary electron with accelerated ion with the energy E_1 can be expressed:

$$E_{\max} = 4\frac{m_e M_i}{(m_e + M_i)^2} E_1, \tag{7.12}$$

where m_e is the mass of the electron and M_i is the mass of the ion. Energy $E_{\max}$ depends on the mass of the ion by the inverse proportionality.

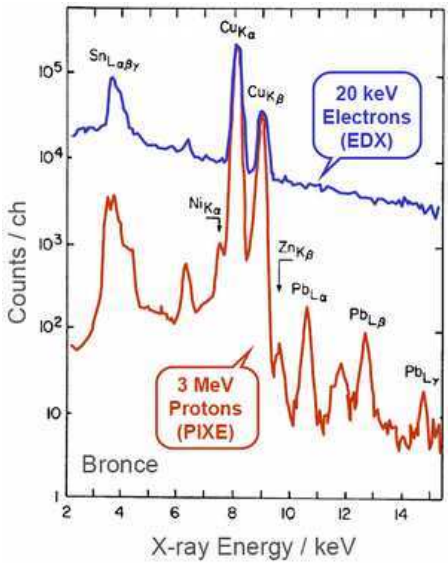

Figure 7.7: Comparison of PIXE and Electron microprobes (EDX). PIXE is generally approx. 100 times more sensitive than EDX, (ETH, Swiss Federal Institute of Technology, Zurich)

Detailed description of PIXE was done for example by Govil (2001). Since 1990 many publications were written in magazine International Journal of PIXE (IJPIXE) which was

created due to the description of this phenomenon. PIXE is under the strong focus of research for last two decades due to its using for a surface analysis.

7.3.6 X-ray emission during thunderstorms

One of the last processes of X-ray generation mentioned here was observed by Gurevich (1997). Process is determined by the multiple runaway breakdown caused by thunderstorm electric field. Generation of X-ray fluxes in thunderstorms has been attributed to bremsstrahlung of high energy electrons produced by runaway breakdown. The runaway breakdown is triggered by secondary cosmic-ray electrons, which are accelerated by the thunderstorm electric field producing next generation of high energy electrons. In the presence of thunderstorm electric fields, the beam of runaway electrons can propagate over hundreds of meters in the atmosphere and ultimately transfer a significant amount of charge. Since the critical field for runaway breakdown is an order of magnitude less than the threshold of conventional air breakdown, the multiple runaway breakdown triggered by cosmic rays develops during the preconditioning stage of a thunderstorm which precedes a lightning flash. That process leads to X-ray emission, and to fast transfer of electric charge in thunderstorm electric fields.

7.3.7 X-ray flashes produced by stick-slip friction in peeling tape

Putterman with his colleagues observed an interesting production of X-rays by the friction in peeling tape. They explained it by the process called triboluminiscence which has been known process to produce visible light by the relative motion between two contacting surfaces. They observed nanosecond flashes of electromagnetic radiation in X-rays area by the peeling of common adhesive tape in vacuum system. The detector used for this study consisted a scintillating detector. The main observed peak was at 15 keV but some energy was more than 60 keV. Their report was published in Nature, see Camara (2008).

Example 7.1: *Simple calculation of emission of freed electrons in Manning region (explained in detail in chapter8) can be done using non-relativistic Larmor formula. Lets calculate initial kinetic energy of the electron accelerated in external electric field*

Strength of the external electrostatic field E (see chapter 8) affecting the electron is:

$F = eE = 1{,}602\times10^{-19}\ 150\times10^{9}\ \mathrm{N} = 240\mathrm{x}10^{-10}\ \mathrm{N}$

Acceleration of the electron in external electric field can be calculated as:

$$a = \frac{F}{m_0} = \frac{240\times10^{-10}}{9.109\times10^{-31}} m/s^{-2} = 26.348\times10^{21} m/s^{-2}$$

Kinetic energy of electron given by external electric field on the track length of typical nanofiber's diameter $s = 100nm$:

$$W_k = Fs = 240\times10^{-10}\ 100\times10^{-9}\ J = 2.4\times10^{-17} J$$

Radiation power R calculated according to Larmor formula (7.5):

$$R = \frac{e^2a^2}{6\pi\varepsilon_0 c^3} = \frac{(1.602\times10^{-19})^2(26{,}348\times10^{21})^2}{6\pi(8.854\times10^{-12})(299\times10^6)^3} W = \frac{1782\times10^{-38}\times10^{42}}{(166.9\times10^{-12})(2.673\times10^7\times10^{18})} W =$$

$$= 3.9941\frac{10^4}{10^{13}} W = 3.9941\times10^{-9} W$$

The time during which this electron travels the path of $s = 100nm$

$$t = \sqrt{\frac{2s}{a}} = \sqrt{\frac{2\times100\times10^{-9}}{26.348\times10^{21}}} s = \sqrt{7.59\times10^{-30}} s = 2.755\times10^{-15} s$$

Energy loss of the electron

$$W_r = Rt = 3.9941\times10^{-9}\ 2.755\times10^{-15} J = 1.1\times10^{-23} J$$

The ratio of the lost and kinetic energy of the electron is:

$$\frac{W_r}{W_k} = \frac{1.1\times10^{-23}}{2.4\times10^{-17}} = 4.5833\times10^{-7}$$

Some relativistic calculations:

Speed *v* of the accelerated electron:

$$v = a\times t = 26.348\times10^{21}\ 2.755\times10^{-15}\ m/s = 72.6\times10^6\ m/s$$

Ratio of the speed of the electron and speed of the light:

$$\frac{v}{c} = \frac{72.6}{299} = 0.243$$

Relativistic change of the electron's mass for speed $v = 0.243\times c$:

$$m = \frac{m_0}{\sqrt{1-\frac{v^2}{c^2}}} = \frac{m_0}{\sqrt{1-0.243^2}} = 1.0309\times m_0$$

Conclusion:

Radiation loss of kinetic energy of accelerated electron in Manning zone on the track length 100 nm can be neglected (around 10^{-6} times smaller) with regard to the kinetic energy given by the external electric field. It is therefore necessary to explain the process of generation of X-rays during electrospinning by some another mechanism.

8. Theoretical approach

It is necessary to find theoretical explanation of X-rays produced by electrospinning and detected by radiographic films and Silicon Lithium drifted detector (chapter 6). We have to start with classical Poisson-Boltzmann theory and with finding the maximal value of linear charge density of the cylinder. Counterion condensation theory will be implemented as reasonable description of gigantic potential difference necessary for acceleration of electrons and ions to produce X-rays by the processes mentioned in chapter 7.

8.1 Poisson – Boltzmann theory

One has to count with ions distribution and their interactions in the real experiment. This can be determined by principles of statistical physics. Particles in thermal equilibrium are described by Boltzmann's distribution. It tells us about distribution of the states of the system:

$$\frac{N_i}{N} = \frac{1}{Z(T)} g_i e^{-\frac{E_i}{k_B T}}, \tag{8.1}$$

where N_i/N is fractional number of particles occupying a set of states *i* possessing energy E_i, k_B is the Boltzmann's constant, *T* is the absolute temperature and g_i is the degeneracy (number of states with same energy), *N* is the total number of particles and *Z(T)* is the partition function. More can be found in Kittel (1980) and Landau (1959b).

Distribution of ions in our system can be presented by above mentioned theory. Volume density of the particles n at the position *x* is given by:

$$n(x) = n_0 e^{-\frac{U(x)}{k_B T}}, \tag{8.2}$$

where $U(x) = e\varphi(x)$ is the potential energy of an ion in an external field and *e* is the elementary charge. It is necessary to include positive and negative ions into our equation and then charge density has a form: $\rho(x) = e \cdot n(x)$. Therefore the total charge density of all ions is:

$$\rho(x) = \rho_+(x) - \rho_-(x) = n_0 e(e^{-\frac{e\varphi(x)}{k_B T}} - e^{\frac{e\varphi(x)}{k_B T}}) = -2n_0 e \sinh(\frac{e\varphi(x)}{k_B T}), \tag{8.3}$$

which is called Poisson-Boltzmann equation. For small exponent values one can use linearization of Poisson-Boltzmann equation by the form $\lim_{x\to 0} \sinh(x) = x$ and then nonlinear PB equation becomes linear. Using first Maxwell equation which is as well called Gauss law in electrostatics (2.6) one can obtain one dimensional Debye- Hückel limiting law

$$\frac{\partial^2 \varphi(x)}{\partial x^2} - \frac{2n_0 e^2}{\varepsilon_0 k_B T}\varphi(x) = 0, \tag{8.4}$$

which is the combination of principles of statistical mechanics and electrostatics is called in general as Poisson-Botlzmann theory (PB). Solution of equation [8.4] gives us an important parameter according to Feynman (1971) denoted as Debye's length

$$D^2 = \frac{\varepsilon_0 k_B T}{2e^2 n_0}. \tag{8.5}$$

The Debye's length is the measure of the thickness of the ion sheath that surrounds a large charged particle in an electrolyte. It is the distance from the electrode where the potential decreases by factor of 1/e, where e is Euler's number. Its importance will become evident later in this chapter. More details can be found in Feynman (1971).

Linear charge density can be expressed as: $\rho = \sum_i n_i q_i \cdot e$, where *q* is the ion's valence. Only *q = 1* will mostly be considerd for our purpose. Equation (2.5) can be for large numbers of ions for charged cylinder with respect to the Boltzmann distribution rewritten in general form:

$$\Delta\varphi = -\frac{1}{\varepsilon_0 \varepsilon_r}\sum_i q_i n_i e \cdot 2\sinh[\frac{-q_i e \varphi(x)}{k_B T}]. \tag{8.6}$$

It is helpful to implement another parameter called Bjerrum length

$$l_B = \frac{e^2}{\varepsilon_0 \varepsilon_r k_B T}, \tag{8.7}$$

which can be simply expressed as a minimal length between charges with the same polarity where PB theory can still be valid. It is as well border of Manning zone for $\leq l_B$: Manning (1969, 1977). Detailed explanation of this area will be done later. One can find correlation with Debye's length as: $\kappa^2 = 1/D^2 = l_B \sum_i c_i q_i^2$ which can be explained as Bjerrum's length multiplied by ionic strength and is called Debye-Hückel screening parameter κ. From these

two parameters we can form dimensionless Manning parameter $\xi = l_B/b$, where b is average spacing between charges on the fiber. Combining of (8.6) and (8.7) and using substitution $y = e\varphi/k_BT$ the PB equation can be modified as:

$$\Delta y = -l_B \sum_i q_i c_i \cdot 2\sinh[-q_i y], \tag{8.8}$$

where *y* is the reduced non dimensional potential. It is convenient to use cylindrical due to the cylindrical shape of fibers coordinates (see appendix A1). The PB equation will have form:

$$\frac{\partial^2 y(x)}{\partial r^2} + \frac{1}{r}\frac{\partial y}{\partial r} = 2\sinh y(r) \tag{8.9}$$

It is necessary to find boundary conditions (Debye-Hückel approximation) to solve this equation. One of them can be found by applying Gauss's law at the surface of the polyion (charged cylinder with condensed ions see Fig. 8.1) with linear charge density $\tau = e/b$,

$$\lim_{r\to a} r\frac{dy}{dr} = -\frac{1}{2}\xi, \tag{8.10}$$

where a is the fiber radius. Another boundary condition for open systems is:

$$y(r) \to 0 \quad \text{as} \quad r \to \infty, \tag{8.11}$$

which means that the electrostatic potential goes to the zero when the distance from the fiber is large.

Using both boundary conditions (8.10) and (8.11) the linearized Debye-Hückel solution of (8.9) in has a form:

$$y_{DH}(r) = 2\xi K_0(r), \tag{8.12}$$

where K_0 is the modified Bessel function. This approximation works quite well for potentials far enough from the surface of our polyion. The exact solution of (8.9) gives the form for $r \to 0$:

$$y(r) = -2\xi \log r + 6\xi \log 2 + 2\log\frac{\Gamma(\frac{1+\xi}{2})}{\Gamma(\frac{1-\xi}{2})} + o(1), \tag{8.13}$$

where Γ is the gamma function and $o(1)$ is the integration constant. This exact solution of nonlinear PB equation is very complicated, Tracy and Widom (1996,1997).

The solution of (8.13) can be studied in more details. There is a singularity, when $\xi = 1$. It simply tells us, that when the average distance between ions b is equal to or lower

then Bjerrum length l_B, the PB theory becomes unsolvable. The equation (8.9) has to be linearized here. This phenomenom has received a great deal of attention in recent decades and is called: Counterion condensation.

8.2 Counterion condensation theory

To find the solution of (8.9) for critical value of Manning parameter $\xi_c = 1$, the counterion condensation theory (CC) was created. The fiber is represented here as a linear chain of point charges, with a finite cylindrical volume around it. The "condensed counterions" are uniformly distributed around the fiber as was described by Manning (1969, 1977). The CC theory will be explained here as a consequence of cylindrical symmetry of homogenously charged fiber. Manning zone is represented by a tube around a thin charged fiber where counterions circulate, (see Fig 9.1).

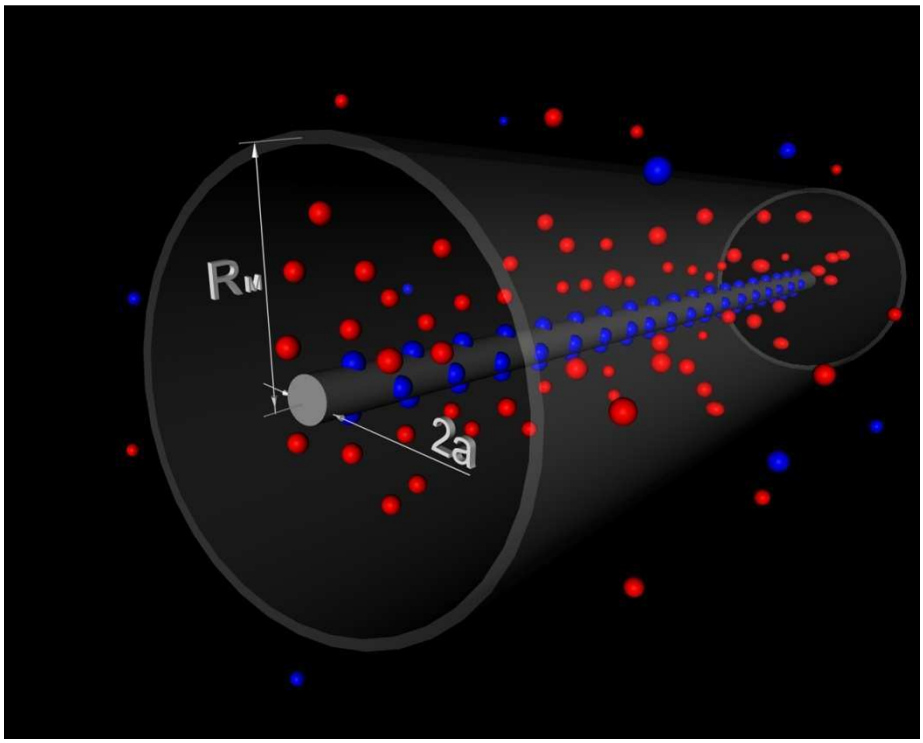

Figure 8.1. Imagination of Manning zone. Negative ions (blue) are localized on the surface of the fiber and positive ions (red) are trapped condensed inside the Manning zone forming high concentrated plasma.

CC theory was primarily developed for description of anomalous behavior of counterions around the polyions in electrolytes. It was found by Le Bret and Zimm (1984) that the PB equation predicts that polyelectrolyte ion associates closer with the "condensed" than with the "uncondensed" fraction of counterions. The CC theory does not use the nonlinear equations as PB theory, it uses only the linearized equation, which is assumed to be satisfactory. In this view, the CC is a physical process caused by the instability of highly charged cylindrical bodies. But in the other hand, it does not confront with the question of fluctuations – it just neglects them in a different way. The CC theory is an approximation to the PB theory insofar as it predicts counterion distribution that is unstable relative to the PB theory. So we can mention here two main regions: the ion distribution in the region close to the fiber (the Manning region) and the distribution of ions in the distant region (the Debye-Hückel region).

One possible solution of (8.9) for $\xi \leq 1$ was found by Kornev (1999). He considers counterions to be present in Manning zone because of the solubility of Poisson-Boltzmann equation for $\xi \leq 1$. Ions are simply excluded from the Manning zone. Ions are sitting on the cylinder (fiber) and they quickly recombine when they are pushed out from the cylinder. Equation (8.9) can be rewritten as:

$$\frac{\partial^2 y(r)}{\partial r^2} + \frac{1}{r}\frac{\partial y(r)}{\partial r} = \exp y(r), \tag{8.14}$$

which is the PB equation in cylindrical coordination where on the left side is Laplace's operator affecting non dimensional potential $y(r)$ on the right side. If we follow Kornev's (1999) steps, one can reach the solution for the dimensionless potential $y(r)$ close to the surface of the fiber:

$$y(r) = -\ln\left[\left(\frac{ka}{2z}\right)^2 R^2 \cos^2\left(z \ln\frac{R}{R_M}\right)\right], \tag{8.15}$$

where $R_M = r_M / a$ is the dimensionless radius of Manning region of counterion condensation, r_M is real radius of Manning zone a is a radius of our fiber, R is the dimensionless radial distance from the center of the fiber. The border of Manning zone holds $R = R_M$, $z = \exp(-C_E)$ and $C_E = 0.577215....$ is the Euler's constant. Dimensionless radius of Manning region can be, according to Kornev (1999), on the border of Manning zone calculated by the formula

$$R_M = \exp\{-e^{C_E} \arctan[e^{C_E}(1-q)]\}, \tag{8.16}$$

where $q = (e/2\pi\varepsilon_r\varepsilon_0 k_B T)\tau$ is the dimensionless linear charge density on cylindrical nanofiber and τ is the linear charge density [C/m]. Linear charge density for our example can be calculated from Bjerrum length: $\tau = e/b$ and for Manning zone $b \le l_B$. Since q is in our case of the order of 10^3, Manning region spans to $R_M \cong 16.4$ according to (7). So the Manning zone reaches up to 16.4 fold of fiber's diameter *a*. In this zone, ions sit on the fiber with distance $b \le l_B$. Oppositely charged counter ions are highly condensed in Manning zone at the distances $r \in (a, a \cdot 16.4)$.

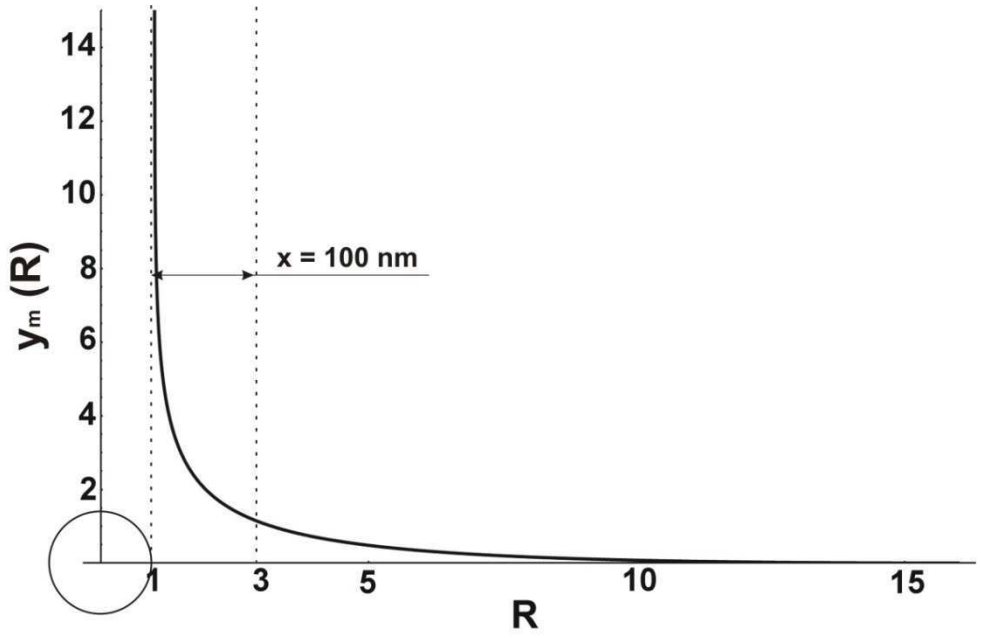

Figure 8.2. Dependency of reduced electrostatic potential on distance R from center of fiber in Manning region.

Figure 8.2 has to be interpreted carefully due to the drastic decrease of electrostatic potential in fibre vicinity. It tells us about high potential difference between the fiber's surface and the border of Manning region. The severe potential decay can accelerate charged particles inside the Manning zone to high velocities. These high accelerated particles can be a source for emission of radiation up to energies of X-ray's subtype of electromagnetic spectrum.

The dimensionless potential value $y_M(1)$ on a surface of a nanofiber is supposed to be $(3\times10^5 V)\times e/(k_B T)$ in our experiments. The numerical treatment of the Equation (8.15) needs a precise coupling between parameters $z \cong \exp(-C_E)$ and $R_M \cong 16.407$ that fulfils the relation $z \ln R_M = \pi/2 - 1/\exp[u(1)+2] \approx 10^{-868589}$. The drop of the dimensionless potential $u_M(R)$ with an increasing distance *R* from the fiber surface is so precipitous that the potential reaches a negligible value at the distance shorter than a particle's mean path at atmospheric pressure, wide Fig. 8.2. Therefore the field strength value E_M inside the Manning region will be further estimated using its average value determined from the difference of potentials on the fiber surface $\varphi(a)$ and on the edge on Manning region $\varphi(r_M)$ as

$$E_M = \frac{\varphi(a) - \varphi(r_M)}{r_M}. \qquad (8.17)$$

This roughly estimated mean field strength value inside the Manning region is about 150 GV/m, since the potential difference $\varphi(a) - \varphi(r_M)$ is roughly one half of the voltage applied, i.e., 15kV. This field is sufficient for gas phase ionization of deuterium (>25 GV/m) and undoubtedly such strength causes ionization of neutral air molecules nearby a jet; Tracy (1996). Ions or electrons, kicked by an increasing chemical potential inside the thinning electrospinning jet into the Manning region, can be significantly accelerated by the predicted gigantic field strength at a short distance *x* comparable with their mean path in the air at atmospheric pressure. The total energy radiated by one accelerating electron at this distance is, according to Larmor formula (example 7.1), only 0.0001% of the obtained kinetic energy and hence relativistic effects are negligible. Therefore the theoretically predicted field strength enables electrons to reach over the short distance x=100nm a massive kinetic energy, $W_1 \cong [\varphi(a) - \varphi(b)] \cdot e$, which is about 15 keV. This estimation is in broad agreement with the measured maximal X-ray energies in the spectra obtained from our electrospinning experiments.

The closest vicinity of individual nanofibrous in electrospinnig jets in our experimental setup operates, according to our hypothesis, as a 'microscopic' particle accelerator acting over an unusually short distance. Accelerated particles collide with other gas particles inside the Manning region, including ions, or with other materials.

9. Deposition of radon progeny

The last unexpected phenomenon of electrospinning process will be explained in this chapter. It has been proved that nanofibres keep some amount of charge during their deposition and some of them even few hours after that. Radon decay creates progenies which are positively charged due to their β decay and these positively charged radon daughters are then attracted and stored by negatively charged nanofibers.

Electrospinning is the process to make submicron fibers by application of high voltage on the surface of the polymer solution. The surface of solution can be positively or negatively charged depending on the polarity of source. Polymeric jets are then created by the destabilization of the surface of the polymeric solution by electric forces (Lukas 2008). There is a massive evaporation of the solvent during the jet's flying, but some residual charge has been kept on the fiber. This residual charge has been patent mainly for ferroelectric polymers such as for example Polyvinylidene Fluoride (PVDF) which is permanently bipolar. They can attract negatively charged radon daughters.

The description of radiant effects starts here with irradiation caused by Radon. Radon is the chemical element with atomic number 86. It is the invisible, radioactive noble atomic gas, that in the nature results from radioactive decay of some forms of Uranium , *U*, that may be found in igneous rock formations beneath buildings or in certain building materials. Radon is being continuously produced by radioactive decay of Radium isotope ^{226}Ra spread all over the world. Radon is one of the heaviest gases. The most stable Radon isotope, ^{222}Rn, has a half time of 3.8 days, viz Heinrich (1942). Radon gas and its solid decay products are considered to be a serious health hazards since they are carcinogens. However, the pathways linking Radon decay consequences to living tissues are not direct. The crucial links occur via a deposition mechanism of the radioactive Radon daughters, as introduced by Batkin (1998). Detail analysis of toxilogical aspects of Radon was described by Roper (1990). The deposition of Radon decay products on electrospun materials and electrodes of electrospinners was studied using various detecting technologies ranging from etched-track detectors, proportional counters, gamma spectrometers, etc. Radon decay progeny are not gases (*Po, Bb, Bi*) but solids, see Fig. 9.1). They can be attached easily to tiny aerosol particles, and these particles may be trapped in the lungs what results in a lung dose from alpha and beta radiation.

Radon, ^{222}Rn, decay products are also intensively deposited onto surfaces of electrospun materials and electrospinner parts. The deposition is caused by an attraction between any negatively charged solids and positively charged radon daughters. Radon daughters have the electrostatic affinity to negatively charged surfaces since they are positively created as a result of the stripping of electrons from the parent atom during their radioactive decays. The investigation of the deposition of aforementioned heavy metals should be critical for an application of nanofibrous materials in tissue engineering due to health hazards of heavy metals. Recent human health hazards increase because in modern industrial environment a human body often carries a negative static charge since a body potential up to tens of kilovolts can result from everyday activities such as walking across synthetic floors, working with plastic materials or from coming into contact with charged objects.

9.1 Experimental setup for radon daughter's deposition

A series of electrospraying as well as electrospinning experiments have been carried out under special conditions to confirm that even scant mass of electrospun nanofibrous layer, not greater than tens of grams, can exhibit radioactive activity. It should be more than four times higher than the natural background (123 ± 8 nSv/h , where SI unit Sv is the Sievert, derived unit of dose equivalent, Sv = J/kg = m^2/s^2). Samples were prepared and registered by twin Geiger-Müler Tubes of the Radiometer 'VOLTCRAFT HS - 036'. Measurements of this deposition were made with negatively and positively charged collectors, for various temperatures, to exclude effects from an electron shell. All deposited nanofibers were stored on the bending spunbond textile and taken down from the collector before all dose measurements. For all samples we measured the same half-time with various radiation intensities. About one half lower irradiation intensities were detected on positively charged collectors, compared with negatively charged ones under the same conditions.

Complex measurement of this process was done too. Results proved, that radiation observed during electrospinning was a deposition of Radon progeny, what is in accordance with the observed asymmetry of observed radiation intensities from positively and negatively charged collectors covered by collected materials. Positively charged Radon daughters are more attracted by negatively charged bodies. The fundamental general theory which explains process of Radon deposition in details was introduced by Batkin *et. al.* (1989).

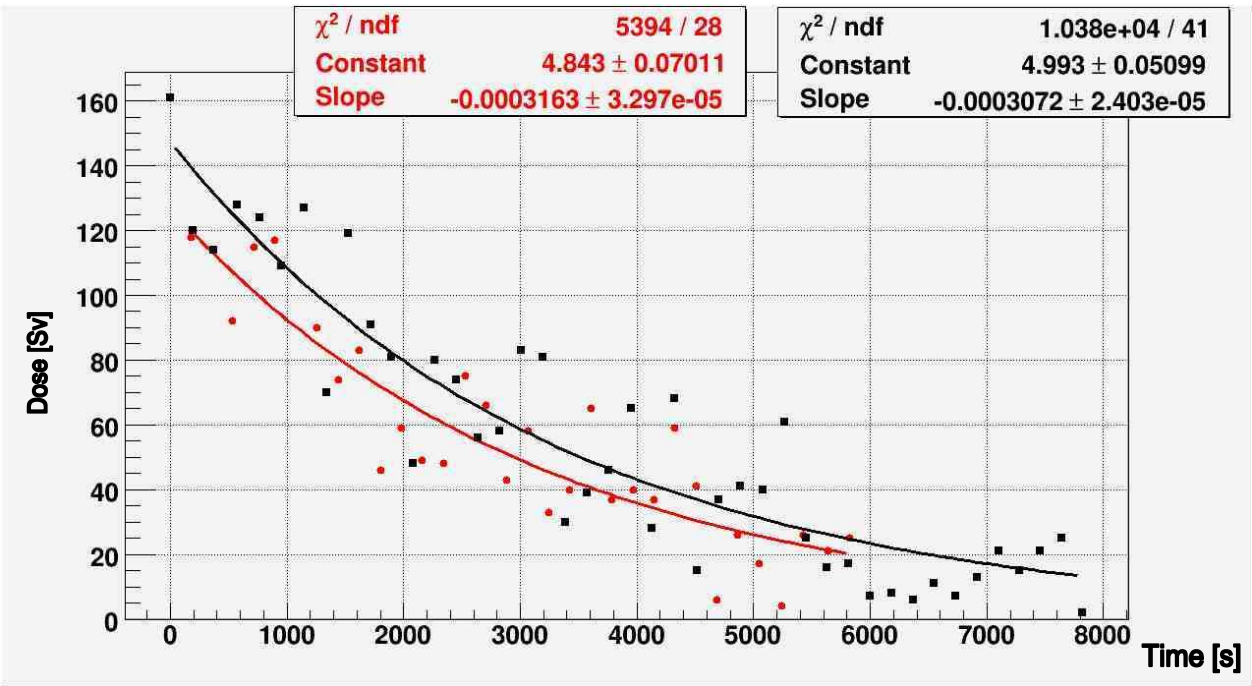

Figure 9.1. Deposits of electrospraying and electrospinning materials of a mass around tens of grams exhibit high-energy excitations four times higher than the laboratory background (123 ± 8 nSv/h). The activity was registered by twin Geiger-Müler Tubes of the Radiometer 'VOLTCRAFT HS - 036'. Two independent samples were measured, one heated up to 100 °C (red) and second under room temperature to exclude effects from the electron shell. Our own measurement.

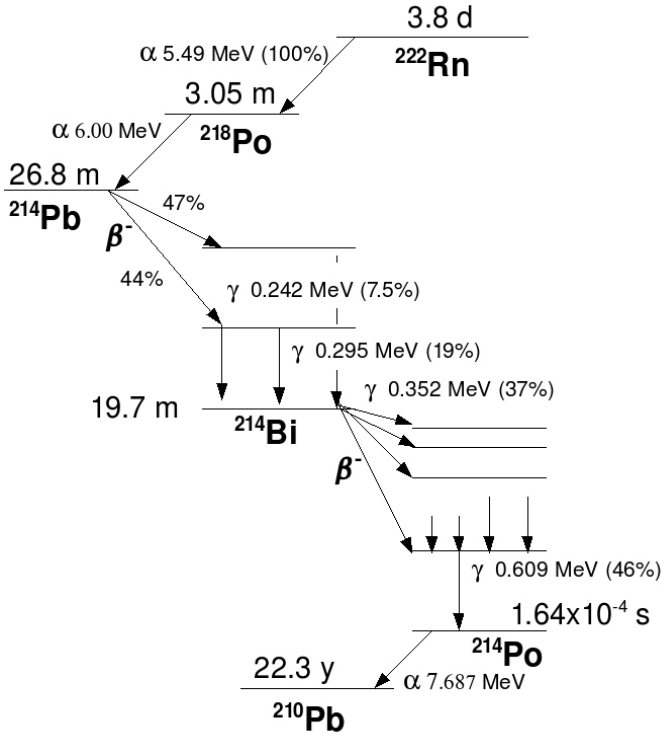

Figure 9.2. The decay scheme of ^{222}Rn: All isotopes are assigned with atomic numbers, half times in minutes [min] and emitted particles. For example ^{218}Po has an atomic number 218, half time 3.05 minutes and disintegrates into ^{214}Pb by emission of 6 MeV energetic alpha particle. Picture was inspirited by Batkin (1998).

It is obvious from (Figure 9.2) that the last product of Radon radioactive decay is Lead isotope ^{210}Pb with half time 22.3 years. This was analyzed by scanning electron microscope JEOL JED-2300 with EDS (energy disperse X-ray analyzer). One can see, that amount of this isotope is immeasurable (Figure 9.3).

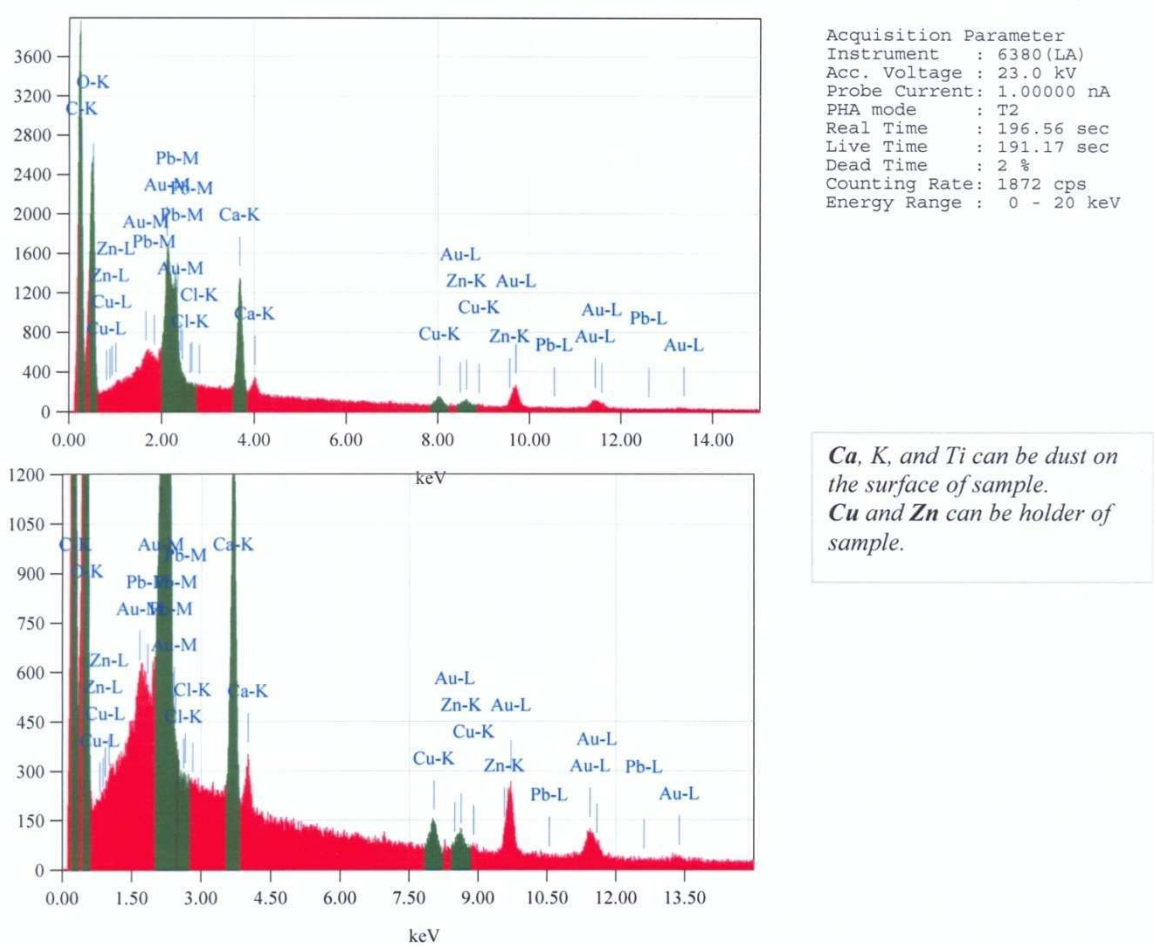

Figure 9.3. Energy disperse X-ray analysis (EDS) of Lead ^{210}Pb amount in sample prepared by electrospinning. The electrospunn nanofibrous sample was prepared from 10% PVA solution in demineralised water. The immediate sample radioactivity was about six times higher than background (Measurement made by Eva Košťáková in Budapest University).

Another idea was to use ferroelectric polymers as active filters for positively charged isotopes. Ferroelectric materials demonstrate spontaneous polarization such as for example Rochelle salt. An example of polymeric material indicates ferroelectric feature is Polyvinylidene fluoride (PVDF). Nanofibers made of PVDF were electrospun, parallelized and then collected. Their ferroelectric property is clearly demonstrated by "ballooning" of stored parallelized nanofibers (Figure 9.4). This "ballooning" is due to the nanofiber's ability

to keep the residual charge and the repulsion force between identically charged fibers. PVDF polymer has to be heated up to 55°C to be able to create nanofibers from the polymeric solution by the needle electrospinning. Nanofibers were then collected by the special device designed for this purpouse which was rotating around its z-axis by the angular frequency around 40 RPM and its schematic picture and photography can be seen in fig 9.5. Deposited nanofibers were then taken down by the two small brushes and then twisted to make precise nanoyarn see fig. 9.6.

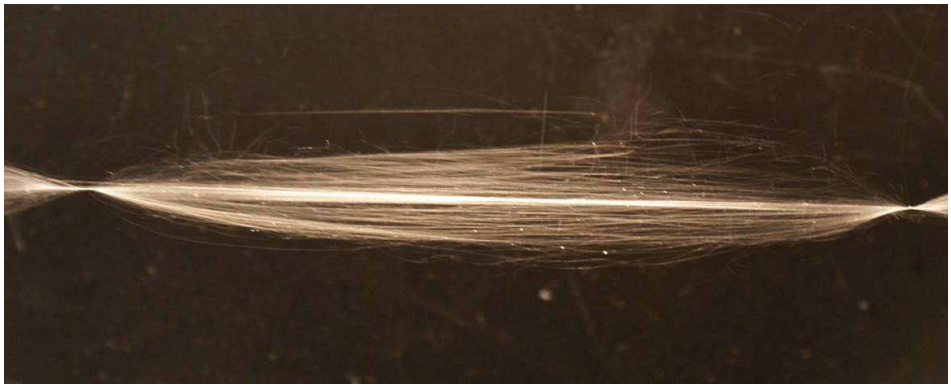

Figure 9.4: Photography of parallelized PVDF nanofibers showing trapped residual charge by its "ballooning".

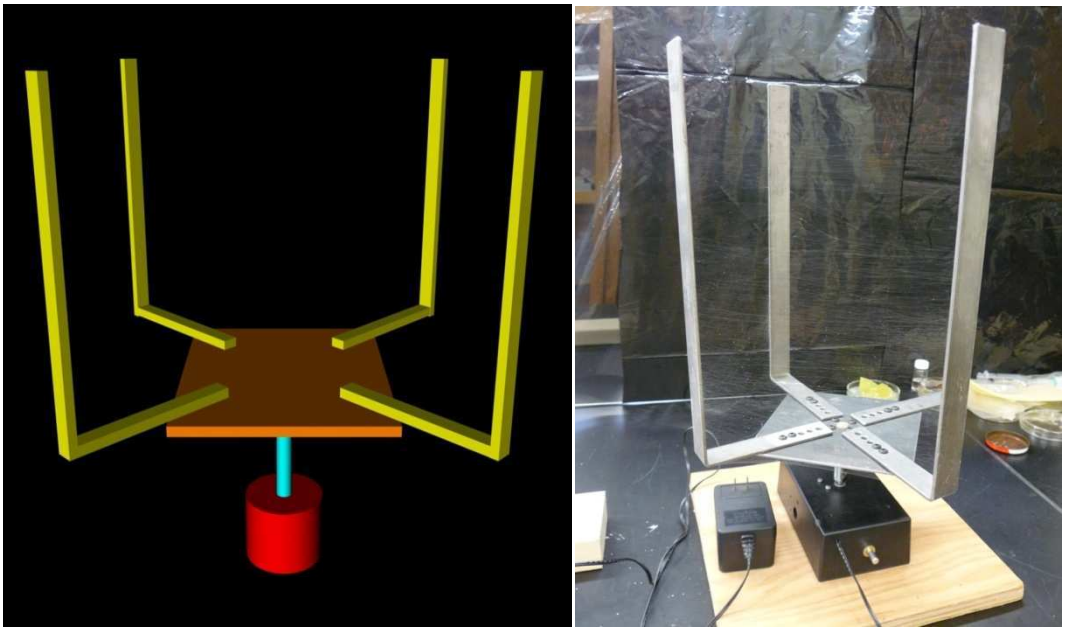

Figure 9.5: Specially designed device for PVDF nanofibers deposition and parallelization. Left is the schematic view and right is the photography of the final product.

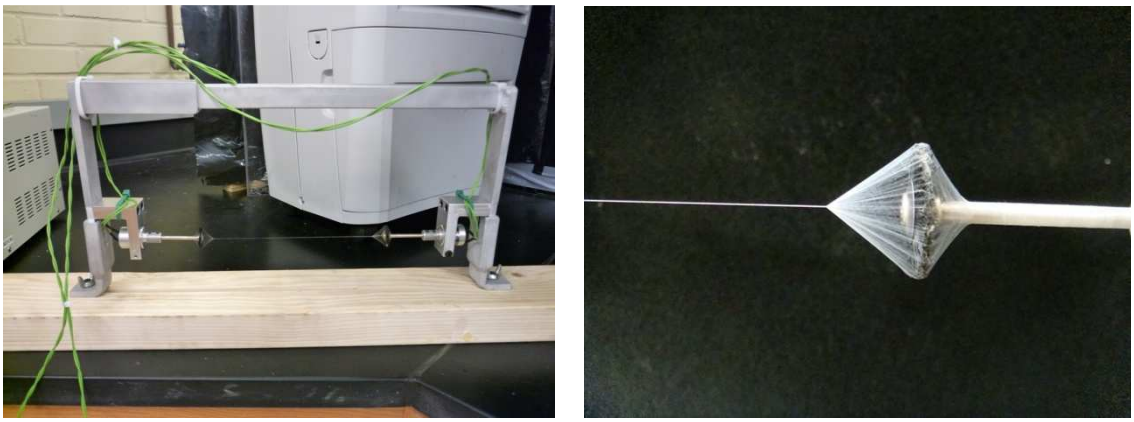

Figure 9.6: The device for taking down of the parallelized nanofibers (left) and the detail of the brush.

This process can be used in several applications to protect humans against charged radio isotopes like for example as active filters of radon daughters or another charged radiation. It was proved, that nanofibers can attract radon daughters and it can be used as active filters for several applications.

10. Summary and Outlook

The final compilation of all achieved results as well as some future prospects will be proposed in this last part of the thesis. As was mentioned already in the introduction, the main effort of this work was detection, measurement and description of X-rays generated by the electrospinning.

This discovery is very unique and no one before never observed such phenomenon. There are some discoveries of productions of X-rays by the process called field emission from nanotubes, but any article such for example written by Bonard (2000) didn't report about energies higher than hundreds of eV. Some articles refer about other alternative methods of X-rays generation. Both of them are mentioned in this work (see paragraphs 6.3.6 and 6.3.7). First of them is the observation of X-rays during thunderstorms. The main difference with our observations is in the value of current necessary for the X-ray generation. Electrospinning needs only a fraction of current which is normal during thunderstorms. The last alternative method of X-ray generation is by the friction in peeling tape. Camara (2008) and his colleagues under leading of Putterman observed a nanosecond X-ray flashes generated by the peeling of common adhesive tape in vacuum system. They explained this process by the process called triboluminiscence but any X-ray radiation wasn't observed in atmospheric conditions. Neither of all mentioned methods are close to our discovery. Here is the first report about the theory called Counterion condensation published by Maning (1969) which counts with critical linear charge density on a fiber in air at atmospheric conditions. It is as well the new step for the better understanding of nano-scale world where physical theories are still missing. The process of Counterion condensation completely erases the decay of field strength caused by grouping the nanofibers into the warp (see example E4 in chapter 2) and brings a new perspective on the point of view of nanofibers.

The Manning zone which is created around the nanofibers can plays the role of particle accelerator. The investigated effect could find its applications in a lot of fields. Let us mention: portable X-ray sources for therapeutic and analytical purposes and the design of anomalous particle accelerators in nuclear physics including fusion apparatus, to mention just Naranjo (2005). This investigation could provide also an important new insight into the mechanism for generating X-rays from lightning and long laboratory sparks.

Another interesting phenomenon, discovered during studies of electrospinning, is firstly published here. It was proved that nanofibers keep some residual charge and can attract positively charged radon daughters (chapter 9). This principle can be used for many

applications as for example active filters of ionized radiation or as a cleaners of natural radon depositions.

Outlook

More detailed analysis of impact of relative permittivity on the electrospinnig process has to be made in the near future. Some preliminary experiments of jet's deflection by the external electrostatic field during their flight were already observed by our colleague Pavel Pokorny and will be published soon in his thesis. Combination of both theoretical and experimental approaches seems to be promising step for better description of electrospinning process. Viscosity is another important parameter influencing mainly thickens of the fibers. Control of the thickness plays a crucial role for generation of X-rays. Many new experiments with various values of viscosities of a polymeric solution have to be prepared.
It is important to repeat spectral measurements of observed X-rays as well as to study its space distribution by the radiographic films. There is a risk of health damage to work with electrospinning in dark room without any aspiration, because the ozone is created when the high voltage is applied. The cooperation with Faculty of Nuclear Science and Physical Engineering of Czech Technical University in Prague will play important role in spectral measurements and better physical explanation of this phenomenon.

More detailed studies of radon daughters deposition caused by nanofibers will be done in cooperation with National Institute for Nuclear, Chemical and Biological Protection in their Radon chamber. Ferroelectric polymers mentioned in chapter 9 will be fully tested.

References

Abraham, M., Becker, R., (1932), *The Classical Theory of Electricity and Magnetism*, Blackie, Glasgow, UK

Andrady, A. L. (2008), *Science and Technology of Polymer Nanofibres*, (Wiley, Hoboken, NJ.)

Ashley, J. C. (1982), *Energy Losses and Inelastic Mean Free Paths of Low-Energy Electrons in Polyethylene*, Radiation research, **90**, 433-436

Bakshi, V. (2008), *EUV Lithography*, SPIE, Bellingham USA, ISBN: 9780819469649

Bass M. et. al. (1995), *Handbook of optics – Vol 2*, second edition, McGraw-Hill, USA, ISBN 0-07-047974-7

Batkin, I. et al (1998), *γ-spectroscopy investigation of radon daughter depositionon electrostatically charged surfaces*, Phys. Med. Biol. **43** 487-499

Bonard, J. M., Kind, H., Stöckli, T., Nilsson, L.O., (2000), *Field emission from carbon nanotubes: the first five years, Solid-State electronics*, no.2586, p.:1-22

Boyers, D.G., and Tiller, W.A. (1973). *Corona discharge photography*. Journal of Applied Physics **44**: 3102–3112.

Bush, J. W. M. (2004). *"MIT Lecture Notes on Surface Tension"* Massachusetts Institute of Technology. Boston USA

Clausius, R. (1879), *Die Mechhnische Warmelehre*, vol. 2. Vieweg, 1879, pp. 62-97

Chadwick, J., (1912) *The γ rays excited by the β rays of radium*, Philosophical Magazine, vol. 24, p. 594-600

Camara, G.C., Escobar, J.V., Hird, J.R., Putterman, S.J. (2008), *Correlation between nanosecond X-ray flashes and stick-slip friction in peeling tape*, Nature, Vol 455.

Dirac, P.A.M. (1938), *Classical theory of radiating electrons*. Proc. Roy. Soc. of London. A929:0148-0169

Dwyer, J. R. et al.(2003), *Energetic radiation produced during rocked-triggered lightning*, *Science*, 299, 694-697.

Feynman, R.P., Leighton, R.B. and Sands, M. (1971), *Feynman lectures on physics* (*Vol. II*), Addison-Wesley Publishing Company, Reading - Massachusetts.

Filatov, Y., Budyka, A. & Kirichenko, V. (2007), *Electrospinning of Micro- and Nanofibers: Fundamentals in Separation and Filtration Processes* (Begell House, Redding)

Formhals, A. (1934), *Process and apparatus for preparing artificial threads*, US Patent, 1,975,504 (1934)

French, A.P., Taylor, E.F. (1978), *An Introduction to Quantum Physics*, Massachusetts Institute of Technology, Boston, ISBN 0-7481-4078-3

Govil, I. M. (2001), *Proton Induced X-ray Emission – A tool for non-destructive trace element analysis*, Current Science, vol. 80, NO. 12.

Griffiths, D. (1999), *Introduction to Electrodynamics -3rd edition*, Prentice Hall - New Jersey

Grigor'ev, A. I. and Sinkevich, O. A. (1985), *Mechanism of development of the instability of a liquid drop in an electric field*, Fuild Dynamics. 20 (6), 341-346.

Grigor'ev, A.I. and Sinkevich (1984), O.A., A *mechanism of St. Elmo's fire, Sov.* Phys. Tech. Phys. **29** (7), July

Grigor'ev, A.I., Grogor'eva, I.D. and Shiryaeva, S.O. (1991), *Ball Lightning and St. Elmo's Fire as Forms of Thunderstorm Aktivity*, Journal of Scientific Exploration, **Vol. 5**, No. 2, pp. 163-190.

Gurevich, A. V., Milib G. M. & Valdivia J. A. (1997), *Model of X-ray emission and fast preconditioning during a thunderstorm*, Physics Letters A, **23** (I) 402-408.

Gurevich, A. V. & Zybin K. P., (2001), *Runaway breakdown and electric discharges in thunderstorms*, Uspekhi Fizicheskikh Nauk, **44** (11) 1119-1140.

Hakim, S.,S., Higham, J.,B., (1962), *An Experimental Determination of the Excess Pressure produced in a Liquid Dielectric by an Electric Field*, Proc. Phys. Soc., Vol. 80, 190

Helmholtz, H., (1868), *On the discontinuous movements of fluids*, Monthly Reports of the Royal Prussian Academy of Philosophy in Berlin, ***23**: 215–228*

Hill, N., E. (1958), *The Application of Onsager's Theory to Dielectric Dispersion, Dep. of Physics*, Bedford College, London

Hohman, M. M., Shin, M., Rutledge, G, Brenner M. P. (2001), *Electrospinning and Electrically Forced Jets, I. Stability theory*, Physics of Fluids, **13** (8), 2201-2220.

Hubell, J.H., Seltzer, S.M. (1989), *Tables of X-Ray Mass Attenuation Coefficients and Mass Energy-Absorption Coefficients*, National Institute of Standards and Technology, Gaithersburg.

Ichimaru, S. (1973), *Basic Principles of Plasmas Physics : A Statistical Approach*, Westview Press, Jackson TN, USA.

Jirsak, O., Sanetrnik, F., Lukas, D., Kotek, V., Martinova, L., Chaloupek, J. (2005), *A method of nanofibres production from a polymer solution using electrostatic spinning and a device for carrying out the method*, US Patent, WO2005024101.

Kirlian, S.D., Kirlian, V., (1939), *Photography and Visual Observation by Means of High-Frequency Currents*, Journal of Scientific and Applied Photography, Vol. 6 No. 6.

Kittel, Ch. (1980), *Thermal physics*, W.H. Freeman and Company, USA

Kittel Ch. (1963) *Introduction to Solid State Physics - 8th ed*. (2005), John Wiley and Sons, USA, ISBN 0-471-11181-3

Kornev, K. (1999), *Lateral interaction of charges in thin liquid films and the Berezinskii-Kosterlitz-Thouless transition.*, Phys. Rev. E, vol 60, n.4.

Kopal, A., Erhart, J., Čmelík, M., Machonský, L.,(2008), *Fyzika II*, Technical University, Liberec, Czech Republic.

Landau, L.D. and Lifshitz, E.M. (1959a), *Fluid Mechanics*, Butterworth-Heinemann, Oxford.

Landau, L.D. and Lifshitz, E.M. (1959b), *Statistical physics*, Butterworth-Heinemann, Oxford.

Landau, L.D. and Lifshitz, E.M. (1960), *Electrodynamics of Continuous Media*, Butterworth-Heinemann, Oxford.

Larmor, J. (1897), *On a dynamical theory of the electric and luminiferous medium*, Philosophical Transactions of the Royal Society **190**, pp. 205-300

Le Bret, M., and Zimm, B.H. (1984), *Distribution of counterions around a cylindrical polyelectrolyte and Manning's condensation theory*. Biopolymers. 23; 287-312.
Liu, L. (2007), Experimets in X-ray physics, MIT undergraduate

Levich, G.,L. (1962), *Physicochemical Hydrodynamics*, Prentice Hall, Englewood Cliffs, New Jersey, USA.

Lukas, D., Sarkar, A., Pokorny, P. (2008), *Self organisation of jets in electrospinning from free liquid surface - a generalized approach*, Vol. **103,** Journal of Applied Physics, pp.084309 1-7.

Lukáš, D., Sarkar, A., Martinová, L., Vodseďálková, K., Lubasová, D., Chaloupek, J., Pokorný, P., Mikeš, P., Chvojka, J., Komárek, M. (2009), *Physical principles of electrospinning (Electrospinning as a nano-scale technology of the twenty-first century),* Textile Progress, Taylor & Francis, Vol. 41, No2, 2009, 59-140, ISBN – 13: 978-0-415-55823-5

Kozawa T. et.al. (1992), *Radiation-Induced Acid Generation Reactions in Chemically Amplified Resists for Electron Beam and X-Ray Lithography*, Japanese Journal of Applied Physics, Vol 31, 4301-4306

Manning, G.S. (1969),*Limiting laws and counterion condensation in polyelectrolyte solutions. I. Colligative properties*, J. Chem. Phys. 51, 924-933.

Manning, G.S. (1977),*Limiting laws and counterion condensation in polyelectrolyte solutions. IV. The approach to the limit and the extraordinary stability of the charged fraction*. Biophys. Chem. 7, 95-102.

Miloh, T., Spivak, B., Yarin, A.L. (2009), *Needleless electrospinning: Electrically driven instability and multiple jetting from the free surface of a spherical liquid layer,* Journal of Applied Physics, 106, 114910

Moseley, H.G.J. (1913), *The high frequency spectra of the elements*, Phil. Mag. p. 1024

Mossotti, O. F. (1850), *Mem. di mathem. **e.** fisica di Modena*, 24, 2, 49

Naranjo B. Gimzewski J. K., Putterman S. (2005), *Observation of nuclear fusion driven by a pyroelectric crystal*, Nature, **434**, 1115-1117.

NRAO, *Free-free radio emission from an HII Region*, National Radio Astronomy Observatory, Carlottesville, Virginia, USA.

Planck, Max. (1901) *On the Law of Distribution of Energy in the Normal Spectrum*, Annalen der Physic, vol. 4, p. 553 ff.

Ramakrishna, S. Fujihara, K. Teo, W. Lim, T. Ma, Z. (2005), *An introduction to electrospinning and nanofibers* (World Scientific Publishing Co., Singapore).

Rayleigh, L. (1882), *On the Equilibrium of Liquid Conducting Masses Charged with Electricity,* Phil. Mag. **14**, pp. 184–186.

Remy, H. (1942), Lehrbuch der Anorganischen Chemie , *Akademische Verlagsgesellschaft Becker and Erler Kom. Ges*; 3rd ed edition.

Reneker, D. H. & Yarin A. L. (2008), *Electrospinning jets and polymer nanofibres*, Polymer, 49, 2387-2425.

Roper, W. L. (1990), *Toxicological profile of radon, Agency for Toxic Substances and Disease Registry,* U.S. Public Health Service.

Röntgen W. C. (1895), *On a New Kind of Rays*, Nature 53: 274–6

Rybicki, G.B.,Lightman, A.P., (1979), *Radiative Processes in Astrophysics*, Wiley, New York

Sarazin, C., L. (1986), *X-ray emission from clusters of galaxies*, Reviews of Modern Physics, Volume 58, Issue 1, p. 1-115

Seliger, H.,H. (1995), *Wilhelm Conrad Rentgen and the glimmer of light*, Physics Today, November.

Shchukin, S. I. and Grigor'ev, A. I. (2000), *Breakup of an Uncharged Droplet in an Electrostatic Field,* Technical Physics, **Vol. 45**, No. 6, pp. 694–697.

Shiryaeva, S. O. and Grigor'ev, O. A. (1999), *Influence of viscosity relaxation on the growth rate of the Tonks–Frenkel instability*, Technical Physics Letters, Vol. 25, No. 1, pp. 41-42.

Shiryaeva, S. O. (2000), *On the Influence of Viscosity on the Characteristic Time of the Instability of a Charged Drop*, Technical Physics, **Vol. 45**, No. 9, pp. 1128–1134

Onsager, L. (1936), *Electric Moments of Molecules in Liquids* , J. Amev. Chem. Soc., 58, 1486.

Taylor, G. (1964), *Disintegration of water drops in an electric field*, Proc. Roy. Soc. London A**, 280**, pp. 383-397.

Taylor, G. F. Van Dyke, M.D. (1969), *Electrically driven jets*, Proc. Roy. Soc. A, **313**, 453-475.

Theron, S.A. Yarin, A.L. Zussman, E. (2005), *Multiple jets in electrospinning: experiment and modelling*, Polymer, **46**, 2889-2899.

Tipler, P (2004). *Physics for Scientists and Engineers: Electricity, Magnetism, Light, and Elementary Modern Physics* (5th ed.). W. H. Freeman. ISBN 0-7167-0810-8.

Tonks, L. (1935), *A Theory of Liquid Surface Rupture by a Uniform Electric Field*, Physical Review, **Vol. 48**.

Tracy, C.A., Widom, H. (1996), *Fredholm determinants and the mKdV/sinh-Gordon hierarchies*, Commun. Math. Phys. 179, 1-10.

Tracy, C.A., Widom, H. (1997), *On the exact solutions to the cylindrical Poisson-Boltzmann equation with applications to polyelectrolytes*. Physica A 244, 402-413

Yarin, A.L. Zussman, E. (2004), *Upward needleless electrospinning of multiple nanofibers*, Polymer, **45**, 2977-2980.

Xiao-Hong Qin, Yu-Qin Wan, Ji-Huan He, Juan Zhang, Jian-Yong Yu and Shan-Yuan Wang, (2004), *Polymer*, **45** 6409

Zeleny, J. (1914), *The electrical discharge from liquid points, and a hydrostatic method of measuring the electric intensity at their surface*, Physical Review, **3**, pp. 69-91.

List of Author's publications

Publications corresponding to the thesis

Pokorný, P., Mikeš, P., Lukáš, D. (2010), *Electrospinning Jets as X-ray Sources at Atmospheric Conditions*, Europhysics letters (IF 2.893).

Lukáš, D., Sarkar, A., Martinová, L., Vodseďálková, K., Lubasová, D., Chaloupek, J., Pokorný, P., Mikeš, P., Chvojka, J., Komárek, M. (2009), *Physical principles of electrospinning (Electrospinning as a nano-scale technology of the twenty-first century),* Textile Progress, Taylor & Francis, Vol. 41, No2, 2009, 59-140, ISBN – 13: 978-0-415-55823-5 (IF 0.864).

Mikes, P., Pokorny, P., Charvát, R., Lukas, D. (2011), *Electrospinning as a source of X-rays*, Fiber Society, Hong Kong, China.

Mikes, P., Lukas, D., Pokorny, P. (2010), *Deposition and filtering of radon progeny driven by electrospinning,* Nanocon 2010, Czech Republic.

Mikes, P., Lukáš, D., Pokorny, P. (2007), *Radon daughters deposition during electrospinning*, Palanga/Lithuania, 2007

Mikes, P., Lukas, D., Pokorny, P. (2009), *Detection of radiation during electrospinning*, Autex conference, Izmir Turkey.

Mikeš, P., Lukáš, D., Pokorný, P. (2009), *Observation of St. Elmo's fire in laboratory conditions*, Nestandardní aplikace fyzikálních polí, sborník GACR

Publications not correspondintg to the thesis

Lukas D., Vodsedalkova K., Chaloupek J., Mikes P., Komarek M., Kostakova E., Raab M., Sarkar A., (2008), *Fyzika polymerů*, Nakladatelství Technická univerzita v Liberci, Liberec (2008). ISBN: 978-80-7372-312-5

Lukáš, D.,Vodsedalkova, K., Mikes, P., Chvojka, J. (2008), *Kognitivni veda dnes a zítra - Kolektivni jevy,* Nakladatelství Bor, ISBN 978-80-86807-55-3

Lukas, D., Pan, N., Sarkar, A., Weng, W., Chaloupek, J., Kostakova, E., Ocheretna, L., Mikes, P., Pociute, M., Amler, E., (2010), *Auto-model based computer simulation of Plateau_Rayleigh instability of mixtures of immiscible liquids,* Physica A 389, 2164_2176

Appendix

A1 Cylindrical polar coordinates

Transformation $(r \geq 0, 0 \leq \theta < 2\pi, -\infty < z < \infty)$:

$$x = r\cos\theta$$

$$y = r\sin\theta$$

$$z = z$$

Gradient: $$\vec{\nabla}\Phi = \frac{\partial\Phi}{\partial r}\hat{r} + \frac{1}{r}\frac{\partial\Phi}{\partial\theta}\hat{\theta} + \frac{\partial\Phi}{\partial z}\hat{z}$$

Divergence: $$\vec{\nabla}\cdot\vec{A} = \frac{1}{r}\left[\frac{\partial}{\partial r}(rA_r) + \frac{\partial A_\theta}{\partial\theta} + \frac{\partial}{\partial z}(rA_z)\right]$$

Rotor: $$\vec{\nabla}\times\vec{A} = \frac{1}{r}\begin{vmatrix} \hat{r} & r\hat{\theta} & \hat{z} \\ \frac{\partial}{\partial r} & \frac{\partial}{\partial\theta} & \frac{\partial}{\partial z} \\ A_r & A_\theta & A_z \end{vmatrix}$$

Laplacian: $$\nabla^2\Phi = \frac{1}{r}\frac{\partial}{\partial r}\left(r\frac{\partial\Phi}{\partial r}\right) + \frac{1}{r^2}\frac{\partial^2\Phi}{\partial\theta^2} + \frac{\partial^2\Phi}{\partial z^2}$$

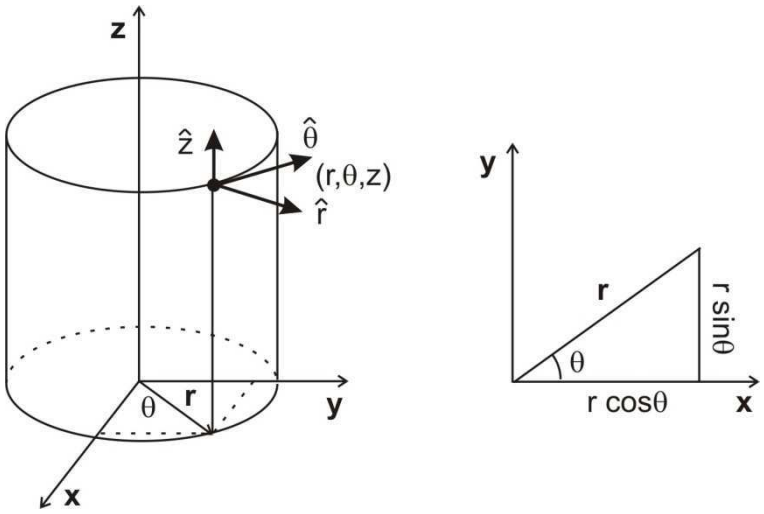

A2 Spherical polar coordinates

Transformation $(r \geq 0, 0 \leq \lambda < 2\pi, 0 < \theta < \pi)$:

$$x = r \sin\theta \cos\lambda$$

$$y = r \sin\theta \sin\lambda$$

$$z = r \cos\theta$$

Gradient $$\vec{\nabla}\Phi = \frac{\partial\Phi}{\partial r}\hat{r} + \frac{1}{r}\frac{\partial\Phi}{\partial\theta}\hat{\theta} + \frac{1}{r\sin\theta}\frac{\partial\Phi}{\partial\lambda}\hat{\lambda}$$

Divergence $$\vec{\nabla}\cdot\vec{A} = \frac{1}{r^2}\frac{\partial}{\partial r}(r^2 A_r) + \frac{1}{r\sin\theta}\frac{\partial}{\partial\theta}(\sin\theta A_\theta) + \frac{1}{r\sin\theta}\frac{\partial A_\lambda}{\partial\lambda}$$

Rotor $$\vec{\nabla}\times\vec{A} = \frac{1}{r^2\sin\theta}\begin{vmatrix} \hat{r} & r\hat{\theta} & r\sin\theta\hat{\lambda} \\ \frac{\partial}{\partial r} & \frac{\partial}{\partial\theta} & \frac{\partial}{\partial\lambda} \\ A_r & rA_\theta & r\sin\theta A_\lambda \end{vmatrix}$$

Laplacian: $$\nabla^2\Phi = \frac{1}{r^2}\frac{\partial}{\partial r}\left(r^2\frac{\partial\Phi}{\partial r}\right) + \frac{1}{r^2\sin\theta}\frac{\partial^2}{\partial\theta}\left(\sin\theta\frac{\partial\Phi}{\partial\theta}\right) + \frac{1}{r^2\sin^2\theta}\frac{\partial^2\Phi}{\partial\lambda^2}$$

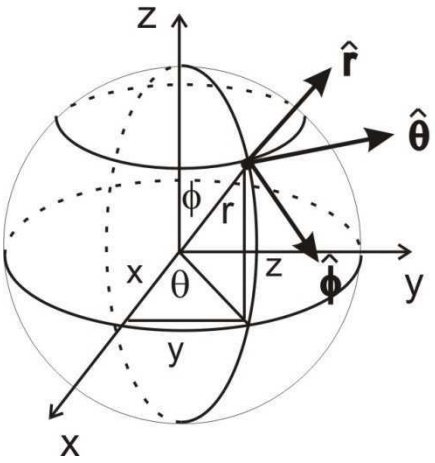

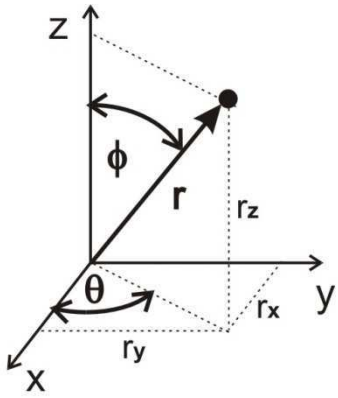

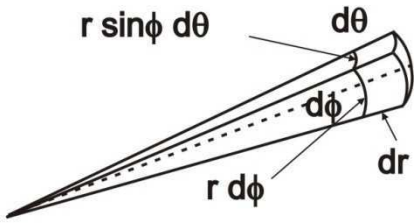

A3: Clausius-Mossotti: Derivation of relative permittivity according to mass density

Clausius-Mossotti relation $\frac{\varepsilon_r - 1}{\varepsilon_r + 2} = \frac{N_A \alpha}{3M} \rho_m$

Substitution $b = \frac{N_A \alpha}{3M}$

and expression of relative permittivity is $\varepsilon_r = \frac{2\rho_m b + 1}{1 - \rho_m b}$

Derivation of relative permittivity according to mass density is

$$\frac{\partial \varepsilon_r}{\partial \rho_m} = \frac{2b(1-\rho_m b) - (2\rho b_m + 1)(-b)}{(1-\rho_m b)^2} = \frac{3b}{(1-\rho_m b)^2} = \frac{3\frac{\varepsilon_r - 1}{\varepsilon_r + 2}}{\rho_m \left(1 - \frac{\varepsilon_r - 1}{\varepsilon_r + 2}\right)^2} =$$

$$= \frac{3\frac{\varepsilon_r - 1}{\varepsilon_r + 2}}{\rho_m \left[1 - 2\frac{\varepsilon_r - 1}{\varepsilon_r + 2} + \frac{(\varepsilon_r - 1)^2}{(\varepsilon_r + 2)^2}\right]} = \frac{3\frac{\varepsilon_r - 1}{\varepsilon_r + 2}}{\rho_m \left[\frac{(\varepsilon_r + 2)^2 - 2(\varepsilon_r - 1)(\varepsilon_r + 2) + (\varepsilon_r - 1)^2}{(\varepsilon_r + 2)^2}\right]} =$$

$$= \frac{(\varepsilon_r - 1)(\varepsilon_r + 2)}{3\rho_m}$$

A4: Asymmetric capacitor composed of a plate and a warp of parallel and equidistant fibers – detailed calculation

Total potential φ_L at the surface of the 0th fibre surface in the lower warp is composed of potential generated by the 0th fibre, the potential of its 0th fibre counterpart from the upper warp, a potential sum from other fibres in the lower warp and ultimately a potential sum from remaining fibres of the upper warp.

$$\varphi_L(r) = \frac{\tau}{2\pi\varepsilon_0}\left(-\ln a + \ln(2h) - 2\sum_{i=1}^{n}\ln\sqrt{a^2+(id)^2} + 2\sum_{i=1}^{n}\ln\sqrt{(2h)^2+(id)^2}\right) = \frac{\tau}{2\pi\varepsilon_0}\left(\ln\frac{2h}{a} + 2\sum_{i=1}^{n}\ln\frac{\sqrt{(2h)^2+(id)^2}}{\sqrt{a^2+(id)^2}}\right) \quad . \quad \text{(A1a)}$$

where *i* is an index assigned to individual fibres in warps. Similarly to the relationship (A1a), the total potential φ_L at the 0th fibre surface in the upper warp is

$$\varphi_U(r) = \frac{\tau}{2\pi\varepsilon_0}\left(\ln a - \ln(2h) + 2\sum_{i=1}^{n}\ln\sqrt{a^2+(id)^2} - 2\sum_{i=1}^{n}\ln\sqrt{(2h)^2+(id)^2}\right) = \frac{\tau}{2\pi\varepsilon_0}\left(\ln\frac{a}{2h} + 2\sum_{i=1}^{n}\ln\frac{\sqrt{a^2+(id)^2}}{\sqrt{(2h)^2+(id)^2}}\right) \quad .$$

(A1a')

Derivations in this paragraph follows the steps from the previous one and so, similar equations are denoted by the same numbers distinguished by "a".

The voltage U_W, i.e. potential difference, between lower and upper warps is

$$U_W = \varphi_L - \varphi_U = \frac{\tau}{2\pi\varepsilon_0}\left(\ln\frac{2h}{a} - \ln\frac{a}{2h}\right) + \frac{\tau}{\pi\varepsilon_0}\left(\sum_{i=1}^{n}\ln\frac{\sqrt{(2h)^2+(id)^2}}{\sqrt{a^2+(id)^2}} - \sum_{i=1}^{n}\ln\frac{\sqrt{a^2+(id)^2}}{\sqrt{(2h)^2+(id)^2}}\right) = \frac{\tau}{\pi\varepsilon_0}\left(\ln\frac{2h}{a} + \sum_{i=1}^{n}\ln\frac{(2h)^2+(id)^2}{a^2+(id)^2}\right) . \quad \text{(A2a)}$$

Equation (A2a) provides with the following τ - *U* relationship.

$$\tau = \pi\varepsilon_0 U\left(\ln\frac{2h}{a} + \sum_{i=1}^{n} \ln\frac{(2h)^2 + (id)^2}{a^2 + (id)^2} \right)^{-1}. \qquad \text{(A3a)}$$

The sum $\sum_{i=1}^{n} \ln\frac{(2h)^2 + (id)^2}{a^2 + (id)^2}$ in (A3a) is estimated using the following integration

$$\lim_{n\to\infty} \sum_{i=1}^{n} \ln\frac{(2h)^2 + (id)^2}{a^2 + (id)^2} \cong \int_1^{\infty} \ln\frac{(2h)^2 + (xd)^2}{a^2 + (xd)^2} dx = \int_1^{\infty} \ln\left[(2h)^2 + (xd)^2\right] dx - \int_1^{\infty} \ln\left[a^2 + (xd)^2\right] dx.$$

Using the relationship

$$\int \ln\left[A + Bx^2\right] dx = x\ln\left(Bx^2 + A\right) - 2x + \frac{2\sqrt{A}}{\sqrt{B}} \tan^{-1}\frac{\sqrt{B}x}{\sqrt{A}}$$

and substituting $A = (2h)^2$ in the first term of the left hand side of (I), or $A = a^2$ in the last term of (I), and $B = d^2$, one arrives to

$$\sum_{i=1}^{n} \ln\frac{(2h)^2 + (id)^2}{a^2 + (id)^2} \cong \int_1^{\infty} \ln\frac{(2h)^2 + (xd)^2}{a^2 + (xd)^2} dx =$$

$$\left[x\ln\left(d^2x^2 + (2h)^2\right) - x\ln\left(d^2x^2 + a^2\right) + 2\left(\frac{2h}{d}\tan^{-1}\frac{xd}{2h} - \frac{a}{d}\tan^{-1}\frac{xd}{a} \right) \right]_1^{\infty} =$$

$$\left[x\ln\frac{d^2x^2 + (2h)^2}{d^2x^2 + a^2} + 2\left(\frac{2h}{d}\tan^{-1}\frac{xd}{2h} - \frac{a}{d}\tan^{-1}\frac{xd}{a} \right) \right]_1^{\infty}.$$

The term $x\ln\frac{x^2d^2 + (2h)^2}{x^2d^2 + a^2}$ goes to zero, for $x \to \infty$, since the L'Hospital rule gives

$$\left(\frac{1}{x}\right)' = -x^{-2} \quad \text{and} \quad \left[\ln\frac{x^2d^2 + (2h)^2}{x^2d^2 + a^2} \right]' = \frac{2d^2\left[a^2 - (2h)^2\right]x}{d^4x^4 + d^2a^2x^2 + (2h)^2d^2x^2 + (2h)^2a^2}$$

And hence

$$\lim_{x\to\infty}\frac{2d^2\left[a^2-(2h)^2\right]x}{d^4x^4+d^2a^2x^2+(2h)^2d^2x^2+(2h)^2a^2}\left(-x^2\right)\cong\lim_{x\to\infty}\frac{1}{x}=0 \quad .$$

Finally we have

$$\sum_{i=1}^{n}\ln\frac{(2h)^2+(id)^2}{a^2+(id)^2}\cong 0+\frac{2}{d}\left(\frac{2h\pi}{2}-\frac{a\pi}{2}\right)-\ln\frac{d^2+(2h)^2}{d^2+a^2}-2\left(\frac{2h}{d}\tan^{-1}\frac{d}{2h}-\frac{a}{d}\tan^{-1}\frac{d}{a}\right)=$$
$$\frac{\pi}{d}(2h-a)-\ln\frac{d^2+(2h)^2}{d^2+a^2}-\frac{2}{d}\left(2h\tan^{-1}\frac{d}{2h}-a\tan^{-1}\frac{d}{a}\right)$$

From the Equation (A4a) one obtains potential difference U_W, between warps as

$$U_W=\frac{\tau}{\pi\varepsilon_0}\left[\ln\frac{2h}{a}+\frac{\pi}{d}(2h-a)-\ln\frac{d^2+(2h)^2}{d^2+a^2}-\frac{2}{d}\left(2h\tan^{-1}\frac{d}{2h}-a\tan^{-1}\frac{d}{a}\right)\right]. \qquad \text{(A4b)}$$

And hence the τ - U relationship sounds as

$$\tau=\pi\varepsilon_0U_W\left[\ln\frac{2h}{a}+\frac{\pi}{d}(2h-a)-\ln\frac{d^2+(2h)^2}{d^2+a^2}-\frac{2}{d}\left(2h\tan^{-1}\frac{d}{2h}-a\tan^{-1}\frac{d}{a}\right)\right]^{-1} \quad . \qquad \text{(A5b)}$$

The field strength at a fibre surface is obtained via the *r* derivative of the potential expressed previously in Equation (A3a).

$$E_W(a)=-\left.\frac{\partial\varphi(r)}{\partial r}\right|_{r=a}=-\frac{\tau}{2\pi\varepsilon_0}\frac{\partial}{\partial r}\left[\ln\frac{2h}{r}+2\sum_{i=1}^{n}\ln\frac{\sqrt{(2h)^2+(id)^2}}{\sqrt{r^2+(id)^2}}\right]_{r=a}=$$
$$-\frac{\tau}{2\pi\varepsilon_0}\frac{\partial}{\partial r}\left[\ln\frac{2h}{a}+\sum_{i=1}^{n}\ln\frac{(2h)^2+(id)^2}{a^2+(id)^2}\right]=\frac{\tau}{2\pi\varepsilon_0}\left[\frac{1}{a}+\sum_{i=1}^{n}\ln\frac{2a}{a^2+(id)^2}\right].$$

The sum $\sum_{i=1}^{n}\ln\frac{2a}{a^2+(id)^2}$ is here estimated using integral.

$$\sum_{i=1}^{n}\ln\frac{2a}{a^2+(id)^2}=2a\int_1^{\infty}\frac{dx}{a^2+(xd)^2}=2a\left[\frac{1}{da}\tan^{-1}\frac{xd}{a}\right]_1^{\infty}=\frac{2}{d}\left(\frac{\pi}{2}-\tan^{-1}\frac{d}{a}\right).$$

Therefore for the field intensity on the fibre surface holds

$$E_W(a)=\frac{\tau}{2\pi\varepsilon_0}\left[\frac{1}{a}+\frac{2}{d}\left(\frac{\pi}{2}-\tan^{-1}\frac{d}{a}\right)\right]=\frac{\tau}{2\pi\varepsilon_0}\left(\frac{1}{a}+\frac{\pi}{d}-\frac{2}{d}\tan^{-1}\frac{d}{a}\right). \qquad \text{(A6a)}$$

The substitution from Equation (A5b) for τ into the Equation (A6a) provides with

$$E_W(a)=\frac{U_W\left(\frac{1}{a}+\frac{\pi}{d}-\frac{2}{d}\tan^{-1}\frac{d}{a}\right)}{2\left[\ln\frac{2h}{a}+\frac{\pi}{d}(2h-a)-\ln\frac{d^2+(2h)^2}{d^2+a^2}-\frac{2}{d}\left(2h\tan^{-1}\frac{d}{2h}-a\tan^{-1}\frac{d}{a}\right)\right]}.$$

Compare it with Equation (A6) and watch the asymptotic for $d\to\infty$, to find their full similarity.

Multiplying both sides of the previous equation by 2*h* gives

$$\frac{hE_W(a)}{U_W}=\frac{\frac{h}{a}+\frac{\pi h}{d}-\frac{2h}{d}\tan^{-1}\frac{d}{a}}{2\left[\ln\frac{2h}{a}+\frac{\pi a}{d}\left(\frac{2h}{a}-1\right)-\ln\frac{\left(\frac{d}{a}\right)^2+\left(\frac{2h}{a}\right)^2}{\left(\frac{d}{a}\right)^2+1}-2\left(\frac{2h}{d}\tan^{-1}\frac{d}{2h}-\frac{a}{d}\tan^{-1}\frac{d}{a}\right)\right]}$$

Introducing dimensionless distances: $\xi=h/a$, $\zeta=h/d$ and $\rho=d/a$ and assuming that $\xi>>1$ one arrives to

$$\frac{E_W(a)}{E_O}=\frac{\xi+\pi\zeta-2\zeta\tan^{-1}\rho}{\ln 2\xi+2\pi\zeta-\ln\frac{\rho^2+(2\xi)^2}{\rho^2+1}-4\zeta\tan^{-1}\frac{1}{2\zeta}+\frac{2}{\rho}\tan^{-1}\rho}=Z_W, \qquad \text{(A7a)}$$

where E_0 is the field strength in a plate capacitor with distance between plates *h* and with a voltage $U' = U/2$, while Z_W is an amplification factor for the warp geometry.

Amplification factor Z_W for a warp of parallel and equidistant nanofibres with a spacing *d* between neighbouring ones is governed by the dimensionless distance $\rho = d/a$, in case that $h >> d >> a$, and is approximately independent on *h*.

$$\frac{E_W}{E_0} \cong \frac{\rho}{2\pi} = Z_W ,$$

The relationship between field strength amplifying factor Z_W and a fibre radius *a* for chosen parameter values is depicted in Fig. E8.